

A Theory of the Mechanics of Information: Generalization Through Measurement of Uncertainty (Learning is Measuring)

Christopher J. Hazard, Michael Resnick, Jacob Beel, Jack Xia, Cade Mack, Dominic
Glennie, Matthew Fulp, David Maze, Andrew Bassett, and Martin Koistinen

Howso Incorporated

October 28, 2025

1 Abstract

Traditional machine learning relies on explicit models and domain assumptions, limiting flexibility and interpretability. We introduce a model-free framework using surprisal (information theoretic uncertainty) to directly analyze and perform inferences from raw data, eliminating distribution modeling, reducing bias, and enabling efficient updates including direct edits and deletion of training data. By quantifying relevance through uncertainty, the approach enables generalizable inference across tasks including generative inference, causal discovery, anomaly detection, and time series forecasting. It emphasizes traceability, interpretability, and data-driven decision making, offering a unified, human-understandable framework for machine learning, and achieves at or near state-of-the-art performance across most common machine learning tasks. The mathematical foundations create a “physics” of information, which enable these techniques to apply effectively to a wide variety of complex data types, including missing data. Empirical results indicate that this may be a viable alternative path to neural networks with regard to scalable machine learning and artificial intelligence that can maintain human understandability of the underlying mechanics.

Contents

1 Abstract	1
Contents	1
2 Introduction	3
3 Intuitive Summary of Techniques	5
4 Foundational Statistics of Uncertainty	6
5 Definitions	7
6 Inference via Surprisal as Distance	9
6.1 Continuous and Ordinal Features Expected Differences	9
6.2 Continuous and Ordinal Features Marginal Surprisal	10
6.3 Nominal Features Marginal Surprisal	10
6.4 Surprisal of One Case Given Another	10
6.5 Influential and Similar Cases	11

6.6	Discriminative Inference (React)	12
6.7	Prediction (React) Residuals	12
6.8	Generative Inference (React)	13
7	Influential Features and Causal Discovery	13
7.1	Prediction Contributions	13
7.2	Accuracy Contributions	14
7.3	Robust Residuals	14
7.4	Information of Accuracy Contribution	14
7.5	Deviations and Feature Influence Probabilities	15
7.6	Additional Inference Optimization for a Single Target	16
7.7	Causal Direction and Guided Causal Discovery of New Features	16
8	Advanced Inference for Single Cases	18
8.1	Semistructured Data Types and Null Values	18
8.2	Derived and Dependent Features	19
8.3	Boundary Values	19
8.4	Boundary Cases	19
8.5	Data Constraining and Goal Features	20
8.6	Residual Conviction: Comparing Anomalousness of Features	20
8.7	Surprisal or Distance Contribution of a Case	21
8.8	Similarity Conviction of a Case	21
8.9	Synthetic Data via Differential Privacy Mechanisms	21
9	Data Compression Via Probability Mass and Hierarchical Sharding	23
9.1	Case Weights, Redundancy Reduction, and Ablation	23
9.2	Hierarchical Data Sharding	25
10	Groups, Clusters, Series, and Anomalies	25
10.1	Rebalancing, Fairness, and Data Volume Privacy	25
10.2	Clustering	26
10.3	Group Anomalousness	27
10.4	Anomaly Detection	28
10.5	Series, Time Series, and Panel Data	28
10.6	Reinforcement Learning and Relation to Active Inference	29
11	Implementation	30
11.1	API, Architecture, and Usability	30
11.2	Amalgam Programming Language	32
11.3	Nearest Neighbors Query Implementation	32
12	Empirical Results	35
12.1	Supervised Learning	35
12.2	Feature Importance	36
12.3	Anomaly Detection	37
12.4	Learning from Demonstration	38
12.5	Reinforcement Learning	40
12.6	Causal Discovery	40
12.7	Data Synthesis	42
12.8	Data Reduction and Ablation	42
12.9	Adversarial Robustness	43
12.10	Compute Performance	44

13 Future Work: Language, Images, and Creativity	45
13.1 Text	45
13.2 Images	46
13.3 Creativity	46
14 Conclusion	47
Acknowledgments	48
Bibliography	48
Appendices	53
A Supporting Mathematics	53
A.1 Derivation of Łukaszyk–Karmowski (LK) with Laplace Distributions	53
A.2 Surprisal Is a Distance Metric	57
B Numeric Example of Deriving a Prediction Using Iris Dataset	58
C Details of Empirical Evidence	61
C.1 Supervised Learning Classification Results	61
C.1.1 Howso (Targetless)	61
C.1.2 Howso (Single-Target)	64
C.1.3 XGBoost	67
C.1.4 LightGBM	70
C.2 Supervised Learning Regression Results	74
C.2.1 Howso (Targetless)	74
C.2.2 Howso (Single-Target)	79
C.2.3 XGBoost	84
C.2.4 LightGBM	89
C.3 Feature Importance Validation Results	96
C.4 Anomaly Detection Results	96
C.5 Reinforcement Learning: Detailed Results	113
C.5.1 CartPole Results	113
C.5.2 Wafer-Thin-Mints Results	113
C.6 Synthetic Data Generation: Detailed Results	115
C.7 Adversarial Robustness Results	115
C.7.1 Aggregate Results	115
C.7.2 Per-Dataset Results	115

2 Introduction

Traditional machine learning methods often rely on explicit models of data distributions, which can obscure trade-offs between accuracy, interpretability, and computational efficiency. These models also require domain-specific assumptions, limiting their adaptability to novel or complex tasks. This paper introduces a model-free framework that operates directly on data using surprisal, a fundamental concept from information theory, to quantify uncertainty and relevance. Unlike conventional methods that require explicit modeling of data distributions, our approach operates directly on raw data, eliminating the need for domain-specific assumptions and reducing the risk of model bias. This shift allows for more flexible and generalizable inference across diverse tasks, such as causal discovery and anomaly detection.

Advances in information theory and probability theory over the past two decades have provided essential insights toward understanding relationships among data. Despite these advances, there remains a significant gap between the theoretical foundations of probabilistic inference and the practical needs of machine learning. Most existing approaches to machine learning require careful tuning of hyperparameters, specification of loss

functions, and selection of models, which can be time-consuming and require significant expertise. Further, most machine learning algorithms are designed for a specific objective function, rather than providing a general framework for learning and inference. In this paper, we propose a new approach to machine learning that addresses these limitations by providing a unified, probabilistic framework for learning and inference that operates directly on the data.

Surprisal, or self-information, quantifies the information gained or lost when observing a particular data element to predict an event or another data point. It is mathematically defined as the negative logarithm of the probability of an event, making it a natural tool for measuring uncertainty in data. In our techniques, we frequently determine how surprising it would be if you could correctly use one particular data point in place of another because they were sufficiently similar. If two data points are very similar, it would be unsurprising that you could use the second data point in place of the first to make a prediction about the first. Surprisal offers a way to easily transform between distance and uncertainty, and surprisal is a flexible tool that enables many types of inferences and results that carries uncertainty characterizations with it.

Performing inference directly from the data is far from a new concept. k-Nearest Neighbors (kNN) is one of the oldest, simplest, and most robust algorithms for pattern classification and regression models [Hastie et al., 2001]. It is a simple technique that is easily implementable [Alpaydin, 1997]. Outputs from the technique are usually traceable back to the exact data that influenced each decision. This traceability enables detailed analysis of the decision inputs and characterization of the data local to the decision. The terms kNN, *case based reasoning* (CBR), and *instance-based learning* (IBL) have been used to describe such algorithms, and which term is used depends on whether the focus is on the algorithm (kNN), reasoning (CBR), or retrieval of data in high dimensional spaces (IBL). The techniques we describe here relate to kNN, CBR, and IBL, as they are all related to finding the relevant data.

k-Nearest Neighbors was previously a dominant machine learning technology [Coomans and Massart, 1982, Breiman et al., 1984, Altman, 1992, Alpaydin, 1997] but was largely abandoned with the growing size of data and the computational complexity of finding the nearest k points [Raikwal and Saxena, 2012, Schuh et al., 2014, Hmeidi et al., 2008]. Recently, these techniques have seen a resurgence for use in vector databases to find embeddings for neural networks [Pan et al., 2024]. The curse of dimensionality has also been known to adversely affect kNN [Hastie et al., 2001, Indyk and Motwani, 1998, Schuh et al., 2013, Tao et al., 2009] and the selection of a distance function can be challenging [V. B. Surya et al., 2017]. Additionally features may have to be scaled or standardized to prevent distance measures from being dominated by one of the features. The accuracy of kNN can be severely degraded by the presence of noisy or irrelevant features, or if the feature scales are not consistent with their relevance. Finally, kNN requires a value of parameter k . If k is too small, the model may have low bias but be sensitive to noisy points and have too high of variance. If k is too large, the neighborhood may include points from other classes and may have too little variance.

Our techniques search for relevant data based on the idea that learning is a process of measuring and characterizing uncertainty in the relationships among the data, rather than optimizing a specific objective function. Nearest neighbor searches using uncertainty have been studied, both with stochastic distances [Mason et al., 2021] and with uncertainty around the data points [Agarwal et al., 2016]. We improve on these techniques by using surprisal as a measure of uncertainty and by measuring the uncertainties among the data. We develop a framework for machine learning that is flexible, scalable, and robust to outliers and missing data. Our approach can be applied to a wide range of machine learning tasks, including supervised and unsupervised learning, reinforcement learning, and time series forecasting. It also has the potential to provide a new foundation for machine learning that is more general, flexible, powerful, and human-understandable than existing approaches. In the following sections, we will describe the theoretical foundations of our approach, demonstrate its effectiveness, and discuss potential future directions. We emphasize that the primary goal is not to create a technique that is the best at one specific task. Rather, our aim is to create a system that meets the following criteria: it is of sufficiently high performance that it is practically usable for nearly *every* task without having to build different models and systems for every task; every step is human understandable and traceable back to the data, with units of measurement and uncertainty every step of the way; the system turns the process of learning and inference into managing data and deriving values in understandable ways rather than attempting to understand and manage models; and that it opens new research to unify fundamental understanding of machine learning to improve to state-of-the-art and beyond without needing to build models.

The software implementing the techniques described in this paper is available at <https://github.com/>

howsoai/, with the primary interface Python module at <https://github.com/howsoai/howso-engine-py>, and example notebooks at <https://github.com/howsoai/howso-engine-recipes>. Throughout this paper we will generally refer to the algorithms and techniques, but in empirical results or when discussing implementation, we will refer to it as Howso or the Howso Engine. This work is the first comprehensive treatment of a research effort that started in 2011, with earlier iterations of some of the core ideas starting from kNN and iterating toward the findings described here [Hazard et al., 2019, Banerjee et al., 2023].

This paper adopts a nontraditional structure to emphasize the interdisciplinary nature of our framework. We begin with an intuitive summary, followed by foundational concepts, then progressively build toward advanced applications and scale, and follow with empirical results. Related work and future directions are largely integrated inline to maintain focus on the core contributions. The appendices contain relevant proofs, a numerical example of deriving a prediction, and details of empirical evidence.

3 Intuitive Summary of Techniques

Due to the novelty of techniques, we will begin with an intuitive summary of our system before introducing more technical formalisms.

Imagine trying to predict the acidity of a particular grape from a particular farm. Having acidity measurements of 3 grapes of similar size picked from the same vine on the same day would likely be a very informative prediction of the acidity of the first grape. Having 3 apples from the same farm may offer little information about the grape’s acidity, but knowing the latitude and longitude of the apple trees they were picked from may be very informative for predicting the street address of the farm.

For a given inquiry, any given piece of data has some probability of being informative. Most data will have a virtually zero probability of being informative most of the time. If we know the probabilities of data elements being informative, we can use those probabilities to find the data most likely to be relevant. From these probabilities, we can compute the best estimate as well as the uncertainty and distribution around that estimate.

Our system estimates all of these uncertainties, and we do so using robust and assumption minimizing techniques around the average uncertainty, the mean of the absolute differences between expected and actual. To estimate the uncertainties of features or columns of data, our system uses all other features including the feature itself to find the relevant data, makes a prediction, and finds the average difference between the prediction and actual value. In the case of measuring grapes, this means it uses the acidity of the grape in question, in addition to that grape’s other properties to predict its own values. This overfitting is intentional as it is a proxy for the potentially relevant features that are not included in the data. We use these uncertainties to compute the probability that one value is informative for another value, and then use these results to compute the probabilities that each feature predicts every other feature. Combining these probabilities, we compute the overall probability that one record is informative for another. There is no model besides the data and its uncertainties; the database is queried with these uncertainties to find any relevant result. Every computation of probability of every inference can be understood, and every data element used in an inference can be traced back to its source.

Because the system is a database, features, records, etc. can be included or excluded in queries, or added to, edited in, or removed from the data. Rather than using traditional cross validation techniques from data science, we can just leave a record out and predict it. Sampling records with replacement provides good estimates of the quality of inference on unseen data that is similar to existing data. Our system can compute how much individual features contribute to a prediction without including the biases included from models via traditional feature importance techniques. Imagine features A , B , and C are being evaluated in how they predict T . We can measure A predicting T , A and B predicting T , A and C predicting T , etc. and even predicting T without any features, and determine each feature’s contribution.

Further, our system can use the same approach to determine how features contribute to reducing the uncertainty in predicting another feature, including uncovering causal relationships. Causality deals with the relationship between two or more events or variables where one event influences the occurrence of another. For instance, moving a lever can open a valve and allow water to flow. This cause-and-effect relationship is asymmetric and not reversible. Our system can detect this asymmetry by analyzing how the uncertainty in one variable changes when another variable is included in the prediction. By doing so, we can identify

potential causal relationships among variables, which can have significant implications for understanding the underlying mechanisms driving a system and predicting the effects of changes to the system. Further, our system can detect asymmetries in both uncertainty and predictability, revealing likely causal relationships and hidden influences (confounders), and the strength of those relationships. This is in contrast to correlational techniques that treat relationships as two-way and can only find associations.

Many more machine learning and AI capabilities are possible and effective with this system. Anomalies can be identified by finding data records whose probability of being informative to their neighbors is much less than their neighbors' probabilities of being informative for each other. Anything in the system can be conditioned, that is, narrowed or focused to specific types of data, by specifying values. This is akin to looking up records in a database but by probability instead of by values or value ranges. Generative outputs are created by drawing from the probability distributions. Reinforcement learning is implemented by finding the data records that are most informative, selecting from those records which best maximize rewards, and then drawing an output from that probability distribution. Larger data sets can be addressed by automatically determining which records are sufficiently duplicative that their probability masses can be combined.

Time series capabilities extend this base of capabilities. By deriving and including additional features which represent the lagged values (values from an earlier time step) and rates (change in value over time), the aforementioned capabilities can be leveraged for nearly any time series workflow, including forecasting and hypothetical modeling. Time series strengthens the quality of causal results by assessing whether one change occurs before another.

Throughout this work, we will frequently leverage information theory, which provides notationally and computationally convenient techniques to handle these probabilities.

4 Foundational Statistics of Uncertainty

Because our system is built around uncertainty, we begin by describing what forms of uncertainty we employ and how we characterize it.

When assessing uncertainty of a data element, it is common to assess the uncertainty of measurement, or measurement error. This is classically performed by repeatedly performing some measurement and characterizing some moment about the mean of those measurements, typically variance. Often, this uncertainty is assigned to the reliability of a measuring device or process. Another form of uncertainty of a data element is the uncertainty of attempting to predict the value via a model. This is typically called a residual or prediction uncertainty, and this residual is typically assigned to a particular prediction or a model if the residuals are aggregated.

In addition to where the uncertainty is measured, uncertainty is also often characterized by its most likely origin [Hüllermeier and Waegeman, 2021]. *Epistemic* uncertainty is uncertainty that stems from not having enough knowledge or data, which can be reduced by obtaining more knowledge or data. *Aleatoric* uncertainty is the irreducible part of uncertainty that comes from underlying stochasticity that cannot be resolved by collecting more data, such as the outcome of a fair coin flip. However, in many practical scenarios, the distinction between these two types of uncertainty is blurred. For instance, a coin flip's randomness (aleatoric) could become predictable with advanced tools like high-speed cameras and physics simulations (reducing epistemic uncertainty). Our framework aims to identify epistemic sources of uncertainty as described in Section 7.7.

Beyond traditional categories, we introduce *substitutability deviation* (often just *deviation* for short), a novel measure of uncertainty that reflects how likely one data element can be replaced by another without compromising predictive or informative value. This concept is critical for tasks like nearest-neighbor searches, where similarity between data points determines relevance. It is not strictly epistemic or aleatoric, but rather represents the combination of the two given the data. As an example of deviations, when using human height in reasoning about physiological information or clothing size, we often make measurements to the nearest centimeter or half inch and declare people to be the same height if within that tolerance. A person's posture, shoe sole depth, and spine compression from sitting and standing can all impart differences on the person's height.¹ In this case, the deviation for this kind of data may be roughly a centimeter or half inch.

¹Undoubtedly, any data set with self-reported human heights is likely to have some skew in the rounding.

The foundation of our techniques rely upon mean absolute error (MAE), the absolute value of the difference between the estimated and the observed. Though standard deviation is widely used for measuring uncertainty, MAE can be considered to be a more suitable measure of risk and uncertainty than standard deviation in many situations. MAE is more robust to outliers, better captures the potential for extreme losses, and is easier for humans to interpret due to half of the expected results being within the value [Taleb, 2007].

Building on these concepts of uncertainty, we use maximum entropy distributions whenever possible to characterize the local uncertainty of our data. Maximum entropy refers to the idea of selecting a probability distribution that makes the fewest assumptions about the underlying data, given the constraints. This approach is useful in situations where the data and information are limited, such as when assessing uncertainty locally, zoomed in to a small amount of data. The maximum entropy distribution of the absolute values of residuals is the exponential distribution. This distribution is widely used in statistics and has several desirable properties, including being robust to outliers and easy to interpret. When dealing with differences between two values, if the absolute value of the difference is used as the mean absolute deviation of the distribution of values, the Laplace distribution (which is two back-to-back exponential distributions) is the maximum entropy distribution. We will rely on this relationship throughout our work.

To determine the surprisal of a particular observation, we use cumulative residual entropy [Rao et al., 2004] to determine the surprisal of a particular value when compared to another data value given its deviation. Here, we derive this surprisal from the cumulative density function (CDF) of the exponential distribution via cumulative residual entropy. Given two observed values, x_1 and x_2 , we can write this well-known CDF with regard to the difference between the actual values d , which is unknown. Using δ as the deviation, this expression becomes

$$P(d \leq |x_1 - x_2|) = 1 - e^{-\frac{1}{\delta}|x_1 - x_2|}. \quad (1)$$

We wish to flip the question. Given the unknown difference between the two actual values d , we would like to determine the probability that the difference between our observations x_1 and x_2 is less than the actual difference. If the actual difference is less than the observed difference, that means the data is at least as relevant as it has been observed. We find this by negating Equation 1 as

$$P(|x_1 - x_2| < d) = e^{-\frac{1}{\delta}|x_1 - x_2|}.$$

As surprisal is the negative logarithm of a probability, we can express the surprisal that we would observe from using the value of x_1 in place of x_2 as

$$\begin{aligned} I(|x_1 - x_2| < d) &= -\ln(P(|x_1 - x_2| < d)) \\ &= -\ln\left(e^{-\frac{1}{\delta}|x_1 - x_2|}\right) \\ &= \frac{|x_1 - x_2|}{\delta}. \end{aligned} \quad (2)$$

In light of this, we observe that to find the surprisal of one value given another, we can simply divide the absolute value of the difference by the deviation.

We note that mean absolute error and mean absolute deviation (MAD) are closely related concepts. MAE refers to the expected difference between actual and predicted when making a prediction or measurement, whereas MAD refers to the expected difference between values and their mean. When using our techniques, this distinction can become blurred. For example, determining the deviation to find the probability that a data point is informative for another could be considered MAE if trying to predict that value or MAD if characterizing the data. We try to use the most appropriate term between MAE or MAD for each context, but a different way of viewing a given technique may suggest the other term.

5 Definitions

Here we define common variables throughout the formulae below. This is meant as a lookup table for the remainder of the work. Further, we define *conviction*, ρ , as the ratio of the expected surprisal to observed surprisal as

$$\rho = \frac{EI}{I}. \quad (3)$$

- \mathcal{F} is the set of all available features.
- \mathcal{C} is the set of all available cases or records or instances that are in the data set.
- F is a set of features, J is used when a second set of features is needed.
- i and n are individual cases, which may or may not be in the set of available cases.
- j and t are individual features, with t generally indicating a feature designated as a target for the particular operation. In our implementation, we often refer to features being used as input or contextualization as “context features” and features being used as output via prediction, generation, or inference as “action features”, as whether a feature is an input or output depends on what is being done rather than a built-in aspect of a model.
- x is a vector of values, with the subscript representing the feature or features. It may be subscripted with i or n to indicate a specific record, either trained or not, or may be omitted if there’s only one vector of values being considered (e.g., x_F).
- w_i is the weight of a given case, when applicable. This is the probability mass that the particular case represents in the data when data reduction techniques are applied. Weights are generally omitted from most of the formulae for simplicity, but may be included in nearly any formula involving case probability masses. See Sections 6.4 and 9.1.
- f_j is the function that estimates the value for feature j .
- $C_{i,F}$ is the influential cases with respect to case i with regard to features F .
- $\mathcal{P}(C)$ denotes the power set of set C .
- $I(x)$ is the self-information of x , also known as surprisal.²
- $I(x | y)$ is the information of x given y .
- S_i is the surprisal contribution of i , indicating the expected surprisal of i given its influential cases C_i .
- σ_i is the surprisal contribution conviction of i , which is the surprisal contribution contextualized as a conviction.
- κ is the value of a particular nominal class. It may be used with a subscript, e.g., κ_1 , to indicate one class versus another.
- $\delta_j(x_{i,F})$ is the deviation, the mean absolute error of of j for the values of x_i over set of features F which indicates the uncertainty of whether the values can be considered the same for inference purposes. This value is at least as large as the measurement error but not greater than the residual. Note that F does not exclude j . If x_j is a nominal value, then $\delta_j(x_F)$ or $\delta_{j,\kappa}(x_F)$ may be used to represent the deviation for the nominal class of x_j or κ respectively. Further, for performance purposes, $E(\delta_j(x_{n,F}) | n \sim \mathcal{C})$ is sufficient to yield strong results from most data sets. See Section 7.5 for computing these values.
- d is the difference between two actual values, which may not be known. When used by itself it is used as a variable, but in context of different observations it will be used as a function of those two data elements for a given feature, e.g. as $d_j(x_{i,j}, x_{n,j})$. In many of our formulae, the real value for d is unknown and so it is treated as a distribution.
- $q_{j,t}$ is the probability that feature j is informative for predicting feature t , which can be a function of F or x_F , and if not, then it is the expected value of the probability. See Section 7.5 for computing these values.
- ϕ is a set of constraints used to subset the data. For example, for a given query, ϕ could be $\{x_j \in \{\kappa_1, \kappa_2\}, 0 \leq x_t \leq 5\}$. See Section 8.5.

²We use I instead of s to reduce the number of letters introduced.

- $\Omega_j(x_F)$ is a goal function on feature j that accepts a vector of values and evaluates to a value representing how close it is to a specific goal, where smaller values are closer to the goal. Without loss of generality, goal features may maximize by simply negating a particular value or may attempt to achieve a value as close as possible to another by minimizing the difference. If written with a set of features as Ω_F , it means a collection of goal functions. See Section 8.5.
- ρ is conviction, a ratio of expected surprisal to observed surprisal, which may be used as an input.
- k denotes a count of cases, typically indicating the cases that comprise the appropriate statistical bandwidth for a query.
- E denotes an expected value over the relevant domains. E_{LK} denotes the expected value assuming an uncertainty using the Łukaszyk-Karmowski metric. Based on the domain, this is either as defined by Equation 4 for Laplace distributions, or as $E_{LK}(|x_{i,j} - x_{n,j}| | x_{n,F}) = |x_{i,j} - x_{n,j}| + \frac{2\delta_j^2}{|x_{i,j} - x_{n,j}| + 2\delta_j}$ for exponential distributions [Łukaszyk, 2003], the maximum entropy distribution for distributions over positive real numbers given a mean, though solutions for other distributions could be used if appropriate.
- P denotes a probability, potentially conditioned.
- η is a generic variable used to represent a real value.
- ξ is a generic variable used to represent a nominal value.
- Q_η is a function that returns the quantile of the set passed in at quantile η .
- e is Euler's number.

6 Inference via Surprisal as Distance

We begin by describing the core operations around determining data relevancy and performing discriminative and generative inference.

6.1 Continuous and Ordinal Features Expected Differences

The Łukaszyk-Karmowski metric finds the expected difference between two values, given the distributions around those values [Łukaszyk, 2003, 2004]. If there is uncertainty around a measurement, this means that even identical measurements still yield a small but nonzero expected distance due to that uncertainty. This is written in their original notation as the expected distance d between uncertainty distributions X and Y as

$$d(X, Y) = \int_{-\infty}^{\infty} \int_{-\infty}^{\infty} |x - y| f(x) g(y) dx dy.$$

We assume the Laplace distribution for uncertainty. This is a maximum entropy distribution given a mean absolute deviation, not unlike the Gaussian distribution being the maximum entropy distribution when given the variance. We assume both probability density functions of the value distributions are parameterized with the same uncertainty, $\delta_j(x_F)$, as derived Appendix A.1. Note that we write it as a conditional expected difference given that the uncertainty is characterized by the uncertainty around $x_{n,F}$. Adopting the notation described above, this expected difference is

$$E_{LK}(|x_{i,j} - x_{n,j}| | x_{n,F}) = |x_{i,j} - x_{n,j}| + \frac{1}{2} e^{\frac{-|x_{i,j} - x_{n,j}|}{\delta_j(x_{n,F})}} (3\delta_j(x_{n,F}) + |x_{i,j} - x_{n,j}|). \quad (4)$$

When using this expected difference, it reduces the distinctiveness of differences that are within the uncertainty, but the effect is insignificant on differences that are far greater than the uncertainty.

6.2 Continuous and Ordinal Features Marginal Surprisal

Given that we have an expected distance between two values, we would like to determine how surprising it would be if one value turned out to be informative for the other. In other words, we want to determine how surprised we would be if we could use one value in place of another given their uncertainties. The uncertainties are the mean absolute deviation around the values, the primary parameter for the Laplace distribution.

As discussed in Section 4, the Laplace distribution is symmetric, which allows us to simplify the distribution of these mean absolute deviations to the exponential distribution. We parameterize this Laplace error distribution as $L(x_{i,j}, \delta_j(x_{i,F}))$, so the exponential distribution of the distribution of the unknown actual difference between values becomes $Exp\left(\frac{1}{\delta_j(x_{i,F})}\right)$. We write the deviation for feature j as δ_j , and write the expected difference between observed value $x_{i,j}$ and another known value $x_{n,j}$ given a set of features F as $E(|x_{i,j} - x_{n,j}| | F)$. The features are relevant to determine what deviation is appropriate for the $x_{n,F}$.

From these aforementioned values, we can rewrite Equation 2 to express the surprisal that $x_{n,j}$ is informative to $x_{i,j}$ for the unknown difference $d_j(x_{i,j}, x_{n,j})$ as

$$I(d_j(x_{i,j}, x_{n,j}) < E(|x_{i,j} - x_{n,j}| | x_{n,F})) = \frac{E(|x_{i,j} - x_{n,j}| | x_{n,F})}{\delta_j(x_{n,F})}. \quad (5)$$

Equation 5 includes the conditional surprisal that the distribution of the uncertainty is a Laplace distribution with the Łukaszyk-Karmowski metric [Łukaszyk, 2003, 2004]. To determine the marginal surprisal, we should remove this extra base surprisal. This base surprisal of a case compared to itself, $I(x_{n,j} | F, x_{n,j}, L(x_{n,j}, \delta_j(x_{n,F}))) = \frac{0 + \frac{1}{2}e^0(3r+0)}{r} = 1.5$ nats, and should be subtracted from the resulting surprisal. We write this surprisal more compactly leaving out the unknown difference between values. The complete formula for marginal surprisal for a continuous feature is thus

$$I(x_{i,j} | F, x_{n,j}) = \frac{|x_{i,j} - x_{n,j}| + \frac{1}{2}e^{-\frac{|x_{i,j} - x_{n,j}|}{\delta_j(x_{n,F})}} (3\delta_j(x_{n,F}) + |x_{i,j} - x_{n,j}|)}{\delta_j(x_{n,F})} - 1.5. \quad (6)$$

The difference between surprisal of an observation versus marginal surprisal of an observation can be illustrated with a coin toss. If the coin is believed to be fair and tossed in normal conditions (e.g., excluding landing on the edge), then 1 bit of surprisal is expected. However, if the coin lands on its edge, approximated to be a 1 in 6000 chance with an American nickel [Murray and Teare, 1993], a person would be surprised. The probability of heads is thus $\frac{2999.5}{6000}$, tails is $\frac{2999.5}{6000}$, and edge is $\frac{1}{6000}$, the surprisal of observing a heads would be 1.00024 bits, a tails 1.00024 bits, and an edge 12.55075 bits. Thus, the marginal surprisal of the coin landing on its edge over the baseline expectation of a normal coin flip is $12.55075 - 1.00024 = 11.55051$ bits.

6.3 Nominal Features Marginal Surprisal

Finding the marginal surprisal of a nominal feature follows similar logic to that of continuous features. First we find how surprising it would be if a given value $x_{n,j}$ were informative for the case we are trying to use it for, x_i , given the relevant deviations. To obtain the marginal surprisal, we must also subtract out the minimum surprisal of all of the possible values, treating that as the baseline surprisal. Typically this will yield zero marginal surprisal for the most probable match. However, it may also yield zero marginal surprisal if several values are statistically indistinguishable. This marginal surprisal for nominal features can be expressed as

$$I(x_{i,j} | F, x_{n,j}) = -\ln \delta_j(x_{n,F}) - \min_{\kappa} (-\ln \delta_{j,\kappa}(x_{n,F})). \quad (7)$$

6.4 Surprisal of One Case Given Another

For set of features F , the surprisal of case i given case n is

$$I(i | F, n) = \sum_{j \in F} I(x_{i,j} | F, x_{n,j}). \quad (8)$$

This can also be written as

$$I(x_i | F, x_n) = \sum_{j \in F} I(x_{i,j} | F, x_{n,j}), \quad (9)$$

which can be transformed to the probability of case x_n being informative for case x_i as

$$P(x_i | F, x_n) = e^{-I(x_i | F, x_n)}. \quad (10)$$

If case weights, w_n are used, then the weighted probability can be written as

$$P(x_i | F, x_n) = e^{-w_n \cdot \sum_{j \in F} I(x_{i,j} | F, x_{n,j})}, \quad (11)$$

which is equivalent to w_n occurrences of the case each having the same probability by exponentiating the probability by the weight.

When computing the surprisal of one case given another with regard to a specific target, we need to consider the probability that a given feature, j , is informative to the target feature being predicted, t . The probability of case x_n influencing inference for case x_i using features F when performing inference to predict feature t is

$$P(x_i | F, t, x_n) = P(x_i | F, x_n) \cdot q_{j,t}(x_F) \quad (12)$$

where

$$P(x_i | F, x_n) = e^{-I(x_i | F, x_n)}. \quad (13)$$

This means that the expected case surprisal for predicting target t is

$$I(x_{i,t} | F, x_n) = \sum_{j \in F} q_{j,t} I(x_{i,j} | F, x_{n,j}). \quad (14)$$

Equation 14 can be transformed like Equation 9 to the probability of case x_n being informative for case x_i for feature t as

$$P(x_{i,t} | F, x_n) = e^{-I(x_{i,t} | F, x_n)}. \quad (15)$$

Adding surprisals is the logarithm equivalent of multiplying probabilities, and so multiplying a surprisal by a probability of influence is the same as raising the surprisal’s corresponding probability to the probability of influence. This yields the intended behavior that two features which have the same informativeness and probability of influence contribute the same as multiplying together two probability terms, as the former is the square of the probability. From this perspective, Equation 14 closely resembles the conjunction of probabilities of independent distributions that form the core of the no-flattening theorem by Lin et al. [2017] suggesting that there is a relationship between this work and how hierarchical neural network architectures behave.

As proven in Appendix A.2, surprisals are a distance metric when deviations are constant. When deviations are considered approximately constant and smooth locally, surprisals are also a distance metric locally. This property makes surprisal usable in place of distance for many distance-based machine learning techniques beyond kNN as described in Section 6.5, such as distance-based clustering techniques (e.g., HDBSCAN [McInnes et al., 2017]), and visualization techniques (e.g., UMAP [McInnes et al., 2018]).

6.5 Influential and Similar Cases

The set of influential cases $C_{i,F}$ is the set of records that have minimal surprisal with regard to record i for set of features F and comprise the statistical bandwidth that is influential to i . This set can be of size k_{min} to k_{max} where the next incremental case offers marginal probability less than some probability threshold t . The set of influential cases is represented as

$$C_{i,F} = \operatorname{argmin}_{i \in \mathcal{C}}^{k \in [k_{min}, k_{max}]} I(x | i) \text{ s.t. } P(x | \{y \in \mathcal{C} : I(y | i) < I(x | i)\}) < t. \quad (16)$$

Note that by default, $k_{min} = 1$, $k_{max} = \infty$, and $t = \frac{1}{e^3}$, and that “similar cases” are determined by specifying a fixed k .

6.6 Discriminative Inference (React)

Discriminative inference, often contextualized as a prediction, produces an expected value for a feature j given the context of features F and feature values x_F . Our techniques take into account the influential cases and the probabilities that they are informative to predicting j given x_F . For continuous and ordinal features, the expected value for case i is found over the support of all of the influential cases, $C_{i,F}$, by finding the average value given the probabilities of influence as

$$\begin{aligned} f_t(x_{i,F}) &= E(x_t | x_{i,F}) \\ &= \frac{1}{\sum_{n \in C_{i,F}} P(x_{i,t} | F, x_{n,F})} \sum_{n \in C_{i,F}} P(x_{i,t} | F, x_{n,F}) \cdot x_{n,t}. \end{aligned} \quad (17)$$

If case weights, w_n , are used then this equation becomes

$$f_t(x_{i,F}) = \frac{1}{\sum_{n \in C_{i,F}} P(x_{i,t} | F, x_{n,F})^{w_n}} \sum_{n \in C_{i,F}} P(x_{i,t} | F, x_{n,F})^{w_n} \cdot x_{n,t}. \quad (18)$$

For ordinal features, the predicted value is rounded to the nearest ordinal.

For nominal features, the expected value is the mode of the probability masses of the values of the influential cases. We combine the probabilities of each of the influential cases and accumulate their masses by each value, ξ , finding the value with the largest probability as

$$\begin{aligned} f_t(x_{i,F}) &= E(x_t | x_F) \\ &= \arg \max_{\xi} \sum_{n \in \{n' \in C_{i,F} | x_{n',t} = \xi\}} P(x_{n,t}). \end{aligned} \quad (19)$$

Like continuous features, if case weights are used, then the expected value becomes

$$f_t(x_{i,F}) = \arg \max_{\xi} \sum_{n \in \{n' \in C_{i,F} | x_{n',t} = \xi\}} P(x_{n,t})^{w_n}. \quad (20)$$

6.7 Prediction (React) Residuals

We use the definition of residuals as the mean absolute expected difference between the predicted and actual value. The residual for feature j can be computed for an existing data element x_i for features F as

$$r_j(x_{i,F}) = E(|f_j(x_{n,F}) - x_{n,j}| | n \sim C_{x_{i,F}} \setminus \{i\}) \quad (21)$$

if the feature j is continuous. Determining the expected residual across many cases can be computationally expensive, and we have found that using the weighted mean absolute deviation of a prediction matches the actual error more closely than the average of the residuals found by leave-one-out predictions for many variants of nearby cases (e.g., C_i , as well as fixed values such as the 30 nearest cases). The weighted mean absolute deviation of the prediction can be expressed as

$$r_j(x_{i,F}) \approx \frac{1}{\sum_{n \in C_{i,F}} P(x_{i,t} | F, x_{n,F})} \sum_{n \in C_{i,F}} P(x_{i,t} | F, x_{n,F}) \cdot |x_{n,t} - E(x_t | x_{i,F})|. \quad (22)$$

If j is nominal, then the residual can be computed as

$$r_j(x_{i,F}) = E(1 - P(x_{n,t} | C_{x_{i,F}}, F, x_{i,F}) | n \sim C_{x_{i,F}} \setminus \{i\}). \quad (23)$$

We note that if $i \in \mathcal{C}$, then these formulae are computing the residual of a record already in the data set, and so it must be excluded as to not influence itself. If $i \notin \mathcal{C}$, then nothing will be removed. Further, modifying these formulae to account for case weights can be done in the same manner as described in Section 6.6.

6.8 Generative Inference (React)

When performing a generative inference, the default assumption is that it should follow the marginal distribution of the prediction. However, this sharpness of the marginal distribution can be controlled by changing the conviction, ρ from the default value of 1 which follows the marginal distribution. Given a desired conviction ρ , a generative value for a continuous feature j given a context $x_{i,F}$ can be drawn from the Laplace distribution from the relevant uncertainty as

$$g_j(x_{i,F}, \rho) \sim L\left(x_{n,j}, \frac{r_j(x_{n,j})}{\rho}\right), n \sim \{n \in C_{i,F} : P(x_{i,j} | F, x_n)\}. \quad (24)$$

For nominal features, drawing generative for the context $x_{i,F}$ can be written as

$$g_j(x_{i,F}, \rho) = \begin{cases} x_{n,j}, n \sim P(x_{n,t} | C_i, F, x_{i,F}) & \text{if } \eta < \frac{r_j(x_{i,F})}{\rho}, \eta \in U(0, 1) \\ x_{n,j}, n \sim \mathcal{C} & \text{if } \frac{r_j(x_{i,F})}{\rho} \leq \eta < 1 - \left(1 - \frac{r_j(x_{i,F})}{\rho}\right)^2 \\ x_{n,j} \sim U(\{x_{n,j} | n \in \mathcal{C}\}) & \text{if } 1 - \left(1 - \frac{r_j(x_{i,F})}{\rho}\right)^2 \leq \eta \end{cases}. \quad (25)$$

Like residuals, modifying these formulae to account for case weights can also be done in the same manner as described in Section 6.6.

7 Influential Features and Causal Discovery

In this section, we describe how our methods determine how features contribute to predictions and reductions in uncertainty, and link those results to the discovery of causal relationships. Because the system is a database rather than a model, techniques such as leave-one-out validation, where an individual record is held out and predicted, are very efficient. Performing bootstrap sampling with leave-one-out evaluation (selecting cases to be held out randomly with replacement) is an effective way to measure performance aspects of predicting a feature in our system, as validated by experiments performed with extra holdout data. We leverage our system’s efficiency at leaving out records and leaving out features in queries throughout the techniques described in this section.

7.1 Prediction Contributions

Prediction contributions are the measured difference between a prediction in an action feature when each feature (feature prediction contributions) or case (case prediction contributions) is considered versus not considered. When feature prediction contributions are applied in a robust fashion, this means that the samples are collected over the power set of all possible combinations of features. This is an approximation of the commonly used SHAP feature importance measure [Lundberg and Lee, 2017] which addresses many of SHAP’s common issues [Kumar et al., 2020]. Because the feature is actually removed, it closely resembles what is considered to be a ground truth of feature importance, removing the feature and retraining [Hooker et al., 2019], the only difference being that the deviations and probability masses are not recomputed. The nomenclature distinction is because these values are computed as feature importance on the data rather than measuring the feature importance of a particular model, akin to measuring SHAP across many thousands of independently constructed models. The strength of this approach is that inductive biases are reduced or eliminated. For example, if feature f_1 and feature f_2 are highly correlated, a model may remove or reduce the influence of f_2 , when with respect to the data, both f_1 and f_2 were equally informative. Prediction contributions ensure that such relationships are surfaced.

Prediction contributions can be computed either directionally or via absolute values. Directional values show whether the inclusion of a feature increases or reduces a value, and so the sum of the directional prediction contributions over the features will approximate the mean value of a feature. Absolute value prediction contributions indicate the magnitude of impact a feature has on a particular prediction. Prediction contributions can be computed across an entire data set, on a conditioned subset of a dataset, or on the data for a particular prediction. For simplicity, we write the unconditioned prediction contributions across

features, though any aspect of the formulae can be conditioned, and they may be rewritten to apply to cases from some set of cases.

The directional prediction contributions of feature j predicting a target feature t are obtained across the set of features \mathcal{F} as

$$DPC_{j,t} = E (f_t(x_{F \cup \{j\}}) - f_t(x_F) \mid F \sim \mathcal{P}(\mathcal{F} \setminus \{j, t\})). \quad (26)$$

And the corresponding absolute value prediction contributions are obtained as

$$APC_{j,t} = E (|f_t(x_{F \cup \{j\}}) - f_t(x_F)| \mid F \sim \mathcal{P}(\mathcal{F} \setminus \{j, t\})). \quad (27)$$

7.2 Accuracy Contributions

The techniques in Equation 27 can be applied to the uncertainties as well, in the form of mean absolute error. Accuracy contributions measure how much the inclusion of feature j reduces the uncertainty when predicting a given target feature t . Computing this robustly over the power set of all feature coalitions can be written as

$$AC_{j,t} = E (|f_t(x_{F \cup \{j\}}) - x_t| - |f_t(x_F) - x_t| \mid F \sim \mathcal{P}(\mathcal{F} \setminus \{j, t\})). \quad (28)$$

7.3 Robust Residuals

To characterize the uncertainty of prediction and accuracy contributions, we examine the mean absolute error of predicting target feature t over the power set of possible features. These residuals will be at least as large as the residual of predicting the target feature t , and represent useful information of the uncertainty of prediction and accuracy contributions. To signify that these residuals are computed over the power set, we call these *robust* residuals, and denote them as

$$rr_t = E (r_t(x_{n,F}) \mid F \sim \mathcal{P}(\mathcal{F} \setminus \{t\}), n \in \mathcal{C}). \quad (29)$$

7.4 Information of Accuracy Contribution

Using the same derivation from Equation 6, we can transform the uncertainties of the accuracy contributions from Equation 28 with regard to their differences from zero into surprisals using the uncertainty characterized by robust residuals from Equation 29. Accuracy contributions are measured across the power set of features, so to keep the uncertainties on the same scale, robust residuals fits better than residuals or deviations.³ We call this value the information of accuracy contribution and compute it as

$$IAC_{j,t} = \frac{AC_{j,t} + \frac{1}{2} e^{-\frac{AC_{j,t}}{rr_t}} (3rr_t + AC_{j,t})}{E(rr_t)} - 1.5. \quad (30)$$

These IAC values can be assembled into a matrix comparing all features to all other features. Causal relationships require asymmetries in the entropy relationships between features, in particular, see Definition 8 in the work of Simoes et al. [2023]. These asymmetries can be found as

$$IAAC_{j,t} = IAC_{t,j} - IAC_{j,t}, \quad (31)$$

and may be computed for every pair of features to characterize causal entropy apparent in the data. These entropies may be left as entropies or transformed into probabilities for assessing those relationships with the strongest causal signal. The values for $IAAC_{j,t}$ above a given threshold can be used as edges to characterize a portion of the underlying causal graph. This technique relates to knockout features [Candes et al., 2018]. The difference is that knockout features are copies of the features with added noise to give a baseline to detect causal relationships, whereas our techniques attempt to assess the uncertainty directly and compare it from the opposite direction.

³There are a few circumstances where other residuals still give slightly better results than robust residuals, particularly for feature influence probabilities as derived in Section 7.5. This is an area for future investigation.

7.5 Deviations and Feature Influence Probabilities

Determining what neighbors are relevant in a high dimensional space is a challenging problem. Solving this problem involves contextualizing what is locally relevant based on the data. We extend the ideas of finding relevant features [Hinneburg et al., 2000] and data [Beyer et al., 1999] into probability space, achieving dynamic behaviors that resemble attention mechanisms [Soydaner, 2022].

Deviations, as described in Section 4, is the uncertainty measured in mean absolute error that surrounds each data element, measuring the probability that one value is representative of another. For example, the difference of a centimeter is irrelevant when measuring the height of a redwood tree, as wind can move branches and other factors including time of day can affect the angle of the pine needles, whereas a centimeter may be relevant when measuring the height of an early-growth sapling. We compute these deviations by sampling the data with replacement and determining the uncertainty in predicting each value given that the value itself was used to find the relevant data. Using the value being predicted to find the relevant data, and then determining the mean absolute error of predicting the value, deliberately underestimates the residual with the intent of approximating features absent from the data that might help with the predictability. In other words, deviations are an estimate of the lower bound of the expected residual of predicting a particular data element. If the data does not have extremely long tails and more consistent uncertainty, the expected deviation as measured across the data set can be estimated via sampling with replacement as

$$\delta_j = E(r_j(x_{n,\mathcal{F}} | n \in \mathcal{C})). \quad (32)$$

However, for data sets that have long tails, highly variable uncertainty, or nominal classes of varying similarity, we can compute and store deviations that are locally relevant to the data as

$$\delta_j(x_{i,F}) = E(r_j(x_{i,F} \cup x_{n,J} | J \in \mathcal{F} \setminus F, n \in \mathcal{C})). \quad (33)$$

Using local deviations or deviations for pairs of nominal classes can improve results but incurs additional performance and storage costs. Empirically, we have found that using a single value for a feature’s deviation works very well for many data sets. In the case of nominal features, sometimes different nominal classes are unlikely to be confused with one another. For example, if dealing with a text corpus using tokens or words, it is unlikely that the word “tree” would be confused with the word “square” in virtually any context, so storing a deviation between those two tokens would neither have sufficient statistical support nor would it be computationally efficient. Conversely, the words “tree” and “bush” may be confused on occasion, for example, with regard to coffee plants. Instead, we have implemented what we call a *sparse deviation matrix* for nominal classes, where only the deviations that have sufficient statistical evidence are maintained, and anything that is not statistically significant we bundle together for the deviations of nominal values not found in the sparse deviation matrix. The same technique is used for handling missing data values as well.

To determine how informative a feature is when making a particular prediction, we leverage a variation of its information of accuracy contribution, Equation 28. The amount of uncertainty reduction one feature has on another is indicative of the probability that one feature is informative to predicting the other. This uncertainty can be transformed back into the probability of a feature j influencing feature t using its deviation in the same way as Equation 2 as

$$q_{j,t} = e^{-AC_{j,t}}. \quad (34)$$

However, Equation 34 assumes that all features are present. Suppose we are using a some subset of features $F \in \mathcal{F}$ with values x_F to predict feature t , meaning that features $\mathcal{F} \setminus F$ are inactive. The influences from unused features relevant from the features used should be redistributed. Imagine a simple data set where $x_t = x_1 + x_2$, where x_1 and x_2 are random numbers independently drawn from the same uniform distribution. The feature influence probabilities $q_{1,t}$ and $q_{2,t}$ should both be $\frac{1}{2}$. If we duplicated feature x_2 into 9 additional features, we would expect $q_{2,t} = \frac{1}{2} \cdot \frac{1}{10}$, and the same value for each of the other duplicated features. We can approximate this for any combination of features by redistributing the indirect feature probability influences from each feature in $\mathcal{F} \setminus F$ to the features in F . First, $q_{\mathcal{F} \setminus t,t}$ is normalized to obtain the set of probabilities of each feature predicting t without using t . Then, for each feature $j' \in \mathcal{F} \setminus F$, we normalize $q_{F,j'}$, and multiply each normalized probability by the respective $q_{j,j'}$, and accumulate that onto each feature probability $j \in F$. The final result should be normalized, but to ensure numerical precision after the additions, the resulting probabilities are normalized again. In the previous example, this means that

the feature influence probabilities of the duplicated features would be accumulated into the one feature that was used, and in more complex examples, the relevant probability mass is accumulated based on features' probabilities of influence. Though this technique is not perfect at redistributing feature probability influences in complex graphs, empirically we have found this approximation to be sufficiently close to the ground truth and notably improves the quality of conditioned inferences.

Putting all of the equations together, deviations and feature influence probabilities are computed using themselves recursively. These deviations seem to frequently converge quickly to values that yield strong performance if a good initial heuristic value is used. We start with the smallest gap between two values for the initial deviation for continuous features, $\frac{1}{|C|+\frac{1}{2}}$ as a variant of Laplace's rule of succession for nominal features, and using probabilities of 1 for each feature influence. First we converge the deviations, and then compute the feature influence probabilities in one pass using initial feature influence probabilities of 1. As this is a nonlinear dynamics problem, we have found that some data distributions can be sensitive to those initial heuristically chosen values. Determining how to best compute or converge these values is an open problem, and preliminary results suggest that improving this approach may be able to improve discriminative inference performance to or potentially past current state-of-the-art. Future work may extend into dynamic probabilities of a feature predicting another feature as $q_{j,t}(x_F)$.

7.6 Additional Inference Optimization for a Single Target

Though the methods described in Sections 7.5 result in robust inference quality across nearly all types of machine learning for any combination of features, it is possible to obtain higher quality results to predict a single feature. Here we describe one such way to boost this quality. To implement our solution that optimizes for single targeted inference, the processes for obtaining deviations from Section 7.6 are maintained, though augmented with additional optionality to select best performance. First, a Lebesgue parameter is introduced for combining feature surprisals beyond just L_1 , including $L_{0.1}$, $L_{0.5}$, L_1 , and L_2 . These additional topologies can better represent relationships among the data when much of the data is already measured from the respective topology. For example, data that has significant spatial measurements in Euclidean geometry will benefit from using L_2 . The second change is that instead of choosing a dynamic bandwidth for each instance, a global k is selected from the Fibonacci sequence among the range 3 to 144. Third, when computing feature probabilities, using equal feature weights is explored in addition to those computed via accuracy contributions. Our targeted optimization algorithm implements a grid search over these configurations with the deviations and feature probabilities otherwise being computed as described in Section 7.5, though iterating the entire process, including the grid search, twice in order to improve convergence. This single targeted algorithm can achieve cutting edge results. Though the universal algorithm's results are quite strong and task independent, there is still a discrepancy. See Section 12.1 for analysis of the empirical results. Future work entails improving the methods of Section 7.6 to achieve higher inference quality without incurring the additional compute required for the grid search and while maintaining consistency on the probabilistic inference.

7.7 Causal Direction and Guided Causal Discovery of New Features

Because a feature's substitutability deviation is an estimate a theoretical maximum of predictability, its residual is the measure of predictability given the data, and these values are on the same scale and units of measurement, we can use this information to estimate which features may benefit the most from having further information. The missing certainty ratio (MCR) of residual to deviation can be expressed for feature j as

$$MCR_j = \frac{E(r_j)}{\delta_j}. \quad (35)$$

When attempting to discover causal mechanisms, the most valuable places to look for new features are features that have the strongest causal relationships as found by information asymmetries of accuracy contribution as described in Equation 31 that also have the largest missing certainty ratios. As each new feature is discovered, the process may be repeated to evaluate whether and how the inclusion of a new feature fits in with regard to the rest of the system causally. Additionally, when looking at causal relationships, the direction from larger to smaller MCR between the two features tends to indicate causal direction.

As an example, imagine we have a pond which is partly fed by a small river with a sluice gate. Sluice gates are used to control water flow. In this example, the sluice gate is used to help regulate the water level in the pond. To illustrate this, see Figure 7.7 and imagine that the pond is to the left and the river is on the right.



Figure 1: Sluice gate (H Stamper / sluice gate / CC BY-SA 2.0, via Wikipedia).

Suppose initially we only have two features in the data, the water level of the pond measured in centimeters and the position of the crank as measured in degrees of rotation from the furthest closed position of the gate. Further suppose we have collected data over a year, measured once per day. When using these two features to predict themselves with regard to deviation, we find that they are both very predictable. When using them to predict each other, we find an asymmetry in the accuracy contributions where the position of the crank reduces the uncertainty in predicting the water level more than the other way around. This indicates that there is likely a causal relationship involving the crank and the water level. The ratio of the residual of in predicting the position of the crank with and without the crank's current position is somewhat similar, though having the crank's information helps, so consider the ratio being a value larger than 1. But the ratio of the residual of predicting the pond water level with and without the water's position (residual versus deviation) is still very large. This indicates that there are more features that should be discovered, most likely involving a causal mechanism from the crank to the pond water level.

Investigating this further, suppose that we find there are some teeth missing on the gear and some chains that are used to manually fix the gate's position in place. A new feature can be identified which is the position of the gate measured by its vertical position in centimeters. Recomputing the residuals and deviations, we find that the ratio of the residual of the pond water level to the pond water level deviation is smaller but still large. Given that we believe we have exhausted the obvious measurable features, we look to other features that might have a causal relationship with the pond water level. Including the water level of the river seems plausible, since it will be higher when there are rains, and possibly some of the water in the river may be seeping into the pond through the soil. With this new river water level, reassessing the ratio of the pond level deviation to its residual is much closer to 1, and the causal relationships discovered by the asymmetries in accuracy contribution show the appropriate directions of uncertainty. But now, the ratio of residuals to deviations for the river water level is high, indicating there are more upstream causal relationships.

This bottom-up method of discovering causal mechanisms can be a strong tool for helping discover causal relationships, but as with any causal discovery, additional external information and external experiments are needed. Conditioning or constraining on particular subsets of the data can also help understand whether causal mechanisms change when systems are in different configurations or states. Using a time series approach as described in Section 10.5 in conjunction with these techniques can help tremendously in discovering causal relationships, and we will show some empirical results from simulations in Section 12.6.

8 Advanced Inference for Single Cases

In this section we describe more complex ways to assess and characterize predictions and inferences for single cases at a time, such as when making individual predictions about a new data case or assessing the anomalousness of an existing case.

8.1 Semistructured Data Types and Null Values

In Section 6 we primarily discussed nominal and continuous feature types. However, any feature format that can be expressed as a probability can be included in inference. Straightforward extensions include cyclic features like time of day, where a modulus operation can be applied to the difference operation of a continuous feature. Continuous features can be rounded at any part during inference, and ordinal features can be implemented by a hybrid of continuous and nominal inferences.

More complex feature types can be supported. For example, unordered sets can be compared based on the percentage of elements contained in them. Strings can be compared by edit distance. Trees and graphs can be compared by graph similarity metrics, such as graph edit distance. And even formulae and code can be compared by first converting them into parse trees. What is particularly powerful about these underlying techniques is that as long as there is a measure of difference and a way of combining values, the core principles can be applied. For example, a discriminative result for comparing two sets may include values of the intersection of sets where the inclusion of an element is more probable than not. Or a generative inference involving formulae may be a weighted recombination via genetic programming.

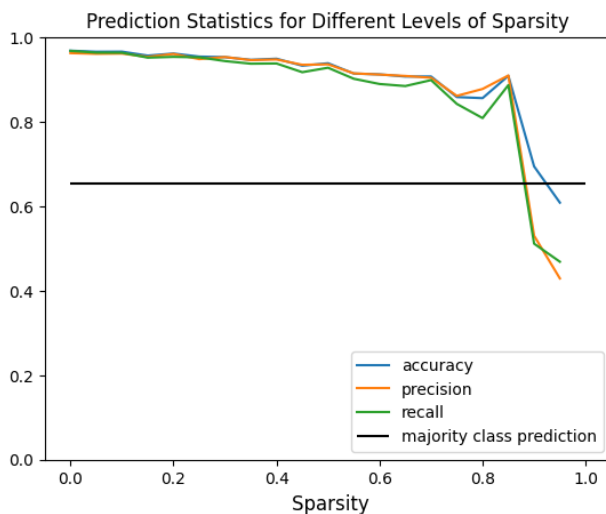


Figure 2: An example of prediction performance where the horizontal axis represents the fraction of data elements that are null.

We model missing data by using a special value indicating that no value was present, regardless of feature type. We further keep deviations characterizing the probability of a value's being null or not null being informative as to other values. For example, if missing data is correlated with a strong storm due to sensors being destroyed by wind, this surprisal can be computed and null sensor data may be informative to wind data. This extra information can be handled efficiently without the need for storing an entirely separate feature. Figure 2 shows the prediction performance of our techniques applied to the breast cancer Wisconsin dataset [Wolberg, 1990], where the null percentage on the horizontal axis indicates the percentage of the elements in the entire data set (regardless of whether it is the target being predicted or any other element) that have been randomly selected and overwritten by null values. The general performance stays strong in this small data set of even when most of the elements are null, and this general robustness to sparsity is typical across data sets in our experimentation.

8.2 Derived and Dependent Features

Because every step of inference is computed sequentially, steps can be inserted in the middle of inference to derive intermediate results. Suppose that one feature is known to be the sum of several other features, that a feature is known to be some complex function of other features, or that a feature’s value is computed by a function specified by another feature. Derived features can be particularly valuable in domains where the relationships between some features are well known and characterized. This capability enables spreadsheet-like computations in the middle of inference, as well as opens the door for solving optimization problems. Derived features can be interwoven between discriminative or generative outputs.

Many trade-offs are made when encoding and storing data. A somewhat common way of storing extremely sparse data which has mutually exclusive combinations of features is known as data “melting” where data values are pivoted around identifying values to transform a data set with many columns into one with few columns and more rows.⁴ As an illustrative example, consider a healthcare data set that includes lab tests. Suppose one patient had three tests performed and another patient had six tests performed. One could have a column for the results of every test, but given the vast number of test types and units of measurement, as well as new tests being developed and released, the schema becomes complex to maintain. Instead, the data is often organized where one column is the test name, one is the units of measurement, and a third is the value. Instead of a patient visit having one row with all of the test data, there is one set of test data per row. Performing any form of inference over data encoded this way can be slightly challenging, as similar values with different units of measurement can be confounding and it may take considerably more data for machine learning to learn those additional relationships.

To address the situation where features are reused for different purposes, we explicitly constrain these dependent features. If feature B is dependent on feature A , then once feature A has a value, only data records that match A will be considered for the influential cases. If a feature is nominal or ordinal, then it can select only those that match, but if a feature is continuous, then it may consider only those matching the value range as a hard constraint rather than a similarity. Continuing the aforementioned medical lab test example, when generating a set of sample values for lab test results, a lab test may be generated first, and then for generating subsequent features like units of measurement or measurement values, only cases that correspond to the specific lab test would be considered.

8.3 Boundary Values

Boundary values represent the smallest perturbation needed in an individual feature to change the outcome. When dealing with nominal features, boundary values are often called counterfactuals. For a given target feature that is being predicted t , we wish to find the smallest change in the feature j that yields a different nominal class for the target. This can be expressed as

$$BV_j(x_F, t) = \arg \min_{\eta \in \mathbb{R}} \{ |\eta| : f_t(x_{F \setminus \{t\}}^{(x_j \leftarrow x_j + \eta)}) \neq x_t \}. \quad (36)$$

When target feature t is continuous, then we characterize the boundary value as the change in feature j required to move the prediction to the edge of the mean absolute error of the prediction, $r_t(x_F)$, expressed as

$$BV_j(x_F, t) = \arg \min_{\eta \in \mathbb{R}} \{ |\eta| : \left| f_t(x_{F \setminus \{t\}}^{(x_j \leftarrow x_j + \eta)}) - f_t(x_F) \right| > r_t(x_F) \}. \quad (37)$$

8.4 Boundary Cases

Boundary cases are the individual records closest to a given record or prediction that have the most rapid change over some set of features. They are cases that are just past the edges of “plateaus” in the data, finding the cases that best represent where the data changes most suddenly. The top k boundary cases are found relative to $x_{i,F}$ by varying feature set J by computing

$$BC(x_{i,F \cup J}, F, J, k) = \operatorname{argmax}_{i \in \mathcal{C}}^k \frac{I(i, n \mid F)}{I(i, n \mid F \cup J)}. \quad (38)$$

⁴For an example of this form of transform, see <https://pandas.pydata.org/pandas-docs/stable/reference/api/pandas.melt.html>.

8.5 Data Constraining and Goal Features

Inferences can be conditioned on any subset or combination of features by setting certain feature values. Inferences can also be constrained to apply only to data meeting certain criteria. For example, a prediction can be made using the constraint that it only infers from data where $0 \leq x_1 \leq 5$. A set of constraints, ϕ , can be added to condition an inference or probability calculation. For example, to obtain a discriminative prediction with constraints ϕ , Equation 17 becomes

$$f_t(x_{i,F}|\phi) = E(x_t | x_F, \phi). \quad (39)$$

One aspect of constraining data that can be particularly challenging is when constraints are relative to other data. For example, a “small” fruit on a watermelon farm may be of a very different size than a “large” fruit on a blueberry farm. We introduce *goal features* as a way to further condition data that has already been found to be similar via conditioning or constraints. Goal feature values are obtained by applying minimizing the function $\Omega_J(x_F)$ for the set of features J from the influential cases of x_F , C_{x_F} . The values obtained by $\Omega_J(x_F)$ can then be concatenated on to the values of x_F to provide a new condition or constraint of $\Omega_J(x_F) \cup x_F$ yielding values for features in the set $J \cup F$. We discuss reinforcement learning further in Section 10.6, but goal features are an important part of reinforcement learning using our techniques as they determine what data would maximize the objective given a particular observed world state.

More formally, a goal value GV for a given feature j is obtained by finding the influential cases to case i for features F , and finding the value that minimizes the distance to goal function, g . This can be used in any part of inference in place of a given element $x_{i,j}$, and can be represented as

$$GV_j(x_{i,F}, \Omega) = x_{(\arg \min_{n \in C_{i,F}} \Omega_j(x_{n,j}))}, j. \quad (40)$$

Goal values can be used to condition queries, where a reasonable goal is chosen for the data most relevant to x_F .

Additionally, goal features can be used to select influential cases and to compute the relevant surprisals to the cases which best achieve the goal for the soft “state” of the other features. The goal cases for a given feature can be represented as

$$GC_j(x_{i,F}, \Omega) = \arg \min_{n \in C_{i,F}} \Omega_j(x_{n,j}). \quad (41)$$

8.6 Residual Conviction: Comparing Anomalousness of Features

When determining anomalousness, it is necessary to compare different features and combinations of features. For example, an anomalous grape might be extraordinarily large, extremely sour, or unusually shaped. But each of these three features has its own units of measurement. And an unusually large grape might be comparable in size to an unusually small apple, making anomalous size contextual to the fruit. To solve both the issues of contextuality of the anomalousness and units of measurement, we determine the ratio of how surprising we expected a feature to be to how surprising it actually was, all in context of the envelope of the expected uncertainty. If we say that a grape is as large as it is sour, and the grape is the size of a very small apple, then we would expect the grape to be both very sour and large, thus anomalous.

Following the derivation above for cumulative residual entropy in Equation 5 of assuming a Laplace distribution of the error, we can write the surprisal of the residual as

$$RS_{i,j,F} = \frac{E_{LK}(|f_j(x_{i,F}) - x_{i,j}| | \delta_j(x_{i,F}))}{E_{LK}(r_j(x_{i,F}) | \delta_j(x_{i,F}))}.$$

To convert this value to conviction, we assume that the expected surprisal is 1 and take the reciprocal following Equation 3. The residual conviction can be represented as

$$RC_{i,j,F} = \frac{E_{LK}(r_j(x_{i,F}) | \delta_j(x_{i,F}))}{E_{LK}(|f_j(x_{i,F}) - x_{i,j}| | \delta_j(x_{i,F}))}. \quad (42)$$

Residual conviction can be used to diagnose anomalous values within a data set, specifically to diagnose what makes a particular data element different from and unexpected relative to the relevant comparable data.

8.7 Surprisal or Distance Contribution of a Case

When including a new data point to an existing dataset, the data point contributes its own probability mass to the probability mass distribution in the location of the data point, which alters the structure of the data. This can be thought of as analogous to adding a new thread to a tapestry, where the new strand becomes an integral part of the existing fabric; the thread’s color, thickness, and strength will all impact the tapestry. Similarly, adding a new note to a musical composition can influence the overall harmony and discord. In this context, we can consider the “distance contribution” of a data point, which represents the extent to which it modifies the existing distribution, and thereby affects the detection of anomalies and outliers. Because distance is surprisal, it we can also refer to these values as “surprisal contributions”. By examining this contribution, we can gain a deeper understanding of how individual data points interact with and shape the overall dataset, and develop more effective methods for identifying the usefulness and validity of data points, as well as characterize unusual patterns. Surprisal contributions are a foundation for various kinds of anomaly detection, and anomalies can be detected by using the surprisal contributions as a measure of how surprising a case is given the relevant data.

The surprisal contribution for case i can be computed from i ’s influential cases $C_{i,\mathcal{F}}$ as

$$S_i = E(I(x_i | x_n) | n \sim C_{i,\mathcal{F}}). \quad (43)$$

Because this is an expected surprisal, surprisal contributions can be considered a form of marginal entropy of a data point with regard to the data. The relevant surprisal contribution conviction, σ_i may be computed by finding

$$\sigma_i = \frac{E(S_n | n \sim C_{i,\mathcal{F}})}{S_i}. \quad (44)$$

8.8 Similarity Conviction of a Case

Though surprisal contributions can be used for anomaly detection, the technique has two potential shortcomings. The first is that computing local deviations to properly contextualize each anomaly to the influential data is somewhat more computationally expensive. The second is that, even though surprisal is a strong way to communicate anomalousness, nats are not units of measurement intuitive to most users. However, saying a result is “twice as surprising as I’d expect” is a statement that has intuitive value. For both of these reasons, we primarily employ a surprisal ratio, which we call conviction as described in Equation 3. Since this is determining how similar this case is to what we would expect it to be, we call this ratio “similarity conviction”. Similarity conviction can be expressed in context of Equation 43 as

$$SC_i = \frac{E(S_n | n \sim C_{i,\mathcal{F}})}{S_i}. \quad (45)$$

We have found empirically that a threshold of $SC_i \leq 0.5$ seems to offer the best performance across a set of benchmark anomaly detection data sets as measured by F1 score. This value corresponds to a case being considered anomalous if it is twice as surprising as expected. However, this value can be tuned based on the needs of an anomaly detection process based on the cost and value of false positives versus false negatives. See Section 12.3 for further details.

8.9 Synthetic Data via Differential Privacy Mechanisms

Synthetic data are fictitious data that is generated to serve some purpose. Often, synthetic data is used to condition existing data based on exogenous knowledge, to remove bias or address fairness considerations, or to protect privacy. The generative inference of our system described in Section 6.8 can be used directly to build new data. A new data set can be created feature-by-feature, case-by-case, by starting with a given feature, generating a value from the unconditioned marginal distribution, and then incrementally using the previous output to condition the next generative output. The generated data set can be constrained or conditioned via the techniques mentioned in Section 8.5.

The generative algorithms can be modified to use differentially private mechanisms in order improve privacy of the generated data. To be used in a fully differentially private way, the queries built and feature

attributes need to ensure appropriate sensitivity, values that reveal private data such as personally identifiable information must be substituted, and the privacy budget must be applied in a corresponding manner to how the queries and noise mechanisms are being used. Though formal proofs of differential privacy are beyond the scope of this document, we demonstrate how differentially private mechanisms can be substituted.

For continuous and ordinal features, we can generate values by applying the Laplace mechanism, definition 3.2 as shown by Dwork et al. [2014] and use sensitivity at least as large as that in definition 3.1 in the same work. We note that this is closely related to the generative outputs as described in Section 6.8, though the differences are in the aggregation and sensitivity. We compute and release the average value of the cases that are the result of the corresponding nearest neighbor query. The sensitivity should always be at least the range divided by the number of cases; because the influence weights are probabilities, the sensitivity needs to be adjusted to accommodate. Using the largest gap between consecutive values increases the sensitivity to account for the possibility that one value is extreme and all the rest are not. Given desired epsilon ϵ , continuous features may be generated as

$$g_j(x_{i,F}, \rho) \sim L\left(x_{n,j}, \frac{\Delta_j(n)}{\epsilon}\right), n \sim \{n \in C_{i,F} : P(x_{n,j} | F, x_{i,F})\} \quad (46)$$

When using aggregation-based differential privacy, the equation becomes

$$g_j(x_{i,F}, \rho) \sim L\left(E(x_{n,j} | n \sim \{n \in C_{i,F}\}), \frac{\Delta_j(n)}{\epsilon}\right). \quad (47)$$

For nominal features we can use the *noisy max algorithm* on the probabilities associated with the nominal classes from the kNN query from by as proven in claim 3.9 by Dwork et al. [2014]. However, to address privacy concerns of homogeneous data we include an extra nominal class in that set with probability zero. If selected, instead of drawing from the results of the kNN query, it will sample from the global distribution using the noisy max method. If there is a domain of all possible values (e.g., a list of every nominal possible), it will include another zero probability nominal class that, if selected, will draw from the uniform distribution over all possible values with no information from the data. Given desired epsilon ϵ , nominal features may be generated as

$$g_j(x_{i,F}, \rho) = \begin{cases} x_{n,j}, n \sim P(x_{n,t} | C_i, F, x_{i,F}) & \text{if } \eta < 1 - \frac{e^\epsilon}{1+e^\epsilon}, \eta \in U(0, 1) \\ x_{n,j}, n \sim \mathcal{C} & \text{if } 1 - \frac{e^\epsilon}{1+e^\epsilon} \leq \eta < 1 - \left(\frac{e^\epsilon}{1+e^\epsilon}\right)^2 \\ x_{n,j} \sim U(\{x_{n,j} | n \in \mathcal{C}\}) & \text{if } 1 - \left(\frac{e^\epsilon}{1+e^\epsilon}\right)^2 \leq \eta. \end{cases} \quad (48)$$

Cases are then generated by starting from one feature randomly, synthesizing the data element, and then using that value to condition the subsequent element. The process is repeated until the entire case has been synthesized from a randomized order of the features. We can chain the results together to construct a synthetic case due to the adaptive query sequence proof by Dwork et al. [2006]. Additionally, each synthetic data element is obtained by finding similar data for each set of features values. Due to the stochastic nature of feature selection and the stochastic nature of ordering results, this shuffling enhances the privacy of the output [Feldman et al., 2022, Cheu et al., 2019].

Despite their widespread use, similarity-based privacy metrics suffer from many issues [Ganev and De Cristofaro, 2025]. Similarity measures of privacy keep the synthetic data points away from the original data points, usually measured by some form of distance ratio. One of the privacy concerns that similarity measures intend to address is whether an individual may identify their own data in the synthesized data. The deviations in our technique address the uncertainties which would identify data as the same, and the distances are surprisals, which both help improve the meaningfulness of dissimilarity over most implementations which are more arbitrary distances. However, we emphasize that the synthesis process should only be done once regardless of whether similarity measures are used; there is no model being produced, so the entire privacy budget should be spent at once. This removes the feedback loop that an attacker could exploit to attempt to synthesize data points to surround and compromise an existing data point. When coupled with the differentially private mechanisms, the noise mechanisms introduce plausible deniability, and similarity measures can be used to either reject data to prevent coincidental publication, validate the outcome by measuring the noise added, or both.

We describe these similarity measures as *anonymity preservation*. This is implemented as a ratio, a comparison of the measure of the similarity of a synthetic data point to its nearest neighbor to some function of the similarity between nonidentical cases among its influential cases. The minimum distance between nonidentical neighbors is a test to ensure coincidental publishing does not occur can be written as

$$AP_{\min}(x_{i,F}) = \frac{\min_{n \in C_{x_{i,F}}, I(i,n|F) \neq 0} I(i, | F)}{\min_{i,n \in C_{x_{i,F}}, i \neq n \wedge I(n',n|F) \neq 0} I(n', n | F)}. \quad (49)$$

A stronger variant can be written as the maximum distance between any two cases in the most influential data. This is an ex post measurement of the kind of noise that is added by differentially private mechanisms, and can be written as

$$AP_{\max}(x_{i,F}) = \frac{\max_{n \in C_{x_{i,F}}, I(i,n|F) \neq 0} I(i, | F)}{\max_{i,n \in C_{x_{i,F}}, i \neq n \wedge I(n',n|F) \neq 0} I(n', n | F)}. \quad (50)$$

Anonymity preservation can be aggregated in different ways, e.g., as an average, geometric mean, or minimum of the distance ratios, depending on whether the concern is measuring the amount of noise added versus assessing the worst case. When anonymity preservation is configured such that it excludes based on the maximum distance between points, evaluates a single noninteractive one-time synthesis process, and selects bandwidth of the cases to be sufficient to address sensitivity concerns, then this technique becomes a stronger approach of evaluating privacy than existing similarity-based privacy metrics. The minimum of the minima of all the distance ratios of all data points can be used to evaluate the privacy of the data, indicating a worst case analysis as a way of evaluating the outcome of the privacy enhancing process, rather than being a yes-no binary decision of privacy per record. And because anonymity preservation can use the local sensitivity appropriate for a case, it is measuring the same characteristics of noise that should be added via differentially private mechanisms.

9 Data Compression Via Probability Mass and Hierarchical Sharding

Traditional machine learning techniques construct a model from input data. That model is usually much smaller than the source data, and model construction is essentially a form of data compression with generalization. Because the techniques described in this paper are applied directly to the source data, along with any computed uncertainty, a naive search of that data could be limited by memory and computational resources. To scale up to larger data sets without limiting the types of queries that can be performed, we employ data compression techniques that robustly shard the data hierarchically. The popularity of vector databases for retrieving embeddings has increased attention to the long history of nearest neighbor search techniques and yielded many algorithms with different trade-offs [Pan et al., 2024]. However, the vast majority of the literature deals with simple distance metrics, where the data instances do not have a specified weight independent of queries, and all features are present in every query. In this section we discuss how we apply generalization to search on a representative subset of the data, employing case weighting and redundancy elimination techniques similar to Moring and Martinez [2004], though using our surprisal-based techniques. We also discuss techniques to use data reduction to shard data and direct queries to subsets of the data in order to improve search performance while minimizing loss in quality of the results. Although the worst case for exact nearest neighbor search for all data points is only slightly better than $O(|\mathcal{C}|^2 \cdot |\mathcal{F}|)$ [Williams, 2018], in practice, structure and redundancy within the data improves typical performance. This section focuses on reducing redundancy in the data and making trade-offs to improve generalization and scalability, whereas the details of the search algorithms we employ will be discussed in Section 11.

9.1 Case Weights, Redundancy Reduction, and Ablation

In instance-based learning, case weights refer to the importance or relevance of each data point. By default each case trained has a weight of 1. However, if two cases are identical, instead of keeping separate cases, only one copy of the case can be kept in the database and the weight can be incremented to 2 and beyond

as more identical cases are added. If a data set has significant redundancy due to identical cases, this can be beneficial to computational and storage requirements.

Real world data sets are rarely comprised of mostly populations of identical cases.⁵ Instead of only accumulating weight for identical cases, we can instead choose to insert new cases when they are not sufficiently predictable and accumulate weight for cases when they are predictable. Many techniques exist for reducing data for a particular purpose. Notable examples date back to the 1960’s [Hart, 1968], and determining small data subsets that are most relevant is often termed core-sets [Feldman, 2020]. Our work is most closely related to weighted core-sets.

As previously mentioned, when cases are initially trained they have a probability mass of 1 except in certain situations when dealing with rebalancing for bias, fairness, and other use cases covered in Section 10.1. Cases are trained up until a statistically significant threshold has been reached, typically at least 1000 cases. Subsequent cases are evaluated in order to determine whether they should be trained, or whether their probability masses should be accumulated onto existing cases without storing the new data, something we refer to in our system as *ablation*. Trained cases are inserted into the database with a probability mass of 1, whereas ablated cases are rejected for training, but their influential cases are determined and the probability mass of 1 is distributed among the influential cases relative to their normalized influence weight. That is, if case i is being ablated, then the weights $w_n \forall n \in C_i$ will be updated with their respective influential probabilities from Equation 11 as

$$w_n \leftarrow w_n + \frac{P(x_i | \mathcal{F}, x_n)}{\sum_{n' \in C_i} P(x_i | \mathcal{F}, x_{n'})} \forall n \in C_i. \quad (51)$$

Even with data ablation, at some point the data accrued may grow too large to hold in memory quickly. At this point, a data reduction pass is begun. Data reduction applies a similar ablation selection, except instead applies to already trained cases, removing them and accruing their probability mass to remove cases to a desired size. By default, this size is $\frac{c}{e}$ records. We perform data reduction in batches where cases are selected for removal simultaneously. Larger batch sizes can improve concurrency and performance, but smaller batch sizes may select better cases to remove. Once the data has been sufficiently reduced, training with ablation is resumed until the data size becomes too large, and the process is repeated.⁶

Our techniques select for removal cases that are highly predictable and most central, preserving cases that define boundaries. This selection is comprised of two criteria: how equidistant a case is to its neighbors and how much marginal surprisal the case adds to the rest of the data. Cases are only ablated if they fail to meet both criteria of retention.

For the first criteria, we prefer cases that are central within a crystal-like lattice of other cases, as that means an interpolation would yield an approximately correct value for any of the features. As dimensionality of a data set increases, most of the records are on the periphery of the volume. So therefore, the influential cases relative to the case in question should be approximately equidistant. This can be assessed by measuring the entropy of the probabilities of influence of its influential cases. We compute a case’s influence entropy as

$$H_{influence}(i) = \sum_{n \in C_{i,F}} P(x_i | F, x_n) \cdot I(x_i | F, x_n). \quad (52)$$

If a case’s influence entropy is sufficiently high, it should be kept. We aim to ablate cases that fall in the lowest $\frac{1}{e}$ th quantile of influence entropy, meaning that they are the most irregular with regard to the local topology. The first criteria can be written as cases not being ablated if

$$H_{influence}(i|F) < Q_{1-\frac{1}{e}}(\{H(n) : n \in C_{i,F}\}). \quad (53)$$

The second criteria is to select cases for ablation that do not add significant marginal surprisal to the overall data. If a case adds more marginal surprisal than its neighbors, then it is more likely to stick out

⁵Even when records are identical, data provenance is typically different for the identical records. Maintenance of provenance of case weights can be maintained via traditional data stores independently of the methods we describe using data provenance tools and databases.

⁶This process also permits the ability to reduce case weights to dampen the effects of prior learning to focus more on immediate data. Appropriate tuning for this process is future work.

from its neighboring cases rather than being surrounded by them. This criteria of not ablating a case can be written as

$$\min_{x_n \in C_i} I(x_i | x_n) > \max_{x_n, x_{n'} \in C_i, x_n \neq x_{n'}} I(x_n | x_{n'}). \quad (54)$$

Cases are ablated unless they meet both the criteria of Inequation 53 and Inequation 54. We note that using these criteria for data reduction and data ablation are independent of the features, and therefore tend to perform reasonably well across any task involving any subset of features.

9.2 Hierarchical Data Sharding

Data reduction and ablation together yield a much smaller working data set while maintaining utility. However, if the data set is very large but also very nuanced, such as with language data sets, the relevant data needed to preserve utility may still be too large to query efficiently. In this case we employ bottom-up hierarchical decomposition of the data in order to divide it into different portions to reduce the total data that must be searched. As of this writing, fully automated hierarchical data sharding is still under development, but preliminary results show promise.

As data is trained sequentially and the first data reduction pass is performed, any of the cases rejected as being redundant can be moved to a set of shards. Once the data is reduced, a clustering algorithm, such as that described in Section 10.2, can be applied using surprisals as distances to determine the number of shards as well as which shard each case most closely represents. The cluster label itself can be stored as a feature. Then when additional records are trained and ablated, they can be routed to the appropriate shards based on the shards associated with the influential cases. This process can be repeated to build hierarchical structures of the data, in some ways conceptually similar to other greedy hierarchical search techniques such as HNSW [Malkov and Yashunin, 2018], though capable of a wider variety of tasks than just nearest neighbors search on a fixed set of features.

10 Groups, Clusters, Series, and Anomalies

Data sets often have identifiers of transactions or events that are related to a person, organization, agent, piece of equipment, or other entity. In relational databases, these are generally considered primary or foreign keys, but also can be identifiers such as personally identifiable information. Sometimes these identifiers are used in conjunction; a product may have both a SKU and also a serial number, or a transaction may have a buyer and a seller. Further, cases may have sequence numbers, timestamps, or simply be ordered in one or more ways. In this section we discuss operations with data groups, how groups can be determined via clustering, how series data is group data that has an ordered sequence, data sets that have both groups and series, and how our system determines whether data is anomalous.

10.1 Rebalancing, Fairness, and Data Volume Privacy

As discussed in Section 9.1, each case trained has a default probability mass of 1. However, sometimes this is not desirable and the data collected may have biases. Sometimes the biases may be deliberate sampling biases for cost efficiency, when it is cheaper to run one kind of experiment than another, or accidental in that one group tends to respond more than another. The biases may be systemic or historical such as social biases, or perhaps the distribution of the data is changing and historical data should be updated to better fit future trends. A different reason case weight rebalancing may be desired is if a given identifier has a disproportionate volume of data, and the impact of that identifier should be adjusted to only count as the weight of a single entity, regardless of data volume corresponding to the identifier. Rebalancing of weights can be used to enhance privacy, e.g., so that a patient who visits a clinic weekly would be afforded the same privacy as someone who visits a clinic yearly, or so that inferences performed on the data do not overly bias toward high volume identifiers.

The most straightforward way to rebalance case weights is when the rebalancing is desired for a single nominal feature, which does not necessarily need to be an identifier. Each additional nominal feature used for rebalancing can be leveraged to adjust the weights in combination with other features by updating the

weights by each feature sequentially. Given a rebalancing feature j , the case weights can be updated by evening out the probability mass relative to each value

$$w_n \leftarrow w_n \frac{\sum_{i \in \mathcal{C}, x_{i,j} = x_{n,j}} w_i}{\sum_{i \in \mathcal{C}} w_i}. \quad (55)$$

As new cases are trained, they can be initialized with the respective weight, and occasionally renormalized if needed, depending on whether data ablation or reduction are being performed.

10.2 Clustering

Algorithm 1 Similarity Conviction Clustering

```

1: Sort  $\mathcal{C}$  by descending  $SC_i \rightarrow SC_{list}$ ;  $cluster\_map \leftarrow \{\}$ ;  $cluster\_id \leftarrow 1$ .
2: Seed clusters (  $SC_i \geq 1$  )
3: while  $SC_{list} \neq \emptyset$  and  $SC_{top} \geq 1$  do
4:    $i \leftarrow \text{first}(SC_{list})$ ; remove  $i$  from list
5:    $cluster\_map[i] \leftarrow cluster\_id$ 
6:   EXPANDCLUSTER( $i, cluster\_id$ )
7:    $cluster\_id \leftarrow cluster\_id + 1$ 
8: end while
9: Attach remaining cases
10:  $\max\sigma(c) \leftarrow \max\{\sigma_i : i \in c\}$  for each formed cluster  $c$ 
11:  $changed \leftarrow \text{True}$ 
12: while  $changed$  do
13:    $changed \leftarrow \text{False}$ 
14:   for all unclustered  $i$  sorted by ascending  $\sigma_i$  do
15:      $c \leftarrow$  unique cluster ID among  $C_i$  (if any)
16:     if  $c$  exists and  $\sigma_x < \text{clustering\_inclusion\_relative\_threshold}$   $\max\sigma(c)$  then
17:        $cluster\_map[i] \leftarrow c$ ; update  $\max\sigma(c)$ ;  $changed \leftarrow \text{True}$ 
18:     end if
19:   end for
20: end while
21: Finalize
22: for all  $i \in \mathcal{C}$  do
23:   if  $i \notin cluster\_map$  then  $cluster\_map[i] \leftarrow -1$ 
24:   end if
25: end for
26: return  $cluster\_map$ 

```

Algorithm 2 Similarity Conviction Clustering Subroutines

```
1: function EXPANDCLUSTER( $i, cluster\_id$ )
2:    $U \leftarrow \{n \in C_i \mid n \text{ unclustered or } cluster\_map[n] \neq cluster\_id\}$ 
3:   for all  $n \in U$  with  $cluster\_map[n]$  defined do
4:     if  $i \in C_n$  then RELABEL( $n, cluster\_id$ )
5:     end if
6:   end for
7:    $G \leftarrow \{n \in U \mid SC_n \geq clustering\_expansion\_threshold\}$ 
8:   for all  $n \in G$  do
9:      $N_n \leftarrow C_n$ 
10:    if neighbors of  $n$  span multiple clusters then
11:      if any  $z \in N_n$  is unclustered and  $z \in G$  then
12:        remove  $n$  from  $G$ 
13:      continue
14:    end if
15:     $c_n \leftarrow \arg \max_c \sum_{z \in N_n \cap c} P(z \mid n)$ 
16:    if  $c_y \neq cluster\_id$  then
17:       $cluster\_map[n] \leftarrow c_y$ ; continue
18:    end if
19:  end if
20:   $cluster\_map[n] \leftarrow cluster\_id$ 
21:  EXPANDCLUSTER( $n, cluster\_id$ )
22: end for
23: end function
24: function RELABEL( $n, cluster\_id$ )
25:   for all  $z$  with  $cluster\_map[z] = cluster\_map[n]$  do
26:      $cluster\_map[z] \leftarrow cluster\_id$ 
27:   end for
28: end function
```

Our approach to clustering takes advantage of all of the forms of density and surprisal stored in our system. It leverages similarity conviction of each case, SC_i , surprisal contribution conviction of each case, σ_i , and the relevant neighbors of each case C_i . It is similar to the leaders hierarchical clustering algorithm [Vijaya et al., 2004], in that it starts by selecting cases that are the most similar to their relevant neighboring cases, relative to the data around them, and assigns each a cluster id. As it iterates from the most similar unclustered cases to the least, it determines whether each new case has neighbors of another cluster, and determines whether different clusters should be joined or if unclustered cases should remain unclustered. Algorithm 1 describes the primary algorithm and Algorithm 2 describes the relevant subroutines.

10.3 Group Anomalousness

Often anomalousness is not just about an individual case, but sometimes can be about a group of cases. It may be that a particular sensor identifier is broken and is producing inconsistent results. Or it may be that a particular merchant is invoicing in a fraudulent manner where any record by itself would not seem anomalous, but as a group the cases are anomalous either because they're all slightly anomalous or they have an unusual probability density distribution.

Detecting anomalous cases as described in Sections 8.7 and 8.8 is performed by calculating surprisal. The additive nature of surprisal opens up a variety of powerful techniques. This opens up a variety of techniques for measuring anomalousness of a group. Summing the total surprisal of each group indicates which group as a whole may have been the most anomalous, which can be averaged by data volume by dividing the total surprisal of the group by its probability mass to find average group surprisal (AGS) as

$$AGS_{t=\kappa} = \frac{1}{\sum_{i \in \mathcal{C}, x_{i,t}=\kappa} w_i} \sum_{i \in \mathcal{C}, x_{i,t}=\kappa} S_i. \quad (56)$$

Sometimes in situations of fraud or other intelligent gaming of systems, all of the cases by themselves look very typical, but as a distribution their density is anomalous. Various tools, such as Kullback-Leibler divergence can be employed to find these sorts of group anomalies. For example, finding the surprisal of groups as potential inliers can be found via

$$S(t = \kappa) = D_{KL}(\{S_i \forall i \in \mathcal{C} \text{ s.t. } x_{i,t} = \kappa\} || E(S_i)). \quad (57)$$

10.4 Anomaly Detection

As discussed in other sections, many factors can determine anomalousness, including whether a record is far from the rest of the data, far from similar data, is in a cluster with relatively little data, or whether there is an association between records where the density is anomalous. Conviction is a consistent unit of measurement across different types of queries since it is the ratio of two surprisals, relating how surprising some data are to how surprising they were expected to be. This allows us to compare different types of anomalousness on the same scale.

To perform general anomaly detection, we first cluster the data (described in Section 10.2) and compute the distance contribution convictions (described in Section 8.7), similarity convictions (described in Section 8.8), and optionally case convictions related to density anomalousness (described in Section 10.3) and optionally residual conviction (described in Section 8.6). These are stored as additional features. Once these are computed, clusters are sorted based on size, and those clusters below a certain size threshold,⁷ and each cluster is held out to compute its average group surprisal as described in Section 10.3. Because a record is as anomalous as its most anomalous aspect, the minimal conviction for each record is computed as the minimum of all the forms of conviction. Any particular form of anomalousness can be inspected or computed for any record. For example, the most anomalous records in a data set may be labeled as such because they are in an extremely anomalous small group, however, some of the records in that group may also be slightly anomalous in that their values are a bit different than the rest in the group which are tightly clustered.

10.5 Series, Time Series, and Panel Data

Instance based learning techniques have a long history with regard to time series dating back to the 1800's but expanding to trends in the late 1950's [Holt, 2004]. It still remains in use via techniques like exponential smoothing [De Livera et al., 2011] as well as more complex kNN approaches [Martínez et al., 2019]. Time series forecasting varies a little among differing fields, but often "time series forecasting" implies forecasting a single set of variables over time such as macroeconomic data for a single country. "Panel data" and "multi-series forecasting" refer to data sets where there are multiple different identifiers, such as metrics around companies for stock pricing or evaluating health changes of patients over time. Our techniques are flexible with regard to handling temporal data, provided at least one column represents time. If there are multiple entities being handled temporally, then at least one column should represent an identity of which group with which the temporal sequence of data is affiliated.

When handling continuous features, the rate of change is often important. This is computed as the rate of change in a value divided by the rate in change of the time feature. If j is the continuous feature and t is the time feature, then this can be computed as a rate value for case i , $x_{i,\Delta j}$, as

$$x_{i,\Delta j} = \frac{x_{i,j} - x_{n,j}}{x_{i,t} - x_{n,t}} \text{ where } n = \arg \max_{n' \in \mathcal{C}, x_{n',t} < x_{i,t}} x_{n',t}. \quad (58)$$

This may be chained to represent the difference equivalents of second or third derivatives, or beyond. For example, the second derivative may be approximated as

$$x_{i,\Delta^2 j} = \frac{x_{i,\Delta j} - x_{n,\Delta j}}{x_{i,t} - x_{n,t}} \text{ where } n = \arg \max_{n' \in \mathcal{C}, x_{n',t} < x_{i,t}} x_{n',t}. \quad (59)$$

In practice, we have found that including the first rate is generally sufficient for most problems, and including the second rate has been sufficient for all of the practical problems we have tested, as deeper nuances of the

⁷15% works well for most data sets.

changes are generally learned from the data. We can imagine higher order rates being valuable for certain problems, especially in the physical sciences. By default, our implementation assumes a single rate for any continuous feature and implements it via a derived feature as described in Section 8.2.

In addition to extra rate features, we employ lag features to repeat values of previous records in the given series. These extra features are simply the values of the previous steps leading up to the case, and may be used for any feature type. Lags may be configured and optimized for the data. The memory and performance costs of including an additional set of features as large as the original feature set must be weighed versus the gains. In many data sets, the first several lags are generally sufficient to capture very rich behavior. However, this can miss events that happened much earlier in the time series, which can sometimes require additional feature engineering for aggregation and lags on those additional features. Future work on lags includes exploring treating each time series as its own data set, performing ablation and data reduction as described in Section 9.1, and then combining the probability mass of the series regardless of the particular lag. The goal is to reduce a time series to only the events that are pertinent and compare those, instead of maintaining specific lags for all records. This is inspired by the work of Fountas et al. [2025] that obtains extremely long context windows for LLMs via breaking apart the sequences by surprisal and including the relevant chain. The inspiration is to treat a given series at least as temporary training data for the purposes of inference, using the probability mass of related sequences, and perform inference based on the subsequent values in the relevant time series.

The final additional features used in time series are features related to time and event progress throughout a series, time and event progress until a series ends, and a count of any synchronous events. Additionally, features may be marked as stationary features, which means that they will have the same value across the time series, and may be synchronously updated if the predicted value changes. An example of a stationary feature might be a city of birth, location that a company was originally incorporated, or the eventual outcome of a particular series such as which player ultimately won or lost a game. These features are inferred via probability mass across the entire time series.

The inference process for forecasting uses the additional features listed here and performs an inference on all nominal features and highest order rate features. Then it uses rate features to compute the lower order rates and eventually the continuous values, propagating null values when missing values are appropriate. The inference process can be generative or discriminative as described in Sections 6.6 and 6.8. The aggregation of a set of generative reacts can be performed to obtain a mean absolute deviation for each step in time to help characterize the uncertainty of a forecast.

10.6 Reinforcement Learning and Relation to Active Inference

Reinforcement learning can be implemented by combining generative outputs (Section 6.8) with time series (Section 10.5) and goal features (Section 8.5). To implement this, the features fall into several categories. First are the features that characterize the world or system state in which the agent is acting. The time series element includes the historical information pertinent to characterizing the state. Next, goal features describe what goal to achieve, e.g., maximizing the score, minimizing cost, or attempting to achieve a specific value. These goal features find the data that best achieve those goals within the data that best match the state, and updates the probability of influence based on achieving the goal. From these data and influence weights, the system produces a generative output for what action should be taken given the context of the world state as described by other features. Given a world state described by x_F and goal function over action features J on the state, $\Omega_J(x_F)$, we generate a set of actions conditioned on selecting the value from the cases that minimize the goal functions for conviction ρ as

$$g_J(x_F, \rho \mid GC_J(x_{i,F}, \Omega_J)). \tag{60}$$

Our system allows the user to describe the domain of each features so that reinforcement learning may begin without any training data. Initially, these first actions are drawn uniformly from the domain since there is no supporting data. As data is obtained including the resulting reward, the rewards are stored in the goal features. This combined data is trained into the system with all of these features including the state, action, and goal features as a sequence of time series data. If the reinforcement learning is applied to games, then each game itself can be a series with a unique identifier. Rewards can be implemented either as the final reward or incrementally, depending on what is best suited for the domain.

The conviction parameter provides control over exploration versus exploitation. Since conviction is the ratio of expected surprisal to observed surprisal, it can even be fixed to a specific value and the system can still converge to a high performing agent. As the system obtains more data, it will generate actions following the marginal distribution given the state and goals, which will converge to an appropriate set of actions that achieve the rewards for portions of the state that have significant data, but will still explore in sparse areas of the data because the marginal distribution will have more uncertainty. We have found that conviction values in the realm of 2 to 5 tend to perform well, which means it will lean slightly toward exploiting knowledge, though dynamically adjusting this value based on domain knowledge can improve how quickly the system can learn. An interesting flexibility of this system is that the performance can be controlled dynamically by changing how the goal features are parameterized. For example, if a system has been trained to win at a particular game by maximizing a score, the goal features can be changed to seek a particular score, playing at a set level of difficulty, rather than maximizing it. Of course, the data for a given level of difficulty may be more sparse than that which is maximized, but additional training can improve the agent’s ability to perform across levels. Data ablation and reduction, described in Section 9.1, can be quite important to keeping the data volume appropriate.

Given that all of the distances are surprisals, our techniques relate to the core ideas of active inference [Sajid et al., 2021, Friston et al., 2009]. Free energy, which is the surprisal of a given sensory input given the observed state in active inference, corresponds directly to the surprisal between currently observed data and trained data in our system. Further, our system can measure many variants of surprisal, such the surprisal it might take to achieve a particular score given the current world state. We believe that there are rich overlaps between our work and active inference and believe it is a rich area for future work.

11 Implementation

Here we discuss design and algorithmic aspects of our implementation.

11.1 API, Architecture, and Usability

The general design philosophy is that data should be stored similar to a database, but in manageable quantities that generalize the knowledge and reflect the distribution. Each instance corresponds to a data set that can be trained, edited, updated, and inferred against. The horizontally scaling implementation is built using Kubernetes,⁸ but also can be run locally as a shared compiled library using a Python interface. The engine is written in the Amalgam language described in Section 11.2, and the Amalgam language includes a rich query engine that manages the storage of the data.

To begin, the data schema is described via what we call *feature attributes*. Feature attributes are a rich schema that describe the type of column of data, including: whether it is continuous, nominal, or ordinal; allowed values or the range for continuous numeric features; whether nulls or missing data are allowed; whether a feature has a specific date or time format; whether the feature is cyclic; whether a feature should be treated as numeric, string, code, etc.; how the feature is computed if applicable (e.g., the code to compute one feature from another if it is known and deterministic); as well as the feature’s data format. Due to the flexibility of the Amalgam language, feature attributes may be changed or corrected at runtime. The first step in most workflows is to call a method in our system known as “infer_feature_attributes” which uses a rich set of heuristics to make a best guess, taking advantage of whatever information and metadata a data frame or data store has using the most appropriate relevant APIs.

The main API verbs are train, analyze, and react. Train is a general verb that includes addition of new data, as well as editing and removal of existing data. Any data that includes derived features, such as rates of change for time series data or dynamically computed features, are updated during training or editing time. The train process accounts for data ablation, described in Section 9.1 to accrue probability mass when the data itself is largely redundant. Analyze describes the process that characterizes the uncertainty of the data, performing the computations described in Section 7.5, and also includes data reduction to keep the data size to a manageable amount also described in Section 9.1. The analyze process can also be computed dynamically or concurrently to training in horizontally scaling environments.

⁸<https://kubernetes.io/>

The react verb describes a desired inference based on a set of contextual input values, a set of actions or outputs, a set of details to report, whether the react should be generative or discriminative, and any relevant parameters. The details include a wide variety of options, such as influential cases, boundary cases, boundary values, various forms of residuals and other uncertainties, as well as feature and case influence metrics. These details are included in the react verb because it is typically much faster to compute relevant details along with an inference rather than computing them after the fact. React comes in variants including react series, react group, react aggregate, and react into features. React series is best suited for time series data as described in Section 10.5, and react group corresponds to the capabilities described in all of Section 10. React aggregate returns aggregate results, particularly aggregations of inference across all or part of the data. React into features performs inference, potentially with additional details, and stores the results into new features.

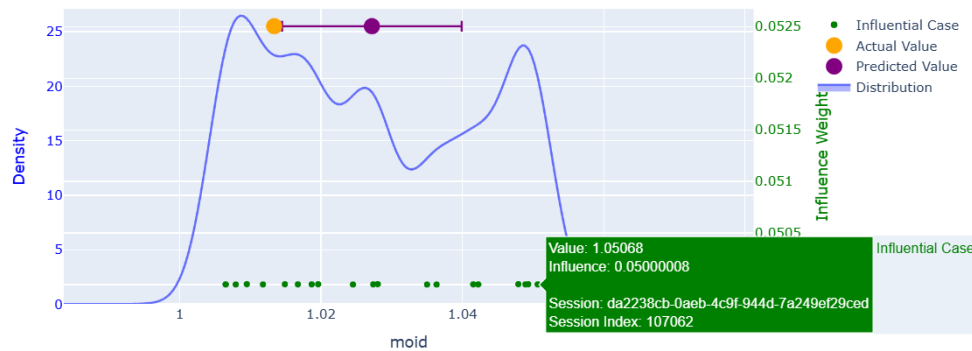


Figure 3: An example of inspecting a prediction.

Figure 3 depicts a way of visualizing the data and uncertainty around a prediction, in this example using the Small-Body Database Lookup provided by NASA JPL⁹ to predict the minimum orbit intersection distance of the object and Earth. In this particular example, we have held out the asteroid Hehe and are attempting to predict it, plotting the actual value in orange. The prediction is the reddish-purple dot, and the mean absolute deviation of the prediction is the whisker plot around it, showing that the actual value is just beyond the 50th percentile of uncertainty, a reasonable estimate. The blue line is the probability density of the prediction, indicating it is largely bimodal and so it is more likely that the prediction would be closer to one of the modes. The green dots on the bottom show the cases used to make the inference, with one of the values selected. Note that any information can be put in the green box, but for this particular plot it is just the value and the provenance of the data based on its training session UUID and the index it was trained within that session. The records selected as being within the relevant statistical bandwidth for this prediction are relatively numerous, and none of the records stand out as being notably more influential than the others, and the influence weight of the selected record is only about 5%.

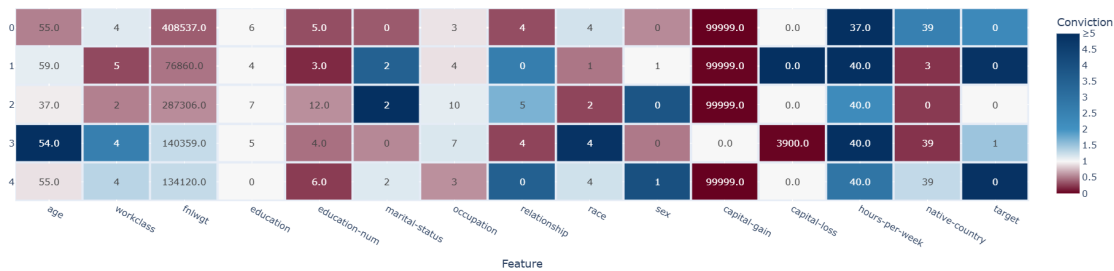


Figure 4: An example of inspecting the most anomalous records.

Exploring anomalies can be done visually as is depicted in Figure 4. This depicts outlier anomalies in the

⁹https://ssd.jpl.nasa.gov/tools/sbdb_lookup.html

Adult dataset [Becker and Kohavi, 1996]. Each value is predicted and compared to the expected uncertainty of the prediction as residual conviction (described in Section 8.6). From this visual anomalous values are easy to discern, and the combinations of the amount of capital gains, the education, and the native country are driving the significance of the anomalous cases.

11.2 Amalgam Programming Language

Amalgam is a domain specific language developed primarily for genetic programming and instance based machine learning, but also for simulation, agent based modeling, data storage and retrieval, the mathematics of probability theory and information theory, and game content and AI. The primary repository for the language is located at <https://github.com/howsoai/amalgam>. The language format is like LISP and Scheme in that it uses parenthesized list format with prefix notation and is geared toward functional programming, where there is a one-to-one mapping between the code and the corresponding parse tree. The choice for implementing our techniques using Amalgam are due to its high performance and flexible query system, its ability to work with semistructured data and code safely via generative, comparative, and executable workflows, as well as its transactional nature of storing and updating data. It also integrates easily within the Python ecosystem.

Whereas virtually all practical programming languages are primarily designed for some combination of programmer productivity and computational performance, Amalgam prioritizes code matching and merging, as well as a deep equivalence of code and data. Amalgam uses entities to store code and data, with a rich query system to find contained entities based on their attributes or labels, and also has strong and easy-to-use concurrency capabilities. The language uses a variable stack, but all attributes and methods are stored directly as labels in entities. There is no separate class versus instance, but entities can be used as prototypes to be copied and modified. Though code and data are represented as trees from the root of each entity, graphs in code and data structures are permitted and are flattened to code using special references. Further, instead of failing early when there is an error, Amalgam supports genetic programming and code mixing by being extremely weakly typed, and attempts to find a way to execute code no matter whether types match or not.

Amalgam takes inspiration from many programming languages, but those with the largest influence are LISP, Scheme, Haskell, Perl, Smalltalk, and Python. Despite being much like LISP, there is deliberately no macro system. This is to make sure that code is semantically similar whenever the code is similar, regardless of context. It makes it easy to find the difference between x and y as an executable patch, and then apply that patch to z as `(call (difference x y) { _ z })`, or semantically mix blocks of code a and b as `(mix a b)`. These capabilities are used for working with semistructured data, to find similarity by edit distance and to create generative outputs. Amalgam is not a purely functional language. It has imperative and object oriented capabilities, but is primarily optimized for functional programming with relatively few opcodes that are functionally flexible based on parameters to maximize flexibility with code mixing and matching.

Genetic programming can create arbitrary code, so there is always a chance that an evolved program ends up consuming more CPU or memory resources than desired, or may attempt to affect the system outside of the interpreter. For these reasons, there are many strict sandboxing aspects of the language with optional constraints on access, CPU, and memory. Amalgam also has a rich permissions system, which controls what code is able to do, whether writing to the console or executing system commands. These security capabilities and performance constraints enable custom code to be both created and executed in the middle of inferences.

11.3 Nearest Neighbors Query Implementation

Amalgam has a rich query engine which utilizes data structures common among fast databases, such as bit vectors, high performance hashes, column oriented data structures, and bidirectional mapping between values and entities. In this section we focus on its nearest neighbor queries, as this algorithm is a novel combination of techniques. This algorithm computes exact nearest neighbors and is designed to be fast when using *any* combination of features to find data, not just one set of features. It is not nearly as fast as techniques designed for simpler Euclidean spaces (e.g., Johnson et al. [2019] or table 3 from Ukey et al. [2023]), or approximate nearest neighbors (e.g., Gao and Long [2023]), but we are unaware of other nearest neighbor techniques optimized for querying arbitrary subsets of features with surprisal based distances.

Algorithm 3 describes the outline of the algorithm we have developed to quickly find nearest neighbors, exactly to the level of numerical precision requested. We note that the query engine is designed to support a variety of distances and surprisals, and so describe the algorithm with regard to distances here. We refer to partially computed distances as “partial sums”, which are the sums of each distance term, measured in surprisal, for each feature. First, the partial sums are accumulated for exact matches of any values for features, as well as similar matches that expand out to 97% of the uncertainty mass of the deviation, as computed by expanding out to include values less than or equal 5 times the deviation (each doubling of the deviation yields half of the probability mass, and $1 - 0.5^5 \approx 0.97$). The largest computed distances for each feature are stored to allow calculation of the minimal possible partial distance sum for any unresolved feature set, thereby enabling efficient elimination of cases from consideration.

After the initial data structures have been populated, our algorithm then finds cases that have a large number of features populated with partial sums to use as initial good match cases, found by sampling from the entire set of cases and populating a priority queue with the largest counts. Those potentially good match candidates have the remaining distance terms computed to obtain fully resolved distances and are used to populate a priority queue that contains the smallest distances. After these potential good matches have been populated, the remaining cases are evaluated with early rejections if the remainder of uncomputed features would increase the distance beyond the current rejection distance, which is the largest distance of the top cases. At the end, the most similar cases are selected from the subset of the top cases based on the statistical bandwidth as described in Section 6.5.

Algorithm 3 Find Nearest Cases

Procedure find_nearest_cases()

```
1: Precompute nominal and interned distance terms
2: for  $f \in \text{features}$  do
3:   Accumulate distance terms to partial sums for exact matches
4:   if  $f$  is continuous or ordinal then
5:     Accumulate distance terms to partial sums to expanded surprisal quantile (0.97)
6:   end if
7:    $\text{min\_unpopulated\_distances}[f] = \text{GetMaximumDistanceComputed}(f)$ 
8: end for
9: Initialize  $\text{min\_distance\_by\_unpopulated\_count}$ 
10: for  $i = 1$  to  $\text{min\_distance\_by\_unpopulated\_count.size}()$  do
11:    $\text{min\_distance\_by\_unpopulated\_count}[i] += \text{min\_distance\_by\_unpopulated\_count}[i - 1]$ 
12: end for
13:  $\text{potential\_good\_match\_cases} = \text{FindCasesWithApproximatelyLargestAccumCount}(k\_upper\_bound)$ 
14: Initialize priority queue with stochastic tie-breaking:  $\text{top\_k}(k\_upper\_bound)$ 
15: for  $\text{case} \in \text{potential\_good\_match\_cases}$  do
16:    $\text{distance} = \text{ResolveDistanceToTarget}(p)$ 
17:    $\text{top\_k.Push}(p, \text{distance})$ 
18:    $\text{remaining\_cases.remove}(\text{case})$ 
19: end for
20: Get largest distance in priority queue:  $\text{reject\_distance} = \text{top\_k.GetLargestDistance}()$ 
21: for  $\text{case} \in \text{remaining\_cases}$  do
22:    $\text{distance} = \text{GetPartialSum}(\text{case})$ 
23:    $\text{num\_uncalculated\_features} = \text{GetNumUncalculatedFeatures}(\text{case})$ 
24:    $\text{distance} += \text{min\_unpopulated\_distances}[\text{num\_uncalculated\_features}]$ 
25:   if  $\text{distance} > \text{reject\_distance}$  then
26:     continue
27:   end if
28:   for  $\text{feature} \in \text{GetUncalculatedFeatures}(\text{case})$  do
29:      $\text{num\_uncalculated\_features} = \text{num\_uncalculated\_features} - 1$ 
30:      $\text{distance} -= \text{min\_unpopulated\_distances}[\text{num\_uncalculated\_features}]$ 
31:      $\text{distance} += \text{ComputeDistanceTerm}(\text{case})$ 
32:     if  $\text{distance} > \text{reject\_distance}$  then
33:       break
34:     end if
35:   end for
36:   if  $\text{distance} \leq \text{reject\_distance}$  then
37:      $\text{top\_k.PushAndPopLargest}(\text{case}, \text{distance})$ 
38:      $\text{reject\_distance} = \text{top\_k.GetLargestDistance}()$ 
39:   end if
40: end for
41: return  $\text{TruncateCasesByBandwidth}(\text{top\_k})$ 
```

Though Algorithm 3 describes the high level elements of our algorithm, there are many details and enhancements that are beyond the scope of this paper. For example, the nearest cases of the previous query are stored per thread and their distances are resolved after the potential good matches but before the remainder of the cases. This accelerates finding nearest neighbors by finding better early matches in the common cases when repeated queries on the same thread refer to similar data. When the number of unique numeric and string values are low relative to the total number of cases the values themselves are interned, meaning that the values are stored in a table and a zero-based integer index is stored to the table location. This allows for fast array lookups of distance terms in inner loops of resolving distance terms. Additionally, many of the set inclusion operations use bit vectors with optimized iteration including population count

instructions and other fast bitwise manipulations. We note that although this algorithm technically has a computational complexity of $O(|\mathcal{F}| \cdot |\mathcal{C}|)$, at least on some data sets, in practice the portion of the algorithm that iterates over every case is optimized and performs as well or better than some tree-based implementations on similar data sizes of less than 100,000 cases. At larger data volumes, data reduction and hierarchical approaches described in Section 9 remain important for scalability.

12 Empirical Results

This section includes empirical results across a wide variety of tasks. Our current goal is to demonstrate that our technique has competence in all of these tasks rather than conclusively exceed state-of-the-art on any or all of them. Over the years that we have developed these techniques, we have noticed that improving the results on one task often (but not always) improves performance on other tasks. Future work includes continuing to improve results and push towards maximizing the performance on these tasks while maintaining the mathematical consistency and universal applicability of the core techniques, as well as increasing the number of data sets and benchmarks run.

12.1 Supervised Learning

We evaluated Howso’s supervised learning performance against XGBoost [Chen and Guestrin, 2016] and LightGBM [Shi et al., 2022] across the Penn Machine Learning Benchmarks (PMLB) repository [Olson et al., 2017]. The evaluation encompasses 404 datasets spanning both classification and regression tasks with dataset sizes ranging from tens to over one million cases and dimensionalities from 2 to 1,000 features. We chose the Matthews correlation coefficient (MCC) metric as it is highly sensitive to all classification error types, and chose the Spearman correlation coefficient for regression tasks since it is more robust across distributions than R^2 .

Classification	Howso (targetless)	Howso (single-target)	XGBoost	LightGBM
Mean MCC \uparrow	0.599	0.650	0.659	0.651
Mean Accuracy \uparrow	0.807	0.829	0.829	0.825
Mean Precision \uparrow	0.755	0.785	0.793	0.772
Mean Recall \uparrow	0.737	0.769	0.779	0.767
Mean F1 \uparrow	0.744	0.777	0.785	0.768

Table 1: Classification Results across 145 PMLB Datasets. Top score bolded.

Regression	Howso (targetless)	Howso (single-target)	XGBoost	LightGBM
Spearman \uparrow	0.918	0.924	0.919	0.916
R^2 \uparrow	0.848	0.834	0.808	0.787

Table 2: Regression Results across 258 PMLB Datasets. Top score bolded.

When optimizing for a single target feature as described in Section 7.6 (as XGBoost and LightGBM do), Howso demonstrates competitive performance on MCC (0.652 vs XGBoost 0.661/LightGBM 0.654) and accuracy (0.830 vs XGBoost 0.830/LightGBM 0.826) as shown in Table 1, and exceeds both competitors on regression as measured by Spearman correlation (0.924 vs XGBoost 0.919/LightGBM 0.916) as shown in Table 2. Additionally, Howso can operate in a targetless configuration as described in Section 7.5 (a capability not available in other supervised learning approaches) where, despite not optimizing to predict a specific target feature, it maintains competitive performance with accuracy of 0.808 on classification (vs XGBoost 0.830/LightGBM 0.826) and regression (0.918 vs XGBoost 0.919/LightGBM 0.916). Full experimental details are provided in Appendix C.1.

Even though PMLB specifies whether each feature is categorical (nominal only) or continuous, for these experiments, we let all estimators determine this on their own based on their own heuristics. We ran these

experiments this way because in our experience, many practitioners would prefer the tools figure this out when possible.¹⁰ Running all of these experiments with specified nominal versus continuous features would benefit all estimators, and it may help Howso more than XGBoost or LightGBM. For example, there are data sets in PMLB that have floating point values of -1.0, 0.0, and 1.0 where the values indicate clearly nominal data and have observed that representing 0 being closer to 1 than -1 in continuous space reduces the quality of Howso’s estimations. Future work involves improving our “infer_feature_attributes” heuristics to automatically infer these types from the data better. We also will continue to work on improving the deviation and feature probability computations; preliminary results show that we are able to improve classification tasks with targetless analysis beyond that of the current targeted algorithm, but at the reduction of regression tasks, and vice versa. We believe it is very plausible that we will be able to entirely merge these flows to include one targetless algorithm of superior quality inference.

12.2 Feature Importance

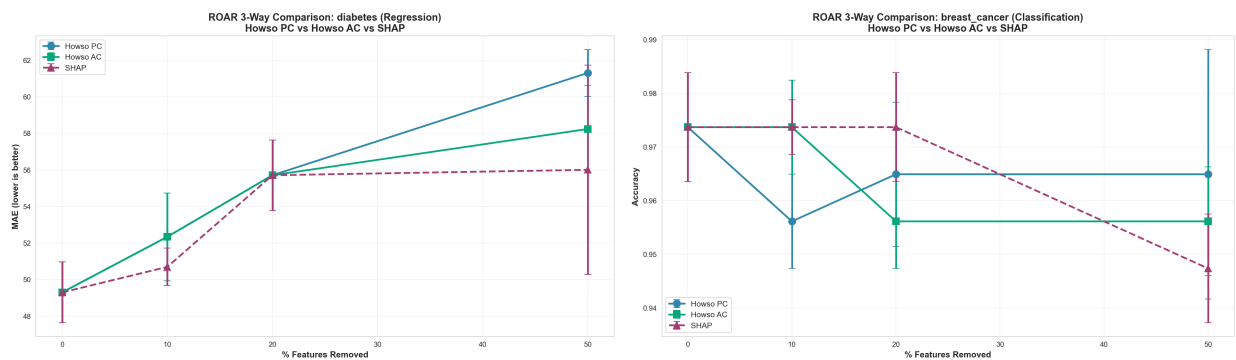


Figure 5: ROAR curves comparing Howso Prediction Contributions, Howso Accuracy Contributions, and SHAP on diabetes (MAE) and breast cancer (Accuracy) with XGBoost; 3 seeds, no tuning.

We applied ROAR (RemOve And Retrain) validation [Hooker et al., 2019] to compare Howso’s Prediction Contributions (PC) as described in Section 7.2 and Accuracy Contributions (AC) described in Section 7.2 against XGBoost using SHAP [Lundberg and Lee, 2017]. On the diabetes data set, Prediction Contributions shows a slightly steeper degradation (+24.4% at 50%) than Accuracy Contributions (+18.0%) or SHAP (+13.6%), while all methods remain robust on the breast cancer data set (less than 2pp degradation at 50%). Full experimental details are provided in Appendix C.3.

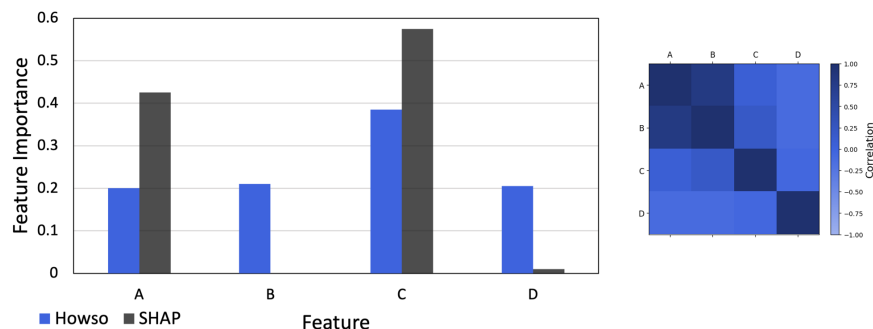


Figure 6: An example of inductive bias influencing feature importance, LightGBM SHAP versus Howso prediction contributions on a generated data set.

¹⁰One example of a typical oddity we have run into is using special extreme values to indicate nominal values. One commercial data set used in production we encountered used specific dates in January of the year 2655 to indicate particular nominal conditions such as unknown or specific types of indefinite values.

Additionally, we created a data set to experiment to test inductive bias. In this experiment, features A, C, and D were generated from uniform random distributions of different scales, C being the largest and D being the smallest. Feature B was just a copy of feature A with a very small amount of noise added. We trained Howso and LightGBM on the data and measured feature importance. As depicted in Figure 6, the feature importance of SHAP indicated how the LightGBM model was built and operating, reflecting the model’s inductive bias of eliminating feature B. When we changed the feature order, it indicated that feature B was important and that A had zero importance. However, when running Howso’s Prediction Contributions, we found that it did not incur inductive bias but accurately reflected the importance and usefulness of the features in predicting the target.

12.3 Anomaly Detection

Since anomalies occur in many different forms, benchmarking a variety of anomaly types yields a more representative and robust assessment of real-world data. ADBench [Han et al., 2022] is widely recognized as a versatile benchmark for tabular anomaly detection. It categorizes anomalies into the four types of local, global, dependency, and cluster. The benchmark system constructs benchmark datasets by removing pre-labeled anomalies from third-party datasets, then regenerates an equal number of synthetic anomalies using one of the four generation methods. Our benchmark extends ADBench’s approach by generating all four anomaly types within each dataset rather than limiting each dataset to a single anomaly category. Specifically, this benchmark applies ADBench’s four generation methods to create one-quarter of the total anomalies from each category, yielding datasets with a greater diversity of anomaly types that better reflects the diversity of real-world anomaly behavior.

Metric	PR-AUC	ROC-AUC
CBLOF [He et al., 2003]	0.1357	0.5851
COF [Pokrajac et al., 2008]	0.2361	0.7783
COPOD [Li et al., 2020]	0.2847	0.8262
ECOD [Li et al., 2022]	0.2895	0.8331
FeatureBagging [Lazarevic and Kumar, 2005]	0.2818	0.8253
HBOS [Goldstein and Dengel, 2012]	0.2826	0.8011
IForest [Liu et al., 2008]	0.2865	0.8510
kNN [Ramaswamy et al., 2000]	0.3029	0.8799
LODA [Pevný, 2016]	0.2539	0.7554
LOF [Breunig et al., 2000]	0.2814	0.8135
MCD [Hubert and Debruyne, 2010]	0.3005	0.8780
MOGAAL [Liu et al., 2019]	0.0976	0.5432
OCSVM [Schölkopf et al., 2001]	0.2932	0.8367
PCA [Shyu et al., 2003]	0.2821	0.8134
SOD [Zuo et al., 2023]	0.2849	0.8557
SOGAAL [Wang et al., 2021]	0.0959	0.6052
Howso Anomaly Detection	0.3126	0.8955
Howso Surprisal Contribution Conviction Only	0.2906	0.8755
Howso Similarity Conviction Only	0.2520	0.7715

Table 3: Total Aggregation Anomaly Detection Results. Top scores are in bold.

Our results, summarized in Table 3, are based on five independent runs for each of the 41 datasets. Compared to ADBench’s aggregated results, which report average model performance across all four anomaly categories, our findings are generally consistent. The top three models by ROC-AUC in our evaluation, kNN, IForest, and SOD, all achieve above-average performance in ADBench’s benchmark results, with kNN and IForest ranking as the second and third best methods, respectively, in ADBench. Howso Anomaly Detection, described in Section 10.4, achieved the highest overall performance, with a PR-AUC of 0.3126 and an ROC-AUC of 0.8955. The Howso Surprisal Contribution configuration, which is conceptually similar to kNN, exhibited comparable performance to kNN itself. Notably, CBLOF, which was the top-performing model in

ADBench’s aggregate evaluation, performs substantially worse under these more heterogeneous conditions. These results emphasize the increased difficulty of real-world datasets containing a mixture of anomaly types and suggests that methods tuned for controlled or single-type anomaly distributions may struggle with the complexity of mixed anomaly datasets. In contrast, the adaptability of Howso’s anomaly detection approach enables stronger generalization and more robust performance across realistic, heterogeneous anomaly distributions. Full experimental details are provided in Appendix C.4. Preliminary results suggest that improving the clustering techniques positively impacts Howso’s anomaly detection scores. Making sure that the clustering is robust to different data scales using the surprisal-as-distance metrics by Howso is future work that may improve these results even further.

12.4 Learning from Demonstration

The results in this section are more qualitative. We describe two experiments performed in real-time environments. In both, our software was running on the same laptop as the real-time environment, in both cases connected via a C# API. These experiments were performed earlier in the development of this software.

The first learning from demonstration experiment was performed on a drone simulation platform developed by Hazardous Software Inc. The sensory inputs to the agent were simulated preprocessed LiDAR data scanning the area in front of the drone, with a minimum filter to reduce the feature set to around 100 samples each representing the closest distance to an object, and that distance was divided by the velocity in that direction. This meant that the sensory inputs were time-to-impact values. Additionally, random navigation points were generated within a certain radius, though the navigation points were generated regardless of objects or obstacles, as long as the navigation point did not intersect with an object. The last set of input data was Xbox 360 controller input.



Figure 7: Drone approaching a navigation point behind stairs.

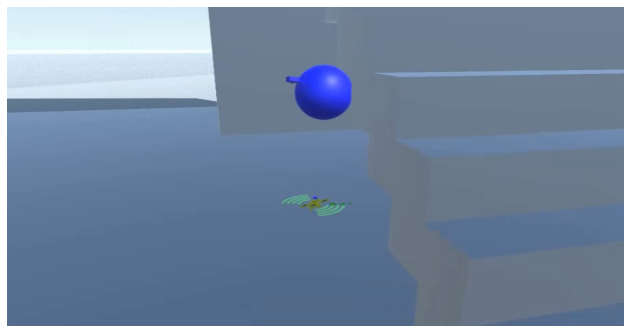


Figure 8: Drone navigating around the stairs.

As is shown in Figures 7 and 8, the drone was shown how to navigate around obstacles, out of windows, around buildings, etc. Typical sessions comprised of 1 to 2 minutes of initial demonstration followed by an additional 4-8 minutes of switching between the agent flying and the human taking over to make corrections

or to redo a maneuver demonstrating how to navigate the obstacle properly. We also implemented a button where the user could delete the most influential training data point, which proved useful on occasion when the drone was, for example, flying in a fixed direction away from a navigation point. After this typical 5 to 10 minute session, our software was able to successfully navigate the drone from navigation point to navigation point. Due to the sensitivity of the drone controls, the system needed to respond within a single digit number of milliseconds some of the time in order to avoid collisions, especially when the navigation points appeared in a challenging relative location. We also observed that the drone’s flying style matched that of the user. For example, if the user flew cautiously or tended to zig-zag, the drone would perform similar behavior. The environment was complex enough that we could tell that the behavior was generalizing to some degree, and the drone did not have access to global coordinates.



Figure 9: Driving while avoiding crowd of pedestrians.



Figure 10: Driving while staying within tight bounds.

The second learning from demonstration experiment was performed on the video game Grand Theft Auto V (GTAV). In this setting, we used similar inputs, though the simulated LiDAR was cast out circling the car without variation in height. In the experiment shown in Figure 9, the agent was taught to drive faster and faster speeds while avoiding pedestrians who were walking about in a large but sparse crowd. The agent was able to avoid pedestrians successfully at moderately high speeds while avoiding pedestrians in a period of time similar to the drone example of about 5 to 10 minutes. In the second experiment shown in Figure 10, the agent was taught to drive the car around a stadium in a tight lane, an area in GTAV similar to a race track. About 2 minutes of training data was generally sufficient to train the agent to successfully navigate the oval path at high speed. This scenario may have relied on memorization to some degree, but the small amount of training data (usually two laps, sometimes one lap was sufficient) indicate that some generalization was likely occurring because the path for any two laps is slightly different given human error and the controls.

12.5 Reinforcement Learning

On CartPole [Brockman et al., 2016], our implementation meets the environment’s built-in benchmark, having an average score of at least 195 over the last 100 episodes, by a median of 273 episodes across 5 runs, with a 100% solve rate. For context, a small study reported the REINFORCE algorithm needing around 650 episodes to solve CartPole, which improved to about 400 when employing a model-free approach with model dynamics [Shaikh et al., 2019], placing Howso in a comparable or faster sample-efficiency range.

On the Wafer-Thin-Mints game [Bontrager et al., 2019] with a 150-round evaluation, the average score ranges from -10 to 9, with 9 being the highest possible. Our Howso agent achieved a mean score of 6.07 across 20 runs (median 6.59), with a 70% win rate; among winning runs the mean was 6.87 (median 6.98). In prior literature, A2C agents trained from pixels typically failed to converge on this environment (mean score around -6). Only the best planning-based approach, NovelTS, reported scores above Howso with a mean of 8.75, and MCTS averaged a score of 5.73.

Howso performs competitively in both environments using a conviction of $\rho = 1$, which means it is simply exploring the part of the space with as much uncertainty as is in the data. We believe this is somewhat profound in that it is able to perform well without an explicit learning rate, in addition to the system being richly interpretable back to the training data. However, we found that setting $\rho = 3$ improved results for CartPole, so we used that for the performance metrics mentioned. Wafer-Thin-Mints was measured with conviction of $\rho = 1$. Full experimental details are provided in Appendix C.5.

12.6 Causal Discovery

Dataset	Measure	GES	Howso	LiNGAM	PC
GCM Microservice Architecture	F1	0.750	0.805	0.867	0.963
	Jaccard	0.600	0.678	0.765	0.929
GCM Online Shop	F1	0.552	0.665	0.581	0.556
	Jaccard	0.381	0.498	0.409	0.385
Sachs	F1	0.549	0.641	0.635	0.533
	Jaccard	0.378	0.472	0.465	0.364
GCM Supply Chain	F1	0.667	0.390	0.615	0.889
	Jaccard	0.500	0.244	0.444	0.800
Fluid Dynamics	F1	0.571	0.697	0.667	0.714
	Jaccard	0.400	0.536	0.500	0.556
average	F1	0.618	0.639	0.673	0.731
	Jaccard	0.452	0.486	0.517	0.606

Table 4: Causal discovery results scored according to undirected relationships.

We evaluated our causal discovery as described in Section 7.7 against the data sets of Graphical Causal Model (GCM) Microservice Architecture¹¹, GCM Online Shop¹², microbiology protein signaling network (Sachs) [Sachs et al., 2005], GCM Supply Chain¹³, and data from a fluid dynamics simulation which has an inflow, outflow, control valve, level set point, and tank. We evaluated our results versus Greedy Equivalent Search (GES) [Chickering, 2020], Peter-Clark Algorithm (PC) [Spirtes et al., 2000], and Linear Non-Gaussian Acyclic Models (LiNGAM) [Shimizu, 2014]. Figure 4 shows the results for undirected causal discovery and Figure 5 shows the results for directed causal discovery.

PC is generally the strongest performer, but our system was strongest performer of the algorithms whenever LiNGAM was better than PC. These data sets were selected to give a cross section of real-world problems and simulations with known ground truths and GCM implementations. Given that our algorithm looks for signal asymmetries in uncertainty, it is not surprising that systems that look for noise direction could outperform ours in some situations, as we see in the empirical results. Strengthening our methods on

¹¹https://www.pywhy.org/dowhy/v0.11.1/example_notebooks/gcm_rca_microservice_architecture.html

¹²https://www.pywhy.org/dowhy/v0.11.1/example_notebooks/gcm_online_shop.html

¹³https://www.pywhy.org/dowhy/v0.11.1/example_notebooks/gcm_supply_chain_dist_change.html

Dataset	Measure	GES	Howso	LiNGAM	PC
GCM Microservice Architecture	F1	0.667	0.758	0.828	0.923
	Jaccard	0.500	0.615	0.706	0.857
GCM Online Shop	F1	0.240	0.435	0.308	0.471
	Jaccard	0.136	0.279	0.182	0.308
Sachs	F1	0.267	0.434	0.436	0.455
	Jaccard	0.154	0.279	0.279	0.294
GCM Supply Chain	F1	0.545	0.250	0.500	0.889
	Jaccard	0.375	0.144	0.333	0.800
Fluid Dynamics	F1	0.143	0.636	0.571	0.462
	Jaccard	0.077	0.467	0.400	0.300
average	F1	0.372	0.503	0.529	0.640
	Jaccard	0.248	0.357	0.380	0.512

Table 5: Causal discovery results scored according to directed relationships.

these types of problems, as well as further investigating when to use missing information ratios versus entropy asymmetries to decide directionality are avenues for future work. Additional future work includes further causal benchmarking against more data sets [Wang, 2024] and employing richer evaluation metrics [Shimoni et al., 2018].

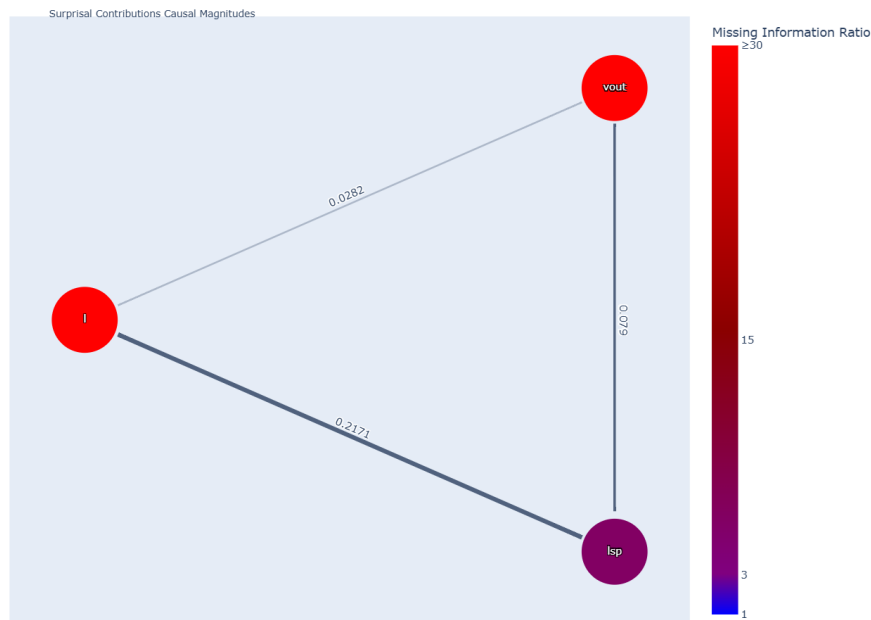


Figure 11: A causal graph discovered for a fluid dynamics simulation using a small subset of features.

We have found that our missing feature discovery and our certainty of edges is also useful for many data sets. We are unaware of any current benchmarks to accurately assess these capabilities, and few causal discovery techniques support this. Figure 11 depicts an example of what the plots look like. The edges are undirected because the missing information ratio is high, meaning that our system is not confident in the direction of the edges. Further, the strongest relationship is between l which is the level of water in the tank and lsp which is the level set point that controls the valve. The level is largely affected by fluid coming into the tank, and the volume of fluid going out $vout$ is also affected by this. In this example, our system correctly assesses that there are additional causal features that are related and important but not included in the system, such as the volume coming in, vin , and the valve control position c , not included in this graph or in the training data for this test. Qualitatively we have tested this system against commercial data

sets and have found it to be very useful, but determining and measuring benchmarks for these capabilities remains a task for future work. Anecdotally, our system seems to give more stable causal graphs than we have experienced with other causal techniques, a notable problem in causal discovery [Hulse et al., 2025]. Characterizing this stability and determining whether and when our system is more stable also remains a task for future work.

12.7 Data Synthesis

We evaluated the quality of synthetically generated data using the techniques described in Section 8.9 by training models on 9 datasets from PMLB (4 regression, 5 classification), generating synthetic versions, and comparing model performance trained on original versus synthetic data across 10-fold cross-validation using LightGBM regressors/classifiers. The synthetic data was generated with desired conviction of 5 and new case generation enabled. Results are shown in Table 6 and we found that there was generally very little loss of predictable signal in the synthesized data. Full experimental details are provided in Appendix C.6. Previous work has found that an earlier version of our synthetic data preserved the most utility of all algorithms compared in the study [Ling et al., 2024].

Metric	Original	Generated
Accuracy	0.959	0.925
F1-Score	0.959	0.927
MCC	0.923	0.868
Spearman	0.921	0.908

Table 6: Synthetic Data Generation Results: Overall Performance Comparison. Aggregated across 5 classification and 4 regression datasets.

12.8 Data Reduction and Ablation

We evaluated the data reduction and ablation techniques described in Section 9.1 across multiple benchmark datasets. These data sets were selected from the PMLB data sets and are generally more challenging to perform data reduction on than most data sets we encounter in industry which tends to have significantly more redundancy. The ablation process retained cases that contributed significant information while redistributing the probability mass of redundant cases to their influential neighbors.

Dataset	Reduction (%)	Howso Ablated	Howso With Subsample*	Howso With All Data
connect_4	63.12	0.4968	0.4765	0.5696
adult	66.67	0.4907	0.5085	0.5022
sleep	87.89	0.5731	0.6441	0.6353
fars	51.75	0.6918	0.6860	0.7082
krkopt	24.91	0.6094	0.6248	0.6580
letter	27.74	0.9420	0.9524	0.9548

*Randomly subsampled to the same size as ablated.

Table 7: Classification results comparing ablated Howso to Howso with all data using Matthews Correlation Coefficient (MCC).

Tables 7 and 8 show the results for classification and regression tasks respectively. We chose the Matthews correlation coefficient (MCC) metric as it is highly sensitive to all classification error types, and chose the Spearman correlation coefficient for regression tasks since it is more robust across distributions than R^2 .

Across the evaluated datasets, case ablation achieved substantial data reduction while maintaining performance comparable to the full dataset, though the results are stronger over random subsampling for regression tasks than classification tasks. The ablated results demonstrate that appropriate data is retained for accurate predictions. Even though in some cases the subsampling performed as well as or slightly better than

Dataset	Reduction (%)	Howso Ablated	Howso With Subsample*	Howso With All Data
1201_BNG_breastTumor	53.29	0.3348	0.2996	0.3539
feynman_test_1	35.95	0.9915	0.9889	0.9948
feynman_test_20	23.22	0.9866	0.9780	0.9855
215_2dplanes	61.97	0.9653	0.9699	0.9703
344_mv	47.04	0.9973	0.9986	0.9987
564_fried	62.52	0.9538	0.9566	0.9655
1193_BNG_lowbwt	59.23	0.7443	0.7440	0.7484
574_house_16H	21.84	0.7920	0.7909	0.7953

*Randomly subsampled to the same size as ablated.

Table 8: Regression results comparing ablated Howso to Howso with all data using Spearman correlation coefficient.

ablation, the data ablation process was able to find a subsample size that was still able to maintain quality. We emphasize that this method of data ablation and data reduction does not focus on any individual target, but rather is designed to address general representative data selection. Future work includes improving the quality of these results and deeper data reduction.

12.9 Adversarial Robustness

Model	Clean Acc	K=3 Adv Acc	K=1 Adv Acc
Howso	0.819	0.596 (-0.223)	0.737 (-0.082)
Logistic Regression	0.795	0.684 (-0.111)	0.742 (-0.053)
Decision Tree	0.783	0.564 (-0.220)	0.641 (-0.142)
kNN	0.796	0.436 (-0.360)	0.757 (-0.039)
LightGBM	0.835	0.619 (-0.216)	0.717 (-0.119)
XGBoost	0.834	0.633 (-0.201)	0.691 (-0.143)

Table 9: Mean accuracy under adversarial attack (27 datasets)

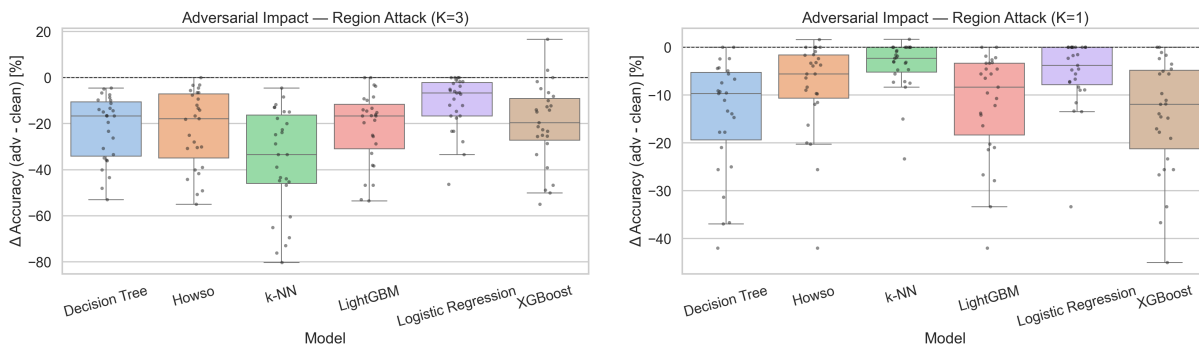


Figure 12: Distribution of accuracy degradation (Δ Accuracy) by model and attack type across 27 datasets. Box plots show median, IQR, and individual dataset results.

We evaluated Howso’s robustness to adversarial attacks using Region-Based Adversarial (RBA) attacks [Yang et al., 2020] across 27 tabular classification datasets. The RBA attack constrains perturbations to the convex region defined by the K most similar training cases, generating adversarial examples that remain within locally plausible feature space. Two attack configurations were tested: K=1 (single-neighbor, tighter constraint) and K=3 (three-neighbor, looser constraint). Howso was compared against five baselines:

k-Nearest Neighbors, Decision Tree, Logistic Regression, LightGBM, and XGBoost. The results are shown in Table 9 and Figure 12.

The K=3 attack was more challenging to all models, with instance-based learners showing greater vulnerability than the parametric logistic regression model. Under the tighter K=1 constraint, all models demonstrated improved robustness. Howso’s was less vulnerable to attacks with K=3 than the other instance-based learner, kNN, and Howso was less vulnerable to attacks with K=1 than everything except the two simpler algorithms, Logistic Regression and kNN. Detailed per-dataset results and analysis are provided in Appendix C.7.

12.10 Compute Performance

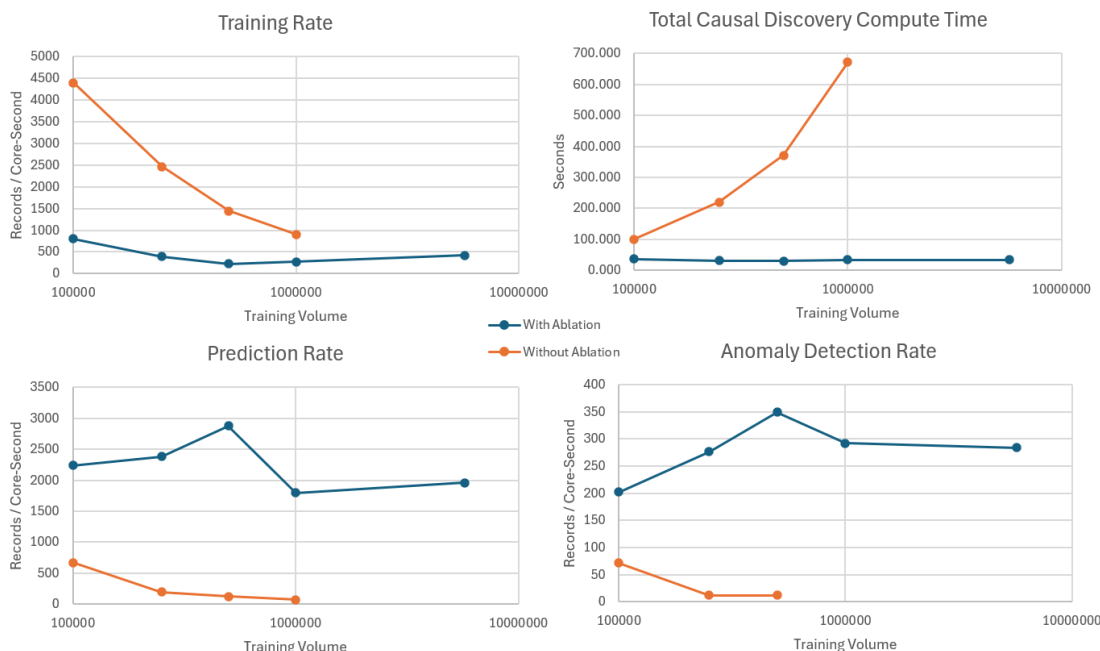


Figure 13: Four measures of performance on different volumes of the NYC arrest dataset.

Figure 13 depicts some performance metrics with different amounts of training data using the New York City historical arrest dataset,¹⁴ which is approximately 6 million records by 18 features, and measured on a modern 16 core processor. The environment and performance metrics include the overhead of loading the data via Python and Python scripts driving all of the interactions, serializing and deserializing the data back and forth via JSON. The orange lines indicate performance without data ablation and data reduction, and the blue lines indicate with. The training time graph includes the relevant analyze, ablation, and data reduction processes in the per-record overhead. Without ablation, the performance degrades, but with ablation, the performance starts notably lower but increases as the scale goes up. With data ablation, causal discovery, anomaly detection, and prediction rates stay steady independent of original data volume, as long as additional data does not add richness to the complexity of the model. In other words, more complex data may require a larger ceiling of data kept to maintain inference quality.

Future work includes advancing the use of hierarchical data sharding as described in Section 9.2 which may logarithmically increase inference times with data. Further, as of the time of this writing, we have focused optimization efforts on inference, and are now working toward a number of optimizations that should continue to improve performance for training times.

¹⁴https://data.cityofnewyork.us/Public-Safety/NYPD-Arrests-Data-Historic-/8h9b-rp9u/about_data

13 Future Work: Language, Images, and Creativity

There are many avenues for future work which would enhance usability and applicability, including improving the quality of inference, causal discovery, anomaly detection, etc., as well as adding support for more data types, and adding more types of dynamic solving of complex expressions (such as combinatorial optimization). In addition to those tactical areas of future work, here we highlight future work to move beyond structured, semistructured, and time series data.

13.1 Text

Prompt	Completed Sentence	Notes
The Solar System has	The Solar System has been relatively well studied, initially through telescopes and then later by spacecraft	The source was the article titled Astronomy, verbatim, except stopping before the period at the end.
The Solar System has	The Solar System has been fairly stable for billions of years, it is technically chaotic, and may be considered a planet.	The source was the article Solar System, changed at the end, gramatically correct, topically correct, but factually incorrect.
Jupiter is the	Jupiter is the most important deity in the Guatemalan Highlands at this time was Q'umarkaj, the capital of the aggressive K'iche' kingdom.	The source was a mixture of articles on the Maya people, and the sentence has strong factual basis, though the grammar is a little off. The K'iche' people and the Maya people in general tracked Jupiter's orbit and incorporated it into their calendars. The K'iche' kingdom was described in the Wikipedia texts as having subdued other Mayan peoples.
Jupiter is the	Jupiter is the largest of the Western Roman Empire, and the the king of the planet's connection with Easter	Example of a nonsensical sentence that is grammatically correct except for the missing period.

Table 10: Typical sentence completions based on approximately 1 million words trained from Wikipedia.

A major future direction for this technology is to apply all of the relevant capabilities discussed in this work to unstructured text. We have begun implementing some early experiments in this domain which have shown promise. In general, we leverage the time series capabilities, and the number of time series lags is effectively the context window. Using basic tokenization around word and punctuation boundaries on small data sets, we find that it is able to effectively memorize text and generalize enough to typically stay topical and produce mostly reasonable grammar with only a few mistakes per sentence. Table 10 shows the results of completing sentences given an initial prompt given a training data set of approximately 1 million words from Wikipedia covering a range of science and history topics. We note that when to terminate a sentence is learned entirely from the training data.

Early experiments with sentiment classification look promising as well. On the MTEB semantic classification benchmark (tweet sentiment extraction) [Enevoldsen et al., 2025] treating the text as time series but the sentiment as a stationary feature as described in Section 10.5, our system's accuracy ranges is currently in the vicinity of 54%. Compared to the public leaderboards,¹⁵ this is in the upper portion of the lower half of all results. However, we are obtaining these results with zero pretraining data and virtually every other technique on the leaderboard has significant pretraining. There is even a column on the leaderboard indicating how many millions of hyperparameters the models have. Future work will include pretraining to boost this score.

Other capabilities interact in interesting ways with text. For example, sparse deviation matrices described in Section 7.5 act essentially as a confusion matrix between interchangeability of words. Data ablation on

¹⁵<https://huggingface.co/spaces/mteb/leaderboard>

time series data, described in Section 10.5, may offer a human-readable alternative to embeddings where unnecessary words are cut out. It is hard to say how the performance and effective compression ratio of these embedding alternatives will compare to embeddings. Simple concepts could be reflected in fewer words than a full vector, however constraints related to grammar may make it harder to remove chunks to improve the compression. Future work will investigate the efficacy of such an implementation.

Another direction is to find ways to vastly improve the time series context length beyond what is currently maximally feasible, which currently is in the realm of 1000-2000 tokens on a single machine. We believe this can be accomplished by performing ablation and data reduction in the context, specifically to dynamically compress the earliest data in the context the most. Using surprisal to mark areas for compression has been shown to vastly improve context windows in LLMs [Fountas et al., 2025], and we believe similar techniques of improving LLM context lengths will have analogues with this system.

Longer term, the hierarchical techniques described in Section 9 will be required to improve performance. The dynamic derivation of code during inference, as described in Section 8.2, may offer paths for tighter, closer tool integration to match rules and derive results for arithmetic, logic, and potentially optimization and symbolic reasoning. Because these mechanisms themselves do not need to be learned, training can be vastly reduced to only include training data to indicate when these tools should be employed. This could potentially significantly reduce training data as compared to LLMs require in order to learn these capabilities due to the vast reduction in dimensionality.

13.2 Images

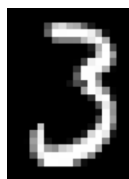


Figure 14: An example of a number generated using the MNIST handwritten digits data set.

Another future direction for the methods described here are to work on image data. Though the scores for the MNIST hand written data set are in the 91% to 92% range, with a little manual tuning we have achieved results in the 96% to 97% range, and we are hopeful that additional work toward improving deviation calculations and feature influence probabilities may be able to make those results achievable automatically. Additionally, preliminary experiments with adversarial attacks on MNIST have shown Howso to be more robust and maintain higher accuracy than any technique other than basic kNN. And we have had some success generating images from the MNIST data set. Figure 14 depicts an example of a generated image using Howso that is slightly better than average but not atypical.

Furthering the work of hierarchical implementation as described in Section 9 will be essential. That capability may help with some of the general problem for some tasks, but including additional features by employing understandable and possibly reversible convolutional transformations may be required to achieve high quality results. KNN has had a long history of being useful in images, even at scale with billions of images [Johnson et al., 2019], and we hope that our work here can help advance these applications. Treating images as time series data may also provide a path for eventually supporting video.

13.3 Creativity

Creativity is often defined as being novel compared to what is known and having value [Runco and Jaeger, 2012], and though there are psychological tests to measure creativity in human subjects via proxy tasks [Kim, 2006], there has been little research into measuring creativity from an information theory perspective (rare exceptions do exist, such as that by Coffman [1992]). As our system can dynamically balance exploration versus exploitation in online learning without specifying a learning or exploration rate (as discussed in Section 12.5), a natural extension for future work is to apply our techniques towards measuring and governing creativity relative to a base data set of knowledge.

Suppose we have a particular configuration or data record, x_F , and we would like to measure its creativity against a set of known data X_F . The relative novelty of x_F to some other configuration x'_F can be expressed as $I(x_F|x'_F)$. Further suppose we have a set of $v \in V$ functions that measure value of a configuration, as $v(x_F)$. Using the geometric mean to combine measurements of achieving different goals has been shown to be an effective objective function for multicriteria optimization which is also scale invariant to the measurements [Harrington, 1965], and so using it to provide contrast between different similarities is a natural use. Leinster and Meckes [2016] show that the generalized diversity index, which can be parameterized to measure the Shannon entropy, is nothing more than the reciprocal of the generalized mean when substituting $p - 1$ for p when dealing with probabilities [Tuomisto, 2010]. Finding a geometric mean of values is the same as finding the arithmetic mean of their logarithms and reversing the transformation. In light of this, we can combine the arithmetic mean of the logarithms with measurement uncertainty to bring these values into surprisal as described in Section 4. This surprisal of value, $I(v(x_F) | v(x'_F))$ can be expressed in terms of the deviation of value, $\delta(x_F)$, as

$$I(v(x_F) | x_F, v(x'_F)) = \frac{1}{|V|} \sum_{v \in V} \frac{|v(x_F) - v(x'_F)|}{\delta(x_F)}. \quad (61)$$

We can condition Equation 61 based on whether the outcome is positive to represent how much surprisal of beneficial value would be gained from data x_F . This caps the loss at zero and can be expressed as

$$I(v_+(x_F) | x_F, v(x'_F)) = \frac{1}{|V|} \sum_{v \in V} \frac{\max\{v(x_F) - v(x'_F), 0\}}{\delta(x_F)}. \quad (62)$$

Recognizing that the surprisal of a loss is just reversed, we can combine both positive and negative into a real valued quasi-surprisal, I^* , as

$$I^*(v_{\pm}(x_F) | x_F, v(x'_F)) = \frac{1}{|V|} \sum_{v \in V} \frac{v(x_F) - v(x'_F)}{\delta(x_F)}. \quad (63)$$

Additionally, in many domains, complexity is a factor of value, and elegance is often associated with creativity in some domains. The difference in complexity of a configuration x_F relative to x'_F can be computed as $I(x_F) - I(x'_F)$.

Putting all of these elements together, we can find the difference between the novelty and value of a given configuration and the best competing configuration of what is known. Measuring the creativity of configuration x_F against a data set of knowledge X_F can be expressed as

$$I^*(x_F|X_F) = \min_{x'_F \in X_F} \left\{ I(x_F|x'_F) - (I(x_F) - I(x'_F)) + \frac{1}{|V|} \sum_{v \in V} \frac{v(x_F) - v(x'_F)}{\delta(x_F)} \right\}. \quad (64)$$

We note that the inclusion of goal features as described in Section 8.5 already implicitly incorporate some aspects of these value functions into the queries, and aspects of Equation 64, are already implicitly performed during reinforcement learning (as will be described in Section 10.6). Future work involves validating this approach to measuring creativity, understanding how best to trade-off novelty versus utility, and applying it further to reinforcement learning and active inference.

14 Conclusion

In conclusion, we have demonstrated that instance-based learning built on information theory is a useful and mathematically powerful way to recontextualize machine learning into probability and statistics while maintaining strong and robust inference capabilities. Our hope is that this work inspires others to continue research on how we can get understanding and knowledge directly from data, where humans can understand every step of the process to debug, diagnose, remediate, and control more complex systems. At larger scales of data with more complex data sets, there will be different emergent layers that will need to be modeled. Our hierarchical approach may be able to decouple these layers when they are easily separable, and future

work may help human understandability for complex systems with information leakage between layers of emergence such as molecular biology [Rosas et al., 2024, 2025]. Rather than continuing to build larger and larger models that are increasingly opaque, we have demonstrated another potential path to help discover the physics of information.

Acknowledgments

This work is the culmination of continuous effort from the entire research and engineering team at Howso Incorporated, formerly Diveplane Corporation. Diveplane was founded in 2017 upon the technology of Hazardous Software Inc., which had began research and development on this technology in 2011. We gratefully acknowledge the effort of our dedicated teams including current and former employees, our government and commercial customers, our individual and institutional investors, and our friends and families on this journey for all of their support.

Bibliography

- P. K. Agarwal, B. Aronov, S. Har-Peled, J. M. Phillips, K. Yi, and W. Zhang. Nearest-neighbor searching under uncertainty ii. *ACM Transactions on Algorithms (TALG)*, 13(1):3, 2016.
- E. Alpaydin. Voting over multiple condensed nearest neighbor. *Artificial Intelligence Review*, pages 115–132, 1997.
- N. Altman. An introduction to kernel and nearest-neighbor nonparametric regression. *The American Statistician*, 46(3):175–185, 1992.
- A. Banerjee, C. J. Hazard, J. Beel, C. Mack, J. Xia, M. Resnick, and W. Goddin. Surprisal driven k -nn for robust and interpretable nonparametric learning. *arXiv preprint arXiv:2311.10246*, 2023.
- B. Becker and R. Kohavi. Adult. UCI Machine Learning Repository, 1996. DOI: <https://doi.org/10.24432/C5XW20>.
- K. Beyer, J. Goldstein, R. Ramakrishnan, and U. Shaft. When is “nearest neighbor” meaningful? In *International conference on database theory*, pages 217–235. Springer, 1999.
- P. Bontrager, A. Khalifa, A. Mendes, and J. Togelius. “superstition” in the network: Deep reinforcement learning plays deceptive games. *arXiv preprint arXiv:1908.04436*, 2019. URL <https://arxiv.org/abs/1908.04436>.
- L. Breiman, J. Friedman, C. Stone, and R. Olshen. Classification and regression trees. 1984.
- M. M. Breunig, H.-P. Kriegel, R. T. Ng, and J. Sander. Lof: identifying density-based local outliers. In *Proceedings of the 2000 ACM SIGMOD international conference on Management of data*, pages 93–104, 2000.
- G. Brockman, V. Cheung, L. Pettersson, J. Schneider, J. Schulman, J. Tang, and W. Zaremba. Openai gym, 2016.
- E. Candès, Y. Fan, L. Janson, and J. Lv. Panning for gold: ‘model-x’ knockoffs for high dimensional controlled variable selection. *Journal of the Royal Statistical Society Series B: Statistical Methodology*, 80(3):551–577, 2018.
- T. Chen and C. Guestrin. Xgboost: A scalable tree boosting system. In *Proceedings of the 22nd acm sigkdd international conference on knowledge discovery and data mining*, pages 785–794, 2016.
- A. Cheu, A. Smith, J. Ullman, D. Zeber, and M. Zhilyaev. Distributed differential privacy via shuffling. In *Advances in Cryptology–EUROCRYPT 2019: 38th Annual International Conference on the Theory and Applications of Cryptographic Techniques, Darmstadt, Germany, May 19–23, 2019, Proceedings, Part I 38*, pages 375–403. Springer, 2019.

- M. Chickering. Statistically efficient greedy equivalence search. In *Conference on Uncertainty in Artificial Intelligence*, pages 241–249. Pmlr, 2020.
- D. D. Coffman. Measuring musical originality using information theory. *Psychology of Music*, 20(2):154–161, 1992.
- D. Coomans and D. Massart. Alternative k-nearest neighbour rules in supervised pattern recognition : Part 1. k-nearest neighbour classification by using alternative voting rules. *Analytica Chimica Acta*, 136:15–27, 1982.
- A. M. De Livera, R. J. Hyndman, and R. D. Snyder. Forecasting time series with complex seasonal patterns using exponential smoothing. *Journal of the American statistical association*, 106(496):1513–1527, 2011.
- C. Dwork, K. Kenthapadi, F. McSherry, I. Mironov, and M. Naor. Our data, ourselves: Privacy via distributed noise generation. In *Advances in cryptology-EUROCRYPT 2006: 24th annual international conference on the theory and applications of cryptographic techniques, st. Petersburg, Russia, May 28-June 1, 2006. proceedings 25*, pages 486–503. Springer, 2006.
- C. Dwork, A. Roth, et al. The algorithmic foundations of differential privacy. *Foundations and Trends® in Theoretical Computer Science*, 9(3–4):211–407, 2014.
- K. Enevoldsen, I. Chung, I. Kerboua, M. Kardos, A. Mathur, D. Stap, J. Gala, W. Siblini, D. Krzemiński, G. I. Winata, et al. Mmteb: Massive multilingual text embedding benchmark. *arXiv preprint arXiv:2502.13595*, 2025.
- D. Feldman. Core-sets: Updated survey. *Sampling techniques for supervised or unsupervised tasks*, pages 23–44, 2020.
- V. Feldman, A. McMillan, and K. Talwar. Hiding among the clones: A simple and nearly optimal analysis of privacy amplification by shuffling. In *2021 IEEE 62nd Annual Symposium on Foundations of Computer Science (FOCS)*, pages 954–964. IEEE, 2022.
- Z. Fountas, M. Benfeghoul, A. Oomerjee, F. Christopoulou, G. Lampouras, H. B. Ammar, and J. Wang. Human-inspired episodic memory for infinite context LLMs. In *The Thirteenth International Conference on Learning Representations*, 2025. URL <https://openreview.net/forum?id=BI2int5SAC>.
- K. J. Friston, J. Daunizeau, and S. J. Kiebel. Reinforcement learning or active inference? *PloS one*, 4(7): e6421, 2009.
- G. Ganev and E. De Cristofaro. The inadequacy of similarity-based privacy metrics: Privacy attacks against “truly anonymous” synthetic datasets. *arXiv preprint arXiv:2312.05114*, 2025.
- J. Gao and C. Long. High-dimensional approximate nearest neighbor search: with reliable and efficient distance comparison operations. *Proceedings of the ACM on Management of Data*, 1(2):1–27, 2023.
- M. Goldstein and A. Dengel. Histogram-based outlier score (hbos): A fast unsupervised anomaly detection algorithm. *KI-2012: poster and demo track*, 1:59–63, 2012.
- S. Han, X. Hu, H. Huang, M. Jiang, and Y. Zhao. Adbench: Anomaly detection benchmark. In *Neural Information Processing Systems (NeurIPS)*, 2022.
- E. C. Harrington. The desirability function. *Industrial quality control*, 21(10):494–498, 1965.
- P. Hart. The condensed nearest neighbor rule (corresp.). *IEEE transactions on information theory*, 14(3): 515–516, 1968.
- T. Hastie, R. Tibshirani, and J. Friedman. The elements of statistical learning. page 63, 2001.
- C. J. Hazard, C. Fusting, M. Resnick, M. Auerbach, M. Meehan, and V. Korobov. Natively interpretable machine learning and artificial intelligence: Preliminary results and future directions. *arXiv preprint arXiv:1901.00246*, 2019.

- Z. He, X. Xu, and S. Deng. Discovering cluster-based local outliers. *Pattern recognition letters*, 24(9-10):1641–1650, 2003.
- A. Hinneburg, C. C. Aggarwal, and D. A. Keim. What is the nearest neighbor in high dimensional spaces? In *26th Internat. Conference on Very Large Databases*, pages 506–515, 2000.
- I. Hmeidi, B. B Hawashin, and E. El-Qawasmeh. Performance of knn and svm classifiers on full word arabic articles. *Advanced Engineering Informatics*, 22(1):106–111, 2008.
- C. C. Holt. Forecasting seasonals and trends by exponentially weighted moving averages. *International Journal of Forecasting*, 20(1):5–10, 2004. ISSN 0169-2070.
- S. Hooker, D. Erhan, P.-J. Kindermans, and B. Kim. A benchmark for interpretability methods in deep neural networks. *Advances in neural information processing systems*, 32, 2019.
- M. Hubert and M. Debruyne. Minimum covariance determinant. *Wiley interdisciplinary reviews: Computational statistics*, 2(1):36–43, 2010.
- E. Hüllermeier and W. Waegeman. Aleatoric and epistemic uncertainty in machine learning: An introduction to concepts and methods. *Machine learning*, 110(3):457–506, 2021.
- J. Hulse, N. U. Eisty, and T. Menzies. Shaky structures: The wobbly world of causal graphs in software analytics. *Empirical Software Engineering*, 30(5):142, 2025.
- P. Indyk and R. Motwani. Approximate nearest neighbors: towards removing the curse of dimensionality. In *Proc. of the 30th ACM Sym.on Theory of Computing*, pages 604–613, 1998.
- J. Johnson, M. Douze, and H. Jégou. Billion-scale similarity search with GPUs. *IEEE Transactions on Big Data*, 7(3):535–547, 2019.
- K. H. Kim. Can we trust creativity tests? a review of the torrance tests of creative thinking (ttct). *Creativity research journal*, 18(1):3–14, 2006.
- I. E. Kumar, S. Venkatasubramanian, C. Scheidegger, and S. Friedler. Problems with shapley-value-based explanations as feature importance measures. In *International conference on machine learning*, pages 5491–5500. PMLR, 2020.
- A. Lazarevic and V. Kumar. Feature bagging for outlier detection. In *Proceedings of the eleventh ACM SIGKDD international conference on Knowledge discovery in data mining*, pages 157–166, 2005.
- T. Leinster and M. W. Meckes. Maximizing diversity in biology and beyond. *Entropy*, 18(3):88, 2016.
- Z. Li, Y. Zhao, N. Botta, C. Ionescu, and X. Hu. Copod: copula-based outlier detection. In *2020 IEEE international conference on data mining (ICDM)*, pages 1118–1123. IEEE, 2020.
- Z. Li, Y. Zhao, X. Hu, N. Botta, C. Ionescu, and G. H. Chen. Ecod: Unsupervised outlier detection using empirical cumulative distribution functions. *IEEE Transactions on Knowledge and Data Engineering*, 35(12):12181–12193, 2022.
- H. W. Lin, M. Tegmark, and D. Rolnick. Why does deep and cheap learning work so well? *Journal of Statistical Physics*, 168(6):1223–1247, 2017.
- X. Ling, T. Menzies, C. Hazard, J. Shu, and J. Beel. Trading off scalability, privacy, and performance in data synthesis. *IEEE Access*, 12:26642–26654, 2024.
- F. T. Liu, K. M. Ting, and Z.-H. Zhou. Isolation forest. In *2008 eighth ieee international conference on data mining*, pages 413–422. IEEE, 2008.
- Y. Liu, Z. Li, C. Zhou, Y. Jiang, J. Sun, M. Wang, and X. He. Generative adversarial active learning for unsupervised outlier detection. *IEEE Transactions on Knowledge and Data Engineering*, 32(8):1517–1528, 2019.

- S. Lukaszzyk. *Probability metric, examples of approximation applications in experimental mechanics*. PhD thesis, Cracow University of Technology, 2003.
- S. Lukaszzyk. A new concept of probability metric and its applications in approximation of scattered data sets. *Computational Mechanics*, 33(4):299–304, 2004.
- S. Lundberg and S.-I. Lee. A unified approach to interpreting model predictions, 2017. URL <https://arxiv.org/abs/1705.07874>.
- Y. A. Malkov and D. A. Yashunin. Efficient and robust approximate nearest neighbor search using hierarchical navigable small world graphs. *IEEE transactions on pattern analysis and machine intelligence*, 42(4):824–836, 2018.
- F. Martínez, M. P. Frías, M. D. Pérez, and A. J. Rivera. A methodology for applying k-nearest neighbor to time series forecasting. *Artificial Intelligence Review*, 52(3):2019–2037, 2019.
- B. Mason, A. Tripathy, and R. Nowak. Nearest neighbor search under uncertainty. In *Uncertainty in Artificial Intelligence*, pages 1777–1786. PMLR, 2021.
- L. McInnes, J. Healy, S. Astels, et al. hdbscan: Hierarchical density based clustering. *J. Open Source Softw.*, 2(11):205, 2017.
- L. McInnes, J. Healy, and J. Melville. Umap: Uniform manifold approximation and projection for dimension reduction. *arXiv preprint arXiv:1802.03426*, 2018.
- B. D. Moring and T. R. Martinez. Weighted instance typicality search (wits): A nearest neighbor data reduction algorithm. *Intelligent Data Analysis*, 8(1):61–78, 2004.
- D. B. Murray and S. W. Teare. Probability of a tossed coin landing on edge. *Physical Review E*, 48(4):2547, 1993.
- R. S. Olson, W. La Cava, P. Orzechowski, R. J. Urbanowicz, and J. H. Moore. Pmlb: a large benchmark suite for machine learning evaluation and comparison. *BioData mining*, 10(1):36, 2017.
- J. J. Pan, J. Wang, and G. Li. Survey of vector database management systems. *The VLDB Journal*, 33(5):1591–1615, 2024.
- T. Pevný. Loda: Lightweight on-line detector of anomalies. *Machine Learning*, 102(2):275–304, 2016.
- D. Pokrajac, N. Reljin, N. Pejcic, and A. Lazarevic. Incremental connectivity-based outlier factor algorithm. In *Visions of computer science-BCS international academic conference*. BCS Learning & Development, 2008.
- J. Raikwal and K. Saxena. Performance evaluation of svm and k-nearest neighbor algorithm over medical data set. *International Journal of Computer Applications*, 50(14):975–985, 2012.
- S. Ramaswamy, R. Rastogi, and K. Shim. Efficient algorithms for mining outliers from large data sets. In *Proceedings of the 2000 ACM SIGMOD international conference on Management of data*, pages 427–438, 2000.
- M. Rao, Y. Chen, B. C. Vemuri, and F. Wang. Cumulative residual entropy: a new measure of information. *IEEE transactions on Information Theory*, 50(6):1220–1228, 2004.
- F. E. Rosas, B. C. Geiger, A. I. Luppi, A. K. Seth, D. Polani, M. Gastpar, and P. A. Mediano. Software in the natural world: A computational approach to hierarchical emergence. *arXiv preprint arXiv:2402.09090*, 2024.
- F. E. Rosas, A. J. Gutknecht, P. A. Mediano, and M. Gastpar. Characterising high-order interdependence via entropic conjugation. *Communications Physics*, 8(1):347, 2025.

- M. A. Runco and G. J. Jaeger. The standard definition of creativity. *Creativity research journal*, 24(1):92–96, 2012.
- K. Sachs, O. Perez, D. Pe’er, D. A. Lauffenburger, and G. P. Nolan. Causal protein-signaling networks derived from multiparameter single-cell data. *Science*, 308(5721):523–529, 2005.
- N. Sajid, P. J. Ball, T. Parr, and K. J. Friston. Active inference: demystified and compared. *Neural computation*, 33(3):674–712, 2021.
- B. Schölkopf, J. C. Platt, J. Shawe-Taylor, A. J. Smola, and R. C. Williamson. Estimating the support of a high-dimensional distribution. *Neural computation*, 13(7):1443–1471, 2001.
- M. Schuh, W. T., and R. Angryk. Mitigating the curse of dimensionality for exact knn retrieval. *Proceedings of the Twenty-Seventh International Florida Artificial Intelligence Research Society Conference*, pages 363–368, 2014.
- M. A. Schuh, T. Wylie, , and R. A. Angryk. Improving the performance of high-dimensional knn retrieval through localized dataspace segmentation and hybrid indexing. *In Proc. of the 17th ADBIS Conf.*, page 344–357, 2013.
- A. Shaikh, A. Zheng, I. Chuang, B. Hsu, R. Su, T. Reutzel, and Q. Zeng. Towards integrating model dynamics for sample efficient reinforcement learning. Technical report, Carnegie Mellon University, 2019. URL <https://sha2nkt.github.io/assets/deep-rl-final.pdf>.
- Y. Shi, G. Ke, Z. Chen, S. Zheng, and T.-Y. Liu. Quantized training of gradient boosting decision trees. *Advances in neural information processing systems*, 35:18822–18833, 2022.
- S. Shimizu. Lingam: Non-gaussian methods for estimating causal structures. *Behaviormetrika*, 41(1):65–98, 2014.
- Y. Shimoni, C. Yanover, E. Karavani, and Y. Goldschmidt. Benchmarking framework for performance-evaluation of causal inference analysis. *arXiv preprint arXiv:1802.05046*, 2018.
- M.-L. Shyu, S.-C. Chen, K. Sarinnapakorn, and L. Chang. A novel anomaly detection scheme based on principal component classifier. 2003.
- F. N. F. Q. Simoes, M. Dastani, and T. van Ommen. Causal entropy and information gain for measuring causal control. In *European Conference on Artificial Intelligence*, pages 216–231. Springer, 2023.
- D. Soydaner. Attention mechanism in neural networks: where it comes and where it goes. *Neural Computing and Applications*, 34(16):13371–13385, 2022.
- P. Spirtes, C. N. Glymour, and R. Scheines. *Causation, prediction, and search*. MIT press, 2000.
- N. N. Taleb. *The Black Swan: Second Edition: The Impact of the Highly Improbable*. Random House Publishing Group, New York, 2007. ISBN 9781400063512.
- Y. Tao, K. Yi, C. Sheng, and P. Kalnis. Quality and efficiency in high dimensional nearest neighbor search. *In Proc. of the ACM SIGMOD Inter. Conf. on Mgmt. of Data*, pages 563–576, 2009.
- H. Tuomisto. A consistent terminology for quantifying species diversity? yes, it does exist. *Oecologia*, 164(4):853–860, 2010.
- N. Ukey, Z. Yang, B. Li, G. Zhang, Y. Hu, and W. Zhang. Survey on exact knn queries over high-dimensional data space. *Sensors*, 23(2):629, 2023.
- V. V. B. Surya, H. Prasath, A. Arafat, O. Lasassmeh, and A. Hassanat. Distance and similarity measures effect on the performance of k-nearest neighbor classifier. *arXiv:1708.04321*, 2017.
- P. Vijaya, M. N. Murty, and D. Subramanian. Leaders–subleaders: An efficient hierarchical clustering algorithm for large data sets. *Pattern Recognition Letters*, 25(4):505–513, 2004.

- X. Wang, X. Wang, and M. Wilkes. *New developments in unsupervised outlier detection*. Springer, 2021.
- Z. Wang. Causalbench: A comprehensive benchmark for evaluating causal reasoning capabilities of large language models. In *Proceedings of the 10th SIGHAN Workshop on Chinese Language Processing (SIGHAN-10)*, pages 143–151, 2024.
- R. Williams. On the difference between closest, furthest, and orthogonal pairs: Nearly-linear vs barely-subquadratic complexity. In *Proceedings of the Twenty-Ninth Annual ACM-SIAM Symposium on Discrete Algorithms*, pages 1207–1215. SIAM, 2018.
- W. Wolberg. Breast Cancer Wisconsin (Original). UCI Machine Learning Repository, 1990. DOI: <https://doi.org/10.24432/C5HP4Z>.
- Y.-Y. Yang, C. Rashtchian, Y. Wang, and K. Chaudhuri. Robustness for non-parametric classification: A generic attack and defense. In *International Conference on Artificial Intelligence and Statistics*, pages 941–951. PMLR, 2020.
- Z. Zuo, Z. Li, P. Cheng, and J. Zhao. A novel subspace outlier detection method by entropy-based clustering algorithm. *Scientific Reports*, 13(1):15331, 2023.

Appendices

A Supporting Mathematics

A.1 Derivation of Łukaszyk–Karmowski (LK) with Laplace Distributions

Theorem 1. *The expected distance between two random variables X and Y given that they both follow the Laplace distribution with a distributional parameter b and with respective means μ_1 and μ_2 can be found as*
 $d(X, Y) = |\mu_2 - \mu_1| + \frac{1}{2}e^{\frac{-|\mu_2 - \mu_1|}{b}} (3b + |\mu_2 - \mu_1|)$.

Proof. We begin with the expected distance between two random variables X and Y given two probability density functions, $f(x)$ and $g(y)$ as

$$d(X, Y) = \int_{-\infty}^{\infty} \int_{-\infty}^{\infty} |x - y| f(x) g(y) dx dy. \quad (65)$$

Using two Laplace distributions with means μ_1 and μ_2 and expected distance from the mean b_1 and b_2 , we can express the probability density functions as

$$f(x) = \frac{1}{2b_1} e^{\frac{-|x - \mu_1|}{b_1}} \quad (66)$$

and

$$g(y) = \frac{1}{2b_2} e^{\frac{-|y - \mu_2|}{b_2}} \quad (67)$$

respectively.

Substituting in the Laplace distributions into the expected distance, we can simplify this slightly as

$$\begin{aligned} d(X, Y) &= \int_{-\infty}^{\infty} \int_{-\infty}^{\infty} |x - y| \cdot \frac{1}{2b_1} e^{\frac{-|x - \mu_1|}{b_1}} \cdot \frac{1}{2b_2} e^{\frac{-|y - \mu_2|}{b_2}} dx dy \\ &= \frac{1}{4b_1 b_2} \int_{-\infty}^{\infty} \int_{-\infty}^{\infty} |x - y| \cdot e^{\frac{-|x - \mu_1|}{b_1}} \cdot e^{\frac{-|y - \mu_2|}{b_2}} dx dy. \end{aligned}$$

We further assume that $b_1 = b_2$, and use b in place of both, which assumes that the error is the same throughout the space and simplify further as

$$d(X, Y) = \frac{1}{4b^2} \int_{-\infty}^{\infty} \int_{-\infty}^{\infty} |x - y| \cdot e^{-\frac{|\mu_1 - x|}{b}} \cdot e^{-\frac{|\mu_2 - y|}{b}} dx dy. \quad (68)$$

Because we only have one value for b , we can assume that $\mu_1 \leq \mu_2$ without loss of generality because we can just exchange the values if this is not true, and in the end we will adjust the formula to remove this assumption. There exist 3 regions of the space for x which are $x \leq \mu_1$, $\mu_1 < x \leq \mu_2$, and $\mu_2 < x$.

Rewriting Equation 68 for the part of the space where $x < \mu_1, y < \mu_1$ is

$$\begin{aligned} d_{x \leq \mu_1, y \leq \mu_1}(X, Y) &= \frac{1}{4b^2} \int_{-\infty}^{\mu_1} \int_{-\infty}^{\mu_1} |y - x| \cdot e^{-\frac{(\mu_1 - x)}{b}} \cdot e^{-\frac{(\mu_2 - y)}{b}} dx dy \\ &= \frac{1}{4b^2} \int_{-\infty}^{\mu_1} \left(\int_{-\infty}^{\mu_1} |y - x| \cdot e^{-\frac{(\mu_1 - x)}{b}} dx \right) \cdot e^{-\frac{(\mu_2 - y)}{b}} dy \\ &= \frac{1}{4b^2} \int_{-\infty}^{\mu_1} \left(\int_{-\infty}^y (y - x) \cdot e^{-\frac{(\mu_1 - x)}{b}} dx + \int_y^{\mu_1} (x - y) \cdot e^{-\frac{(\mu_1 - x)}{b}} dx \right) \cdot e^{-\frac{(\mu_2 - y)}{b}} dy \\ &= \frac{1}{4b^2} \int_{-\infty}^{\mu_1} \left(b^2 e^{\frac{y - \mu_1}{b}} + b^2 e^{\frac{y - \mu_1}{b}} - by + b\mu_1 - b^2 \right) \cdot e^{-\frac{(\mu_2 - y)}{b}} dy \\ &= \frac{1}{4b} \int_{-\infty}^{\mu_1} \left(2be^{\frac{y - \mu_1}{b}} - y + \mu_1 - b \right) \cdot e^{-\frac{(\mu_2 - y)}{b}} dy \\ &= \frac{1}{4b} b^2 e^{-\frac{(\mu_2 - \mu_1)}{b}} \\ &= \frac{1}{4} b e^{-\frac{(\mu_2 - \mu_1)}{b}}. \end{aligned}$$

Rewriting Equation 68 for the part of the space where $x < \mu_1, \mu_1 < y < \mu_2$ is

$$\begin{aligned} d_{x \leq \mu_1, \mu_1 < y \leq \mu_2}(X, Y) &= \frac{1}{4b^2} \int_{\mu_1}^{\mu_2} \int_{-\infty}^{\mu_1} (y - x) \cdot e^{-\frac{(\mu_1 - x)}{b}} \cdot e^{-\frac{(\mu_2 - y)}{b}} dx dy \\ &= \frac{1}{4b^2} \int_{\mu_1}^{\mu_2} (by - b\mu_1 + b^2) \cdot e^{-\frac{(\mu_2 - y)}{b}} dy \\ &= \frac{1}{4b} \int_{\mu_1}^{\mu_2} (y - \mu_1 + b) \cdot e^{-\frac{(\mu_2 - y)}{b}} dy \\ &= \frac{1}{4b} (b\mu_2 - b\mu_1) \\ &= \frac{1}{4} (\mu_2 - \mu_1). \end{aligned}$$

Rewriting Equation 68 for the part of the space where $x < \mu_1, \mu_2 < y$ is

$$\begin{aligned} d_{x \leq \mu_1, \mu_2 < y}(X, Y) &= \frac{1}{4b^2} \int_{\mu_2}^{\infty} \int_{-\infty}^{\mu_1} (y - x) \cdot e^{-\frac{(\mu_1 - x)}{b}} \cdot e^{-\frac{(y - \mu_2)}{b}} dx dy \\ &= \frac{1}{4b^2} \int_{\mu_2}^{\infty} \left(\int_{-\infty}^{\mu_1} (y - x) \cdot e^{-\frac{(\mu_1 - x)}{b}} dx \right) \cdot e^{-\frac{(y - \mu_2)}{b}} dy \\ &= \frac{1}{4b^2} \int_{\mu_2}^{\infty} (by - b\mu_1 + b^2) \cdot e^{-\frac{(y - \mu_2)}{b}} dy \\ &= \frac{1}{4b} \int_{\mu_2}^{\infty} (y - \mu_1 + b) \cdot e^{-\frac{(y - \mu_2)}{b}} dy \\ &= \frac{1}{4b} (b\mu_2 - b\mu_1 + 2b^2) \\ &= \frac{1}{4} (\mu_2 - \mu_1 + 2b). \end{aligned}$$

Rewriting Equation 68 for the part of the space where $\mu_1 < x < \mu_2, y < \mu_1$ is

$$\begin{aligned}
d_{\mu_1 < x \leq \mu_2, y \leq \mu_1}(X, Y) &= \frac{1}{4b^2} \int_{-\infty}^{\mu_1} \int_{\mu_1}^{\mu_2} (x-y) \cdot e^{-\frac{(x-\mu_1)}{b}} \cdot e^{-\frac{(\mu_2-y)}{b}} dx dy \\
&= \frac{1}{4b^2} \int_{-\infty}^{\mu_1} \left(\int_{\mu_1}^{\mu_2} (x-y) \cdot e^{-\frac{(x-\mu_1)}{b}} dx \right) \cdot e^{-\frac{(\mu_2-y)}{b}} dy \\
&= \frac{1}{4b^2} \int_{-\infty}^{\mu_1} \left(e^{\frac{\mu_1-\mu_2}{b}} (by - b\mu_2 - b^2) - by + b\mu_1 + b^2 \right) \cdot e^{-\frac{(\mu_2-y)}{b}} dy \\
&= \frac{1}{4b} \int_{-\infty}^{\mu_1} \left(e^{\frac{\mu_1-\mu_2}{b}} (y - \mu_2 - b) - y + \mu_1 + b \right) \cdot e^{-\frac{(\mu_2-y)}{b}} dy \\
&= \frac{1}{4b} \left(2b^2 e^{\frac{\mu_1-\mu_2}{b}} + e^{\frac{2\mu_1-2\mu_2}{b}} (-b\mu_2 + b\mu_1 - 2b^2) \right) \\
&= \frac{1}{4} \left(2be^{\frac{\mu_1-\mu_2}{b}} + e^{\frac{2\mu_1-2\mu_2}{b}} (\mu_1 - \mu_2 - 2b) \right).
\end{aligned}$$

Rewriting Equation 68 for the part of the space where $\mu_1 < x < \mu_2, \mu_1 < y < \mu_2$ is

$$\begin{aligned}
d_{\mu_1 < x \leq \mu_2, \mu_1 < y \leq \mu_2}(X, Y) &= \frac{1}{4b^2} \int_{\mu_1}^{\mu_2} \int_{\mu_1}^{\mu_2} |y-x| \cdot e^{-\frac{(x-\mu_1)}{b}} \cdot e^{-\frac{(\mu_2-y)}{b}} dx dy \\
&= \frac{1}{4b^2} \int_{\mu_1}^{\mu_2} \left(\int_{\mu_1}^{\mu_2} |y-x| \cdot e^{-\frac{(x-\mu_1)}{b}} dx \right) \cdot e^{-\frac{(\mu_2-y)}{b}} dy \\
&= \frac{1}{4b^2} \int_{\mu_1}^{\mu_2} \left(\int_{\mu_1}^y (y-x) \cdot e^{-\frac{(x-\mu_1)}{b}} dx + \int_y^{\mu_2} (x-y) \cdot e^{-\frac{(x-\mu_1)}{b}} dx \right) \cdot e^{-\frac{(\mu_2-y)}{b}} dy \\
&= \frac{1}{4b^2} \int_{\mu_1}^{\mu_2} \left(\left(b^2 e^{\frac{\mu_1-y}{b}} + by - b\mu_1 - b^2 \right) + \left(b^2 e^{\frac{\mu_1-y}{b}} + e^{\frac{\mu_1-\mu_2}{b}} (by - b\mu_2 - b^2) \right) \right) \cdot e^{-\frac{(\mu_2-y)}{b}} dy \\
&= \frac{1}{4b} \int_{\mu_1}^{\mu_2} \left(2be^{\frac{\mu_1-y}{b}} + y - \mu_1 - b + e^{\frac{\mu_1-\mu_2}{b}} (y - \mu_2 - b) \right) \cdot e^{-\frac{(\mu_2-y)}{b}} dy \\
&= \frac{1}{4b} \left(b\mu_2 - b\mu_1 - 2b^2 + e^{\frac{\mu_1-\mu_2}{b}} (2b\mu_2 - 2b^2) + e^{\frac{\mu_1-\mu_2}{b}} (-2b\mu_1 + 2b^2) + e^{\frac{2\mu_1-2\mu_2}{b}} (b\mu_2 - b\mu_1 + 2b^2) \right) \\
&= \frac{1}{4} \left(\mu_2 - \mu_1 - 2b + e^{\frac{\mu_1-\mu_2}{b}} (2\mu_2 - 2\mu_1) + e^{\frac{2\mu_1-2\mu_2}{b}} (\mu_2 - \mu_1 + 2b) \right).
\end{aligned}$$

Rewriting Equation 68 for the part of the space where $\mu_1 < x < \mu_2, \mu_2 < y$ is

$$\begin{aligned}
d_{\mu_1 < x \leq \mu_2, \mu_2 < y}(X, Y) &= \frac{1}{4b^2} \int_{\mu_2}^{\infty} \int_{\mu_1}^{\mu_2} (y-x) \cdot e^{-\frac{(x-\mu_1)}{b}} \cdot e^{-\frac{(y-\mu_2)}{b}} dx dy \\
&= \frac{1}{4b^2} \int_{\mu_2}^{\infty} \left(\int_{\mu_1}^{\mu_2} (y-x) \cdot e^{-\frac{(x-\mu_1)}{b}} dx \right) \cdot e^{-\frac{(y-\mu_2)}{b}} dy \\
&= \frac{1}{4b^2} \int_{\mu_2}^{\infty} \left(by - b\mu_1 - b^2 - e^{\frac{\mu_1-\mu_2}{b}} (by - b\mu_2 - b^2) \right) \cdot e^{-\frac{(y-\mu_2)}{b}} dy \\
&= \frac{1}{4b} \int_{\mu_2}^{\infty} \left(y - \mu_1 - b - e^{\frac{\mu_1-\mu_2}{b}} (y - \mu_2 - b) \right) \cdot e^{-\frac{(y-\mu_2)}{b}} dy \\
&= \frac{1}{4b} (b\mu_2 - b\mu_1) \\
&= \frac{1}{4} (\mu_2 - \mu_1)
\end{aligned}$$

Rewriting Equation 68 for the part of the space where $\mu_2 < x, y < \mu_1$ is

$$\begin{aligned}
d_{\mu_2 < x, y \leq \mu_1}(X, Y) &= \frac{1}{4b^2} \int_{-\infty}^{\mu_1} \int_{\mu_2}^{\infty} (x - y) \cdot e^{-\frac{(x-\mu_1)}{b}} \cdot e^{-\frac{(\mu_2-y)}{b}} dx dy \\
&= \frac{1}{4b^2} \int_{-\infty}^{\mu_1} \left(\int_{\mu_2}^{\infty} (x - y) \cdot e^{-\frac{(x-\mu_1)}{b}} dx \right) \cdot e^{-\frac{(\mu_2-y)}{b}} dy \\
&= \frac{1}{4b^2} \int_{-\infty}^{\mu_1} e^{\frac{\mu_1-\mu_2}{b}} (-by + b\mu_2 + b^2) \cdot e^{-\frac{(\mu_2-y)}{b}} dy \\
&= \frac{1}{4b} \int_{-\infty}^{\mu_1} e^{\frac{\mu_1-\mu_2}{b}} (-y + \mu_2 + b) \cdot e^{-\frac{(\mu_2-y)}{b}} dy \\
&= \frac{1}{4b} e^{\frac{2\mu_1-2\mu_2}{b}} (b\mu_2 + 2b^2 - b\mu_1) \\
&= \frac{1}{4} e^{\frac{2\mu_1-2\mu_2}{b}} (\mu_2 + 2b - \mu_1) \\
&= \frac{1}{4} e^{-\frac{2(\mu_2-\mu_1)}{b}} (2b + \mu_2 - \mu_1)
\end{aligned}$$

Rewriting Equation 68 for the part of the space where $\mu_2 < x, \mu_1 < y < \mu_2$ is

$$\begin{aligned}
d_{\mu_2 < x, \mu_1 < y \leq \mu_2}(X, Y) &= \frac{1}{4b^2} \int_{\mu_1}^{\mu_2} \int_{\mu_2}^{\infty} (x - y) \cdot e^{-\frac{(x-\mu_1)}{b}} \cdot e^{-\frac{(\mu_2-y)}{b}} dx dy \\
&= \frac{1}{4b^2} \int_{\mu_1}^{\mu_2} \left(\int_{\mu_2}^{\infty} (x - y) \cdot e^{-\frac{(x-\mu_1)}{b}} dx \right) \cdot e^{-\frac{(\mu_2-y)}{b}} dy \\
&= \frac{1}{4b^2} \int_{\mu_1}^{\mu_2} \left(e^{\frac{\mu_1-\mu_2}{b}} (-by + b\mu_2 + b^2) \right) \cdot e^{-\frac{(\mu_2-y)}{b}} dy \\
&= \frac{1}{4b} \int_{\mu_1}^{\mu_2} \left(e^{\frac{\mu_1-\mu_2}{b}} (-y + \mu_2 + b) \right) \cdot e^{-\frac{(\mu_2-y)}{b}} dy \\
&= \frac{1}{4b} \left(2b^2 e^{\frac{\mu_1-\mu_2}{b}} - e^{\frac{2\mu_1-2\mu_2}{b}} (b\mu_2 - b\mu_1 + 2b^2) \right) \\
&= \frac{1}{4} \left(2be^{\frac{\mu_1-\mu_2}{b}} + e^{\frac{2\mu_1-2\mu_2}{b}} (\mu_1 - \mu_2 - 2b) \right)
\end{aligned}$$

Rewriting Equation 68 for the part of the space where $\mu_2 < x, \mu_2 < y$ is

$$\begin{aligned}
d_{\mu_2 < x, \mu_2 < y}(X, Y) &= \frac{1}{4b^2} \int_{\mu_2}^{\infty} \int_{\mu_2}^{\infty} |x - y| \cdot e^{-\frac{(x-\mu_1)}{b}} \cdot e^{-\frac{(y-\mu_2)}{b}} dx dy \\
&= \frac{1}{4b^2} \int_{\mu_2}^{\infty} \left(\int_{\mu_2}^{\infty} |x - y| \cdot e^{-\frac{(x-\mu_1)}{b}} dx \right) \cdot e^{-\frac{(y-\mu_2)}{b}} dy \\
&= \frac{1}{4b^2} \int_{\mu_2}^{\infty} \left(\int_{\mu_2}^y (y - x) \cdot e^{-\frac{(x-\mu_1)}{b}} dx + \int_y^{\infty} (x - y) \cdot e^{-\frac{(x-\mu_1)}{b}} dx \right) \cdot e^{-\frac{(y-\mu_2)}{b}} dy \\
&= \frac{1}{4b^2} \int_{\mu_2}^{\infty} \left(\left(b^2 e^{\frac{\mu_1-y}{b}} + e^{\frac{\mu_1-\mu_2}{b}} (by - b\mu_2 - b^2) \right) + \left(b^2 e^{\frac{\mu_1-y}{b}} \right) \right) \cdot e^{-\frac{(y-\mu_2)}{b}} dy \\
&= \frac{1}{4b} \int_{\mu_2}^{\infty} \left(2be^{\frac{\mu_1-y}{b}} + e^{\frac{\mu_1-\mu_2}{b}} (y - \mu_2 - b) \right) \cdot e^{-\frac{(y-\mu_2)}{b}} dy \\
&= \frac{1}{4b} b^2 e^{\frac{\mu_1-\mu_2}{b}} \\
&= \frac{1}{4} b e^{-\frac{(\mu_2-\mu_1)}{b}}.
\end{aligned}$$

We can combine each of the probability weighted distances as

$$\begin{aligned}
d(X, Y) &= d_{x \leq \mu_1, y \leq \mu_1}(X, Y) + d_{x \leq \mu_1, \mu_1 < y \leq \mu_2}(X, Y) + d_{x \leq \mu_1, \mu_2 < y}(X, Y) + d_{\mu_1 < x \leq \mu_2, y \leq \mu_1}(X, Y) + d_{\mu_1 < x \leq \mu_2, \mu_1 < y \leq \mu_2}(X, Y) \\
&\quad + d_{\mu_1 < x \leq \mu_2, \mu_2 < y}(X, Y) + d_{\mu_2 < x, y \leq \mu_1}(X, Y) + d_{\mu_2 < x, \mu_1 < y \leq \mu_2}(X, Y) + d_{\mu_2 < x, \mu_2 < y}(X, Y) \\
&= \frac{1}{4} b e^{\frac{-(\mu_2 - \mu_1)}{b}} \\
&\quad + \frac{1}{4} (\mu_2 - \mu_1) \\
&\quad + \frac{1}{4} (\mu_2 - \mu_1 + 2b) \\
&\quad + \frac{1}{4} \left(2b e^{\frac{\mu_1 - \mu_2}{b}} + e^{\frac{2\mu_1 - 2\mu_2}{b}} (\mu_1 - \mu_2 - 2b) \right) \\
&\quad + \frac{1}{4} \left(\mu_2 - \mu_1 - 2b + e^{\frac{\mu_1 - \mu_2}{b}} (2\mu_2 - 2\mu_1) + e^{\frac{2\mu_1 - 2\mu_2}{b}} (\mu_2 - \mu_1 + 2b) \right) \\
&\quad + \frac{1}{4} (\mu_2 - \mu_1) \\
&\quad + \frac{1}{4} e^{\frac{-2(\mu_2 - \mu_1)}{b}} (2b + \mu_2 - \mu_1) \\
&\quad + \frac{1}{4} \left(2b e^{\frac{\mu_1 - \mu_2}{b}} + e^{\frac{2\mu_1 - 2\mu_2}{b}} (\mu_1 - \mu_2 - 2b) \right) \\
&\quad + \frac{1}{4} b e^{\frac{-(\mu_2 - \mu_1)}{b}} \\
&= b e^{\frac{-(\mu_2 - \mu_1)}{b}} \\
&\quad + \frac{1}{2} (\mu_2 - \mu_1 + b) \\
&\quad + \frac{1}{4} \left(2b e^{\frac{\mu_1 - \mu_2}{b}} + e^{\frac{2\mu_1 - 2\mu_2}{b}} (\mu_1 - \mu_2 - 2b) \right) \\
&\quad + \frac{1}{4} \left(\mu_2 - \mu_1 - 2b + e^{\frac{\mu_1 - \mu_2}{b}} (2\mu_2 - 2\mu_1) + e^{\frac{2\mu_1 - 2\mu_2}{b}} (\mu_2 - \mu_1 + 2b) \right) \\
&\quad + \frac{1}{4} (\mu_2 - \mu_1) \\
&= b e^{\frac{-(\mu_2 - \mu_1)}{b}} \\
&\quad + (\mu_2 - \mu_1) \\
&\quad + \frac{1}{4} \left(2b e^{\frac{\mu_1 - \mu_2}{b}} \right) \\
&\quad + \frac{1}{4} \left(e^{\frac{\mu_1 - \mu_2}{b}} (2\mu_2 - 2\mu_1) \right) \\
&= b e^{\frac{-(\mu_2 - \mu_1)}{b}} + (\mu_2 - \mu_1) + \frac{1}{2} b e^{\frac{\mu_1 - \mu_2}{b}} + \frac{1}{2} e^{\frac{\mu_1 - \mu_2}{b}} (\mu_2 - \mu_1) \\
d(X, Y) &= \mu_2 - \mu_1 + \frac{1}{2} e^{\frac{-(\mu_2 - \mu_1)}{b}} (3b + \mu_2 - \mu_1).
\end{aligned}$$

To remove the assumption that $\mu_1 \leq \mu_2$, we can rewrite this result as

$$d(X, Y) = |\mu_2 - \mu_1| + \frac{1}{2} e^{\frac{-|\mu_2 - \mu_1|}{b}} (3b + |\mu_2 - \mu_1|). \quad (69)$$

This completes the derivation of LK distance with Laplace Distributions. \square

A.2 Surprisal Is a Distance Metric

Theorem 2. *The function $d(x, y)$ defined as $d(x, y) = \sum_{j \in J} \frac{1}{b_j} \left(|x_j - y_j| + \frac{1}{2} e^{\frac{-|x_j - y_j|}{b_j}} (3b_j + |x_j - y_j|) - 1.5 \right)$ is a valid distance metric for $x_j, y_j \in \mathbb{R}$ and $b_j > 0$.*

Proof. We can rewrite Equation 9 in the style of Equation 69 for multiple dimensions $j \in J$ as

$$d(x, y) = \sum_{j \in J} \frac{1}{b_j} \left(|x_j - y_j| + \frac{1}{2} e^{-\frac{|x_j - y_j|}{b_j}} (3b_j + |x_j - y_j|) - 1.5 \right). \quad (70)$$

To prove that $d(x, y)$ is a distance measure (or metric) when $x_j, y_j \in \mathbb{R}$ and $b_j > 0$, we need to show that it satisfies the four properties of

- *Nonnegativity:* $d(x, y) \geq 0$ for all x, y ,
- *Identity of indiscernibles:* $d(x, y) = 0$ if and only if $x = y$,
- *Symmetry:* $d(x, y) = d(y, x)$ for all x, y , and
- *Triangle inequality:* $d(x, z) \leq d(x, y) + d(y, z)$ for all x, y, z .

We analyze the terms independently when $|x_j - y_j|$ approaches 0. The absolute difference, $|x_j - y_j|$ approaches 0, and the exponential term, $e^{-\frac{|x_j - y_j|}{b_j}}$ approaches 1. Substituting these into the distance function, we have

$$\begin{aligned} d(x, y) &= \sum_{j \in J} \left(\frac{1}{b_j} \left(0 + \frac{1}{2} \cdot 1 \cdot (3b_j + 0) \right) - 1.5 \right) \\ &= \sum_{j \in J} \left(\frac{1}{b_j} \cdot \frac{3b_j}{2} - 1.5 \right) \\ &= \sum_{j \in J} \left(\frac{3}{2} - 1.5 \right) \\ &= 0. \end{aligned}$$

Thus, as the individual differences approach 0, the distance approaches 0. When x and y are exactly equal, $d(x, y) = 0$, confirming the identity of discernables. As x approaches y , $d(x, y)$ will be small approaching zero, indicating nonnegativity.

Because the absolute difference, $|x_j - y_j|$ is symmetric, the function is symmetric because none of the terms change.

To prove the triangle inequality, we need to show that for any points x, y, z , $d(x, z) \leq d(x, y) + d(y, z)$. For any real numbers a, b, c , $|a - c| \leq |a - b| + |b - c|$. Applying this to the absolute terms of the distances, we have $|x_i - z_i| \leq |x_i - y_i| + |y_i - z_i|$. The term $e^{-\frac{|x_j - z_j|}{b_j}}$ can similarly be bounded using the triangle inequality as

$$\begin{aligned} e^{-\frac{|x_j - z_j|}{b_j}} &\leq e^{-\frac{|x_j - y_j| + |y_j - z_j|}{b_j}} \\ &\leq e^{-\frac{|x_j - y_j|}{b_j}} e^{-\frac{|y_j - z_j|}{b_j}}. \end{aligned}$$

Combining all of these terms using the triangle inequality for the absolute values and the properties of the exponential function, maintains $d(x, z) \leq d(x, y) + d(y, z)$. The contributions from each dimension j will satisfy the triangle inequality due to the properties of absolute values and the continuity of the exponential function.

Having established that the distance function $d(x, y)$ satisfies the four properties of a metric, we conclude that $d(x, y)$ is a valid distance metric. \square

B Numeric Example of Deriving a Prediction Using Iris Dataset

This appendix shows each numerical step in predicting a class in the classic iris data set.

Example data:

class	sepal_length	sepal_width	petal_length	petal_width
setosa	5.1	3.5	1.4	0.2
setosa	4.9	3	1.4	0.2
setosa	4.7	3.2	1.3	0.2
setosa	4.6	3.1	1.5	0.2
setosa	5	3.6	1.4	0.2

sepal_length	sepal_width	petal_length	petal_width
5.5	3	2.4	1

Units of measurement	nominal	cm	cm	cm	cm
class	sepal_length	sepal_width	petal_length	petal_width	
Feature uncertainties (estimated lower bound of mean absolute deviation of predictability)	0.005281045	0.029542797	0.047926591	0.069991721	0.037552974
Probability feature is informative when predicting class	0.254527879	0.234701304	0.255385408	0.255385408	

Howso Engine finds the data records (cases) that would be least surprising if substituted for the input using the math below. Those records are in this table.

Influential cases	.session_and_.session_training_index are lineage of the training data	.session	.session_training_index	class	sepal_length	sepal_width	petal_length	petal_width
0		2f050246-5fad-40b0-85b1-68382d3dd1a7	64	versicolor	5.6	2.9	3.6	1.3
1		2f050246-5fad-40b0-85b1-68382d3dd1a7	79	versicolor	5.7	2.6	3.5	1
2		2f050246-5fad-40b0-85b1-68382d3dd1a7	81	versicolor	5.5	2.4	3.7	1
3		2f050246-5fad-40b0-85b1-68382d3dd1a7	98	versicolor	5.1	2.5	3	1.1
4		2f050246-5fad-40b0-85b1-68382d3dd1a7	80	versicolor	5.5	2.4	3.8	1.1
5		2f050246-5fad-40b0-85b1-68382d3dd1a7	88	versicolor	5.6	3	4.1	1.3
6		2f050246-5fad-40b0-85b1-68382d3dd1a7	69	versicolor	5.6	2.5	3.9	1.1
7		2f050246-5fad-40b0-85b1-68382d3dd1a7	95	versicolor	5.7	3	4.2	1.2
8		2f050246-5fad-40b0-85b1-68382d3dd1a7	31	setosa	5.4	3.4	1.5	0.4
9		2f050246-5fad-40b0-85b1-68382d3dd1a7	67	versicolor	5.8	2.7	4.1	1
10		2f050246-5fad-40b0-85b1-68382d3dd1a7	89	versicolor	5.5	2.5	4	1.3
11		2f050246-5fad-40b0-85b1-68382d3dd1a7	20	setosa	5.4	3.4	1.7	0.2

First we compute the differences between each case and the input data for each feature:

Units of measurement	nominal	cm	cm	cm	cm
.session_training_index	class	sepal_length	sepal_width	petal_length	petal_width
64	versicolor	0.1	0.1	1.2	0.3
79	versicolor	0.2	0.4	1.1	0
81	versicolor	0	0.6	1.3	0
98	versicolor	0.4	0.5	0.6	0.1
80	versicolor	0	0.6	1.4	0.1
88	versicolor	0.1	0	1.7	0.3
69	versicolor	0.1	0.5	1.5	0.1
95	versicolor	0.2	0	1.8	0.2
31	setosa	0.1	0.4	0.9	0.6
67	versicolor	0.3	0.3	1.7	0
89	versicolor	0	0.5	1.6	0.3
20	setosa	0.1	0.4	0.7	0.8

Now compute the expected difference given the deviation, which will always be at least as big as the actual difference

This expected difference takes into account the uncertainty of the values using the maximum entropy assumption that, given the mean absolute error, the error follows the Laplace distribution

Units of measurement	nominal	cm	cm	cm	cm
.session_training_index	class	sepal_length	sepal_width	petal_length	petal_width
64	versicolor	0.103195399	0.115128702	1.20000025	0.300070001
79	versicolor	0.200165655	0.400064525	1.100000098	0.056329461
81	versicolor	0.044314196	0.60000136	1.300000006	0.056329461
98	versicolor	0.400000322	0.500009482	0.600076644	0.107415983
80	versicolor	0.044314196	0.60000136	1.400000002	0.107415983
88	versicolor	0.103195399	0.071889887	1.7	0.300070001
69	versicolor	0.103195399	0.500009482	1.5	0.107415983
95	versicolor	0.200165655	0.071889887	1.8	0.200760451
31	setosa	0.103195399	0.400064525	0.900001445	0.600000041
67	versicolor	0.300007557	0.300424267	1.7	0.056329461
89	versicolor	0.044314196	0.500009482	1.6	0.300070001
20	setosa	0.103195399	0.400064525	0.700020632	0.8

Next, we scale the expected differences by the uncertainty to obtain surprisal of each value.

In order to find the marginal surprisal, we remove the baseline surprisal that comes from the underlying assumption of uncertainty (1.5 nats for continuous features based on Laplace assumption)

Units of measurement	nominal	nats	nats	nats	nats
.session_training_index	class	sepal_length	sepal_width	petal_length	petal_width
64	versicolor	1.993081527	0.902188407	15.64488528	6.490578841
79	versicolor	5.275446978	6.847443782	14.2161459	0
81	versicolor	0	11.01917454	17.07362542	0
98	versicolor	12.03969026	8.932819646	7.073537499	1.360385488
80	versicolor	0	11.01917454	18.50236576	1.360385488
88	versicolor	1.993081527	0	22.78858696	6.490578841
69	versicolor	1.993081527	8.932819646	19.93110615	1.360385488
95	versicolor	5.275446978	0	24.21732737	3.846059924
31	setosa	1.993081527	6.847443782	11.35868433	14.47742063
67	versicolor	8.655015223	4.768425525	22.78858696	0
89	versicolor	0	8.932819646	21.25984656	6.490578841
20	setosa	1.993081527	6.847443782	8.501477645	19.8032394

In this step, we scale the surprisals by feature influence probabilities.

(Multiplying by a feature probability of influence is the same as applying the probability exponentially to the probability itself.)

Units of measurement		nominal	nats	nats	nats	nats
.session_training_index	class	sepal_length	sepal_width	petal_length	petal_width	
64	versicolor	0.507294815	0.211744796	3.995475413	1.657599127	
79	versicolor	1.342748333	1.607103985	3.630596226	0	
81	versicolor	0	2.586214635	4.360354798	0	
98	versicolor	3.064436832	2.09654442	1.806478262	0.347422603	
80	versicolor	0	2.586214635	4.725234233	0.347422603	
88	versicolor	0.507294815	0	5.819872585	1.657599127	
69	versicolor	0.507294815	2.09654442	5.090113681	0.347422603	
95	versicolor	1.342748333	0	6.184752038	0.982227584	
31	setosa	0.507294815	1.607103985	2.900842235	3.697324533	
67	versicolor	2.202942697	1.119155689	5.819872585	0	
89	versicolor	0	2.09654442	5.454993133	1.657599127	
20	setosa	0.507294815	1.607103985	2.171153339	5.057458378	

Next, sum the surprisals for each case and convert the surprisals to each case's probability of being the underlying values as the case being predicted.

These probabilities are often small, because it would be highly improbable for them to be an exact match to the data given differing values.

However, this is still the most representative evidence for the prediction in the data set, so the prediction will use this best evidence.

total surprisal	.session_training_index	class	probability
6.37211415	64	versicolor	0.001708543
6.580448543	79	versicolor	0.001387227
6.946569432	81	versicolor	0.000961929
7.314882117	98	versicolor	0.00066556
7.658871471	80	versicolor	0.00047184
7.984766527	88	versicolor	0.000340612
8.041375519	69	versicolor	0.000321866
8.509727954	95	versicolor	0.000201499
8.712565567	31	setosa	0.000164506
9.141970971	67	versicolor	0.000107076
9.209136679	89	versicolor	0.00010012
9.343010517	20	setosa	8.75754E-05
	total probability		0.006518353

Last, we normalize probabilities to find the support of each.

probability of influence	.session_training_index	class
0.262112721	64	versicolor
0.21281862	79	versicolor
0.147572468	81	versicolor
0.102105509	98	versicolor
0.07238632	80	versicolor
0.052254304	88	versicolor
0.04937841	69	versicolor
0.030912506	95	versicolor
0.025237304	31	setosa
0.01642686	67	versicolor
0.015359776	89	versicolor
0.013435202	20	setosa

Summing up the total probability of each class being correct, we take whichever probability is highest.

versicolor	96.133%
setosa	3.867%
virginica	0.000%

C Details of Empirical Evidence

C.1 Supervised Learning Classification Results

Five small regression datasets (first_principles_ideal_gas, first_principles_newton, 1089_USCrime, 659_sleuth_ex1714, 485_analcatdata_vehicle) were excluded from all algorithms due to LightGBM failures (undefined Spearman correlation from constant predictions).

C.1.1 Howso (Targetless)

Table 11: Classification Results across 146 Datasets

Dataset	Accuracy	Precision	Recall	MCC
GAMETES_Epistasis_2_Way_1000atts_0.4H_EDM_1_EDM_1_1	0.5172	0.5202	0.5196	0.0398
GAMETES_Epistasis_2_Way_20atts_0.1H_EDM_1_1	0.5792	0.5853	0.5803	0.1656
GAMETES_Epistasis_2_Way_20atts_0.4H_EDM_1_1	0.7694	0.7797	0.7714	0.5510
GAMETES_Epistasis_3_Way_20atts_0.2H_EDM_1_1	0.5528	0.5578	0.5541	0.1118
GAMETES_Heterogeneity_20atts_1600_Het_0.4_0.2_50_EDM_2_001	0.6316	0.6351	0.6336	0.2687
GAMETES_Heterogeneity_20atts_1600_Het_0.4_0.2_75_EDM_2_001	0.6809	0.6839	0.6821	0.3660
Hill_Valley_with_noise	0.5263	0.5272	0.5268	0.0540
Hill_Valley_without_noise	0.5588	0.5604	0.5601	0.1205
adult	0.8546	0.8047	0.7817	0.5860
agaricus_lepiota	1.0000	1.0000	1.0000	1.0000
allbp	0.9647	0.7226	0.6459	0.5216
allhyper	0.9792	0.4997	0.4744	0.5291
allhypo	0.9492	0.8029	0.6625	0.6124
allrep	0.9666	0.4594	0.2923	0.2054
analcatdata_aids	0.4672	0.4949	0.4904	-0.0080
analcatdata_asbestos	0.7078	0.7193	0.7219	0.4405
analcatdata_authorship	0.9993	0.9996	0.9995	0.9990
analcatdata_bankruptcy	0.8426	0.8599	0.8422	0.6990
analcatdata_boxing1	0.8292	0.8329	0.7936	0.6228
analcatdata_boxing2	0.8118	0.8195	0.8104	0.6293
analcatdata_creditscore	0.8492	0.8276	0.7724	0.5908
analcatdata_cyyoung8092	0.7944	0.7407	0.6406	0.3673
analcatdata_cyyoung9302	0.8703	0.8462	0.7265	0.5555
analcatdata_dmft	0.1668	0.1701	0.1692	0.0007
analcatdata_fraud	0.6685	0.3506	0.5164	0.0000
analcatdata_germangss	0.3514	0.3622	0.3593	0.1441
analcatdata_happiness	0.4631	0.4687	0.5055	0.2327
analcatdata_japansolvent	0.7213	0.7567	0.7100	0.4616
analcatdata_lawsuit	0.9782	0.9050	0.9385	0.8360
ann_thyroid	0.9648	0.8363	0.8204	0.7435
appendicitis	0.8368	0.7435	0.7372	0.4682
auto_insurance_symboling	0.7549	0.6817	0.6896	0.6837
backache	0.8658	0.4329	0.5000	0.0000
balance_scale	0.8480	0.5735	0.6148	0.7300
banana	0.8712	0.8697	0.8699	0.7397
biomed	0.9403	0.9556	0.9218	0.8763
breast_cancer	0.7113	0.5057	0.5140	0.0700
breast_cancer_wisconsin_diagnostic	0.9747	0.9756	0.9701	0.9456
breast_cancer_wisconsin_original	0.9476	0.9495	0.9301	0.8793

(Continued on next page)

(Continued from previous page)

Dataset	Accuracy	Precision	Recall	MCC
bupa	0.5336	0.5394	0.5389	0.0783
calendarDOW	0.6052	0.5784	0.5718	0.5014
car_evaluation	0.9550	0.8945	0.9236	0.9080
cars	0.9098	0.8862	0.8725	0.8339
chess	0.9470	0.9503	0.9449	0.8951
churn	0.9021	0.8766	0.6955	0.5418
clean1	0.9446	0.9426	0.9472	0.8897
clean2	1.0000	1.0000	1.0000	1.0000
cloud	0.6013	0.6340	0.6167	0.4743
coil2000	0.9414	0.6722	0.5038	0.0499
collins	0.9997	0.9995	0.9995	0.9996
confidence	0.8055	0.8079	0.8040	0.7719
congressional_voting_records	0.9553	0.9493	0.9576	0.9068
connect_4	0.7809	0.6605	0.5528	0.5189
contraceptive_method	0.4851	0.4715	0.4663	0.2098
corral	0.9727	0.9751	0.9745	0.9496
credit_approval_australia	0.8454	0.8578	0.8313	0.6882
credit_approval_germany	0.7106	0.6961	0.5495	0.1927
dermatology	0.9416	0.9423	0.9146	0.9291
dis	0.9813	0.6841	0.5976	0.2572
dna	0.7236	0.8199	0.6360	0.5636
ecoli	0.8668	0.8319	0.7916	0.8136
fars	0.7888	0.5839	0.5430	0.7140
flags	0.4080	0.3431	0.3361	0.2328
glass2	0.8647	0.8770	0.8602	0.7367
haberman	0.7356	0.6600	0.5926	0.2388
hayes_roth	0.7235	0.7917	0.7083	0.5612
heart_disease_cleveland	0.7880	0.7918	0.7865	0.5781
heart_disease_hungarian	0.8200	0.8122	0.7977	0.6094
heart_disease_va_long_beach	0.7384	0.4712	0.5014	0.0117
heart_disease_zurich	0.9318	0.5369	0.5698	-0.0006
hepatitis	0.7853	0.5293	0.5233	0.0825
horse_colic_lesion_type	0.4385	0.2783	0.2954	0.1902
horse_colic_outcome	0.6334	0.5090	0.4335	0.2186
horse_colic_surgery	0.6817	0.6605	0.6545	0.3145
hypothyroid	0.9709	0.8650	0.7644	0.6194
ionosphere	0.8828	0.9021	0.8493	0.7491
iris	0.9563	0.9571	0.9573	0.9355
irish	0.9875	0.9867	0.9886	0.9753
kddcup	0.9985	0.7153	0.6949	0.9975
kr_vs_kp	0.9410	0.9439	0.9401	0.8839
krkopt	0.5727	0.5622	0.5026	0.5217
labor	0.8354	0.8215	0.7992	0.6202
led24	0.7097	0.7268	0.7078	0.6786
led7	0.7432	0.7437	0.7422	0.7153
letter	0.9653	0.9659	0.9654	0.9639
lupus	0.7133	0.7067	0.6859	0.3907
lymphography	0.6833	0.5768	0.5490	0.4788
magic	0.8185	0.8188	0.7714	0.5883
mfeat_factors	0.9669	0.9671	0.9672	0.9633

(Continued on next page)

(Continued from previous page)

Dataset	Accuracy	Precision	Recall	MCC
mfeat_fourier	0.8339	0.8406	0.8378	0.8159
mfeat_karhunen	0.9669	0.9677	0.9667	0.9633
mfeat_morphological	0.7123	0.7189	0.7173	0.6805
mfeat_pixel	0.9744	0.9742	0.9741	0.9716
mfeat_zernike	0.8019	0.8075	0.8097	0.7799
mnist	0.9132	0.9142	0.9132	0.9037
mofn_3_7_10	0.9371	0.9626	0.8699	0.8251
molecular_biology_promoters	0.5089	0.2665	0.5020	0.0087
monk1	1.0000	1.0000	1.0000	1.0000
monk2	0.6620	0.6137	0.5954	0.2082
monk3	0.9881	0.9886	0.9875	0.9762
movement_libras	0.8750	0.9201	0.8644	0.8682
mushroom	1.0000	1.0000	1.0000	1.0000
mux6	0.8536	0.8634	0.8649	0.7276
new_thyroid	0.9535	0.9391	0.9408	0.9002
nursery	0.9213	0.9032	0.7934	0.8845
optdigits	0.9813	0.9817	0.9816	0.9793
page_blocks	0.9683	0.8764	0.8635	0.8267
parity5	0.2304	0.1969	0.2828	-0.4505
parity5+5	1.0000	1.0000	1.0000	1.0000
pendigits	0.9934	0.9935	0.9933	0.9927
penguins	0.9855	0.9879	0.9783	0.9775
phoneme	0.8874	0.8732	0.8527	0.7255
poker	0.9176	0.5974	0.3126	0.8519
postoperative_patient_data	0.6389	0.3301	0.4821	-0.0648
prnn_crabs	0.9744	0.9748	0.9745	0.9492
prnn_synth	0.8587	0.8610	0.8586	0.7196
profb	0.6947	0.6424	0.5910	0.2271
ring	0.7573	0.8391	0.7514	0.5838
saheart	0.6627	0.6096	0.5880	0.1959
satimage	0.9088	0.8945	0.8861	0.8873
schizo	0.5520	0.4049	0.3881	0.0923
segmentation	0.9740	0.9756	0.9753	0.9698
shuttle	0.9982	0.7627	0.6884	0.9950
sleep	0.7541	0.6976	0.6334	0.6277
sonar	0.8571	0.8571	0.8365	0.6934
soybean	0.9012	0.9016	0.8782	0.8920
spambase	0.9374	0.9380	0.9302	0.8682
spect	0.6762	0.6705	0.7457	0.4079
spectf	0.9000	0.8532	0.9140	0.7648
splice	0.4817	0.6182	0.6192	0.3817
tae	0.5161	0.5264	0.5189	0.2872
texture	0.9870	0.9872	0.9872	0.9857
threeOf9	0.9458	0.9459	0.9452	0.8910
tic_tac_toe	0.9745	0.9810	0.9640	0.9449
titanic	0.7323	0.7248	0.6304	0.3423
tokyo1	0.9329	0.9285	0.9266	0.8550
twonorm	0.9720	0.9720	0.9721	0.9441
vehicle	0.7235	0.7096	0.7263	0.6334
vowel	0.9798	0.9799	0.9799	0.9778

(Continued on next page)

(Continued from previous page)

Dataset	Accuracy	Precision	Recall	MCC
waveform_21	0.8420	0.8424	0.8425	0.7639
waveform_40	0.8503	0.8509	0.8511	0.7762
wine_quality_red	0.6458	0.4187	0.3461	0.4332
wine_quality_white	0.6507	0.4486	0.3745	0.4718
wine_recognition	0.9722	0.9675	0.9739	0.9572
xd6	0.9892	0.9903	0.9860	0.9763
yeast	0.5688	0.5291	0.5127	0.4372

C.1.2 Howso (Single-Target)

Table 12: Classification Results across 146 Datasets

Dataset	Accuracy	Precision	Recall	MCC
GAMETES_Epistasis_2_Way_1000atts_0.4H_EDM_1_EDM_1_1	0.5164	0.5173	0.5144	0.0316
GAMETES_Epistasis_2_Way_20atts_0.1H_EDM_1_1	0.6493	0.6604	0.6504	0.3106
GAMETES_Epistasis_2_Way_20atts_0.4H_EDM_1_1	0.7910	0.8215	0.7917	0.6124
GAMETES_Epistasis_3_Way_20atts_0.2H_EDM_1_1	0.6569	0.6598	0.6577	0.3175
GAMETES_Heterogeneity_20atts_1600_Het_0.4_0.2_50_EDM_2_001	0.6806	0.6810	0.6805	0.3615
GAMETES_Heterogeneity_20atts_1600_Het_0.4_0.2_75_EDM_2_001	0.7188	0.7295	0.7192	0.4485
Hill_Valley_with_noise	0.5203	0.5261	0.5233	0.0493
Hill_Valley_without_noise	0.5734	0.5769	0.5765	0.1534
adult	0.8168	0.7489	0.7535	0.5022
agaricus_lepiota	1.0000	1.0000	1.0000	1.0000
allbp	0.9589	0.5787	0.5675	0.4829
allhyper	0.9794	0.5519	0.5033	0.5386
allhypo	0.9561	0.7843	0.7043	0.6878
allrep	0.9684	0.6251	0.4630	0.4037
analcatdata_aids	0.5532	0.5962	0.5774	0.1891
analcatdata_asbestos	0.7514	0.7608	0.7586	0.5184
analcatdata_authorship	0.9993	0.9996	0.9995	0.9990
analcatdata_bankruptcy	0.8032	0.8178	0.7913	0.6048
analcatdata_boxing1	0.8138	0.8112	0.7766	0.5841
analcatdata_boxing2	0.7915	0.7965	0.7853	0.5811
analcatdata_creditscore	0.9750	0.9638	0.9829	0.9456
analcatdata_cyyoung8092	0.7625	0.6632	0.5989	0.2601
analcatdata_cyyoung9302	0.8428	0.7883	0.7258	0.5011
analcatdata_dmft	0.1885	0.1548	0.1830	0.0202
analcatdata_fraud	0.6487	0.5563	0.5799	0.1682
analcatdata_germangss	0.3595	0.3674	0.3702	0.1666
analcatdata_happiness	0.5645	0.5955	0.6028	0.3909
analcatdata_japansolvent	0.7786	0.8066	0.7698	0.5714
analcatdata_lawsuit	0.9763	0.9098	0.9201	0.8198
ann_thyroid	0.9683	0.8206	0.8896	0.7911
appendicitis	0.8482	0.7693	0.7266	0.4829
auto_insurance_symboling	0.8273	0.8399	0.8347	0.7773
backache	0.8349	0.5955	0.5752	0.1677
balance_scale	0.8989	0.5993	0.6517	0.8235
banana	0.8961	0.8965	0.8934	0.7898
biomed	0.9648	0.9693	0.9560	0.9249

(Continued on next page)

(Continued from previous page)

Dataset	Accuracy	Precision	Recall	MCC
breast_cancer	0.7237	0.6595	0.6162	0.2706
breast_cancer_wisconsin_diagnostic	0.9766	0.9771	0.9727	0.9498
breast_cancer_wisconsin_original	0.9571	0.9544	0.9471	0.9013
bupa	0.5977	0.6394	0.6081	0.2443
calendarDOW	0.6056	0.5982	0.5723	0.5026
car_evaluation	0.9488	0.8829	0.8916	0.8933
cars	0.9947	0.9919	0.9909	0.9899
chess	0.9870	0.9871	0.9867	0.9738
churn	0.9034	0.8739	0.7052	0.5522
clean1	0.8901	0.8889	0.8940	0.7828
clean2	0.9907	0.9798	0.9854	0.9652
cloud	0.8138	0.8146	0.8071	0.7528
coil2000	0.9330	0.5470	0.5159	0.0566
collins	1.0000	1.0000	1.0000	1.0000
confidence	0.8129	0.8044	0.8079	0.7838
congressional_voting_records	0.9531	0.9474	0.9545	0.9019
connect_4	0.8018	0.7076	0.5741	0.5696
contraceptive_method	0.3785	0.4583	0.4322	0.1419
corral	1.0000	1.0000	1.0000	1.0000
credit_approval_australia	0.8631	0.8637	0.8646	0.7282
credit_approval_germany	0.7033	0.6515	0.6194	0.2675
dermatology	0.9551	0.9475	0.9491	0.9444
dis	0.9841	0.7716	0.6776	0.4183
dna	0.9033	0.8942	0.9144	0.8534
ecoli	0.8725	0.8602	0.8166	0.8211
fars	0.7815	0.5741	0.5397	0.7042
flags	0.4502	0.4271	0.4147	0.2888
glass2	0.8312	0.8432	0.8255	0.6678
haberman	0.7341	0.6523	0.5968	0.2394
hayes_roth	0.7381	0.7942	0.7353	0.5883
heart_disease_cleveland	0.8107	0.8135	0.8055	0.6187
heart_disease_hungarian	0.8245	0.8149	0.8089	0.6235
heart_disease_va_long_beach	0.7198	0.5909	0.5452	0.1252
heart_disease_zurich	0.9011	0.4750	0.4928	-0.0227
hepatitis	0.8046	0.7200	0.6634	0.3740
horse_colic_lesion_type	0.4933	0.3153	0.3288	0.2661
horse_colic_outcome	0.6988	0.6128	0.5383	0.4002
horse_colic_surgery	0.7489	0.7365	0.7215	0.4572
hypothyroid	0.9737	0.8841	0.7826	0.6561
ionosphere	0.9023	0.9019	0.8875	0.7890
iris	0.9662	0.9654	0.9684	0.9502
irish	1.0000	1.0000	1.0000	1.0000
kddcup	0.9995	0.7160	0.6856	0.9991
kr_vs_kp	0.9868	0.9868	0.9868	0.9736
krkoft	0.6947	0.7346	0.6201	0.6580
labor	0.8889	0.8709	0.8577	0.7258
led24	0.7142	0.7143	0.7142	0.6827
led7	0.7349	0.7397	0.7338	0.7064
letter	0.9565	0.9574	0.9567	0.9548
lupus	0.7795	0.7851	0.7446	0.5252

(Continued on next page)

(Continued from previous page)

Dataset	Accuracy	Precision	Recall	MCC
lymphography	0.7583	0.5424	0.5517	0.5517
magic	0.8586	0.8684	0.8170	0.6834
mfeat_factors	0.9531	0.9537	0.9532	0.9480
mfeat_fourier	0.8422	0.8486	0.8462	0.8253
mfeat_karhunen	0.9706	0.9708	0.9708	0.9673
mfeat_morphological	0.7100	0.7187	0.7156	0.6788
mfeat_pixel	0.9750	0.9747	0.9749	0.9722
mfeat_zernike	0.8394	0.8387	0.8422	0.8215
mnist	0.9126	0.9138	0.9126	0.9030
mofn_3_7_10	1.0000	1.0000	1.0000	1.0000
molecular_biology_promoters	0.8106	0.8377	0.8126	0.6489
monk1	1.0000	1.0000	1.0000	1.0000
monk2	0.8195	0.8742	0.7552	0.6165
monk3	0.9796	0.9796	0.9794	0.9589
movement_libras	0.8194	0.8593	0.8149	0.8085
mushroom	1.0000	1.0000	1.0000	1.0000
mux6	0.9712	0.9717	0.9743	0.9458
new_thyroid	0.9360	0.9225	0.9180	0.8627
nursery	0.9525	0.9578	0.8513	0.9306
optdigits	0.9875	0.9878	0.9875	0.9862
page_blocks	0.9641	0.8492	0.8640	0.8084
parity5	0.8616	0.8743	0.9018	0.7968
parity5+5	1.0000	1.0000	1.0000	1.0000
pendigits	0.9945	0.9946	0.9945	0.9939
penguins	0.8802	0.8610	0.8550	0.8129
phoneme	0.8970	0.8877	0.8632	0.7505
poker	0.6303	0.3210	0.2413	0.3298
postoperative_patient_data	0.6389	0.3393	0.4643	-0.0714
prnn_crabs	0.9643	0.9655	0.9642	0.9296
prnn_synth	0.8561	0.8583	0.8562	0.7145
profb	0.6691	0.6047	0.5570	0.1535
ring	0.7064	0.8176	0.6997	0.5037
saheart	0.6638	0.6055	0.5708	0.1715
satimage	0.9099	0.8975	0.8923	0.8888
schizo	0.5409	0.4014	0.3961	0.0983
segmentation	0.9675	0.9682	0.9692	0.9621
shuttle	0.9989	0.9237	0.9346	0.9968
sleep	0.7589	0.6990	0.6413	0.6357
sonar	0.7619	0.7476	0.7476	0.4952
soybean	0.9086	0.9328	0.9341	0.8994
spambase	0.9099	0.9132	0.8986	0.8117
spect	0.7453	0.6844	0.7410	0.4197
spectf	0.9143	0.8707	0.9234	0.7924
splice	0.9112	0.8936	0.9306	0.8656
tae	0.5806	0.5957	0.5842	0.3892
texture	0.9870	0.9869	0.9870	0.9857
threeOf9	0.9857	0.9855	0.9858	0.9712
tic_tac_toe	0.9751	0.9802	0.9654	0.9455
titanic	0.7836	0.7576	0.7297	0.4862
tokyo1	0.9277	0.9218	0.9211	0.8428

(Continued on next page)

(Continued from previous page)

Dataset	Accuracy	Precision	Recall	MCC
twonorm	0.9745	0.9745	0.9746	0.9491
vehicle	0.7294	0.7168	0.7343	0.6435
vowel	0.9663	0.9673	0.9668	0.9631
waveform_21	0.8607	0.8683	0.8604	0.7962
waveform_40	0.8607	0.8647	0.8618	0.7942
wine_quality_red	0.6385	0.3568	0.3179	0.4119
wine_quality_white	0.6551	0.5408	0.3605	0.4699
wine_recognition	0.9833	0.9845	0.9784	0.9732
xd6	0.9977	0.9982	0.9970	0.9952
yeast	0.5851	0.5495	0.5320	0.4589

C.1.3 XGBoost

Table 13: Classification Results across 146 Datasets

Dataset	Accuracy	Precision	Recall	MCC
GAMETES_Epistasis_2_Way_1000atts_0.4H_EDM_1_EDM_1_1	0.4930	0.4941	0.4941	-0.0118
GAMETES_Epistasis_2_Way_20atts_0.1H_EDM_1_1	0.5920	0.5916	0.5914	0.1831
GAMETES_Epistasis_2_Way_20atts_0.4H_EDM_1_1	0.7339	0.7343	0.7342	0.4686
GAMETES_Epistasis_3_Way_20atts_0.2H_EDM_1_1	0.5603	0.5606	0.5607	0.1213
GAMETES_Heterogeneity_20atts_1600_Het_0.4_0.2_50_EDM_2_001	0.6393	0.6391	0.6392	0.2783
GAMETES_Heterogeneity_20atts_1600_Het_0.4_0.2_75_EDM_2_001	0.6813	0.6816	0.6817	0.3633
Hill_Valley_with_noise	0.5556	0.5555	0.5555	0.1110
Hill_Valley_without_noise	0.6032	0.6045	0.6042	0.2087
adult	0.8734	0.8366	0.8005	0.6361
agaricus_lepiota	1.0000	1.0000	1.0000	1.0000
allbp	0.9739	0.7331	0.7249	0.6687
allhyper	0.9866	0.6966	0.5606	0.6771
allhypo	0.9828	0.9193	0.8731	0.8792
allrep	0.9854	0.8291	0.7068	0.7606
anacatdata_aids	0.6000	0.6200	0.6017	0.2184
anacatdata_asbestos	0.7510	0.7581	0.7525	0.5093
anacatdata_authorship	0.9873	0.9886	0.9845	0.9814
anacatdata_bankruptcy	0.8700	0.8696	0.8789	0.7473
anacatdata_boxing1	0.7903	0.7712	0.7527	0.5216
anacatdata_boxing2	0.7333	0.7335	0.7325	0.4658
anacatdata_creditscore	0.9750	0.9614	0.9832	0.9434
anacatdata_cyyoung8092	0.8050	0.7384	0.7262	0.4573
anacatdata_cyyoung9302	0.8355	0.7540	0.7376	0.4843
anacatdata_dmft	0.1926	0.1995	0.1964	0.0309
anacatdata_fraud	0.7333	0.6898	0.6779	0.3396
anacatdata_germangss	0.3212	0.3218	0.3244	0.0977
anacatdata_happiness	0.4500	0.4894	0.4872	0.2056
anacatdata_japansolvent	0.8030	0.8060	0.8077	0.6122
anacatdata_lawsuit	0.9840	0.9383	0.9495	0.8785
ann_thyroid	0.9944	0.9789	0.9564	0.9587
appendicitis	0.8500	0.7513	0.7372	0.4757
auto_insurance_symboling	0.7931	0.7621	0.7528	0.7321
backache	0.8368	0.5936	0.5459	0.1303

(Continued on next page)

(Continued from previous page)

Dataset	Accuracy	Precision	Recall	MCC
balance_scale	0.8635	0.6552	0.6536	0.7591
banana	0.8848	0.8837	0.8831	0.7668
biomed	0.8958	0.8945	0.8835	0.7772
breast_cancer	0.6694	0.5917	0.5845	0.1749
breast_cancer_wisconsin_diagnostic	0.9749	0.9751	0.9725	0.9474
breast_cancer_wisconsin_original	0.9551	0.9506	0.9480	0.8984
bupa	0.5522	0.5550	0.5546	0.1095
calendarDOW	0.6075	0.5888	0.5829	0.5029
car_evaluation	0.9922	0.9806	0.9835	0.9836
cars	0.9547	0.9502	0.9359	0.9150
chess	0.9949	0.9949	0.9948	0.9897
churn	0.9550	0.9407	0.8718	0.8094
clean1	1.0000	1.0000	1.0000	1.0000
clean2	1.0000	1.0000	1.0000	1.0000
cloud	0.6606	0.6747	0.6647	0.5567
coil2000	0.9344	0.5914	0.5264	0.0975
collins	0.9780	0.9742	0.9724	0.9758
confidence	0.7844	0.7862	0.7824	0.7549
congressional_voting_records	0.9569	0.9520	0.9574	0.9093
connect_4	0.8324	0.7352	0.6267	0.6434
contraceptive_method	0.5157	0.4887	0.4853	0.2476
corral	1.0000	1.0000	1.0000	1.0000
credit_approval_australia	0.8768	0.8747	0.8776	0.7523
credit_approval_germany	0.7557	0.7191	0.6819	0.3989
dermatology	0.9617	0.9571	0.9586	0.9521
dis	0.9869	0.8455	0.6909	0.5058
dna	0.9592	0.9506	0.9548	0.9336
ecoli	0.8485	0.7722	0.7922	0.7976
fars	0.8028	0.6171	0.5712	0.7338
flags	0.4167	0.3658	0.4307	0.2761
glass2	0.8689	0.8714	0.8678	0.7390
haberman	0.5806	0.4747	0.4728	-0.0524
hayes_roth	0.9062	0.9299	0.8839	0.8479
heart_disease_cleveland	0.8016	0.7994	0.7977	0.5970
heart_disease_hungarian	0.8085	0.7964	0.7960	0.5920
heart_disease_va_long_beach	0.7163	0.5931	0.5719	0.1601
heart_disease_zurich	0.9190	0.5211	0.5438	0.0382
hepatitis	0.7097	0.6101	0.6005	0.2104
horse_colic_lesion_type	0.5142	0.3386	0.3526	0.3065
horse_colic_outcome	0.7101	0.6566	0.5902	0.4431
horse_colic_surgery	0.7376	0.7203	0.7096	0.4292
hypothyroid	0.9819	0.9082	0.8823	0.7888
ionosphere	0.9197	0.9177	0.9018	0.8190
iris	0.9511	0.9533	0.9518	0.9281
irish	1.0000	1.0000	1.0000	1.0000
kddcup	0.9998	0.8475	0.7990	0.9997
kr_vs_kp	0.9944	0.9944	0.9944	0.9888
krkopt	0.8471	0.8714	0.8584	0.8291
labor	0.8562	0.8486	0.8440	0.6905
led24	0.6915	0.6891	0.6906	0.6572

(Continued on next page)

(Continued from previous page)

Dataset	Accuracy	Precision	Recall	MCC
led7	0.7350	0.7363	0.7345	0.7066
letter	0.9637	0.9634	0.9630	0.9623
lupus	0.7111	0.7011	0.6997	0.4003
lymphography	0.8000	0.5370	0.5508	0.6157
magic	0.8788	0.8739	0.8555	0.7292
mfeat_factors	0.9696	0.9700	0.9695	0.9662
mfeat_fourier	0.8421	0.8450	0.8443	0.8249
mfeat_karhunen	0.9425	0.9417	0.9426	0.9361
mfeat_morphological	0.6817	0.6859	0.6861	0.6462
mfeat_pixel	0.9650	0.9641	0.9656	0.9611
mfeat_zernike	0.7900	0.7859	0.7917	0.7669
mnist	0.9771	0.9770	0.9770	0.9746
mofn_3_7_10	1.0000	1.0000	1.0000	1.0000
molecular_biology_promoters	0.8602	0.8672	0.8608	0.7275
monk1	0.9979	0.9980	0.9980	0.9959
monk2	0.9772	0.9750	0.9772	0.9521
monk3	0.9830	0.9834	0.9826	0.9660
movement_libras	0.7361	0.7567	0.7517	0.7195
mushroom	1.0000	1.0000	1.0000	1.0000
mux6	0.9949	0.9939	0.9961	0.9899
new_thyroid	0.9302	0.9677	0.8704	0.8640
nursery	1.0000	1.0000	1.0000	1.0000
optdigits	0.9769	0.9766	0.9773	0.9743
page_blocks	0.9644	0.8631	0.7786	0.8258
parity5	0.0667	0.0564	0.0731	-0.8676
parity5+5	0.9975	0.9976	0.9974	0.9950
pendigits	0.9930	0.9928	0.9929	0.9922
penguins	0.9754	0.9719	0.9731	0.9613
phoneme	0.9047	0.8880	0.8860	0.7740
poker	0.7756	0.6392	0.2939	0.5891
postoperative_patient_data	0.6111	0.4846	0.4821	-0.0331
prmn_crabs	0.9363	0.9386	0.9372	0.8757
prmn_synth	0.8347	0.8391	0.8344	0.6735
profb	0.6614	0.6029	0.5891	0.1908
ring	0.9720	0.9725	0.9717	0.9443
saheart	0.6503	0.6039	0.5962	0.1996
satimage	0.9270	0.9166	0.9069	0.9099
schizo	0.4930	0.3716	0.3656	0.0272
segmentation	0.9870	0.9846	0.9861	0.9848
shuttle	0.9999	0.9999	0.9958	0.9998
sleep	0.7718	0.7108	0.6559	0.6548
sonar	0.8278	0.8334	0.8301	0.6633
soybean	0.9481	0.9591	0.9459	0.9431
spambase	0.9555	0.9525	0.9552	0.9078
spect	0.8093	0.7171	0.6845	0.3968
spectf	0.8786	0.8504	0.8575	0.7071
splice	0.9545	0.9489	0.9530	0.9276
tae	0.6774	0.6647	0.6667	0.5143
texture	0.9891	0.9889	0.9890	0.9880
threeOf9	0.9989	0.9987	0.9990	0.9977

(Continued on next page)

(Continued from previous page)

Dataset	Accuracy	Precision	Recall	MCC
tic_tac_toe	0.9963	0.9970	0.9953	0.9922
titanic	0.8054	0.7993	0.7260	0.5201
tokyo1	0.9278	0.9222	0.9197	0.8418
twonorm	0.9682	0.9682	0.9683	0.9365
vehicle	0.7412	0.7481	0.7592	0.6551
vowel	0.9019	0.9013	0.9018	0.8922
waveform_21	0.8490	0.8489	0.8490	0.7735
waveform_40	0.8470	0.8470	0.8483	0.7710
wine_quality_red	0.6562	0.4063	0.3481	0.4481
wine_quality_white	0.6745	0.6256	0.4523	0.5059
wine_recognition	0.9722	0.9778	0.9722	0.9590
xd6	1.0000	1.0000	1.0000	1.0000
yeast	0.5807	0.5430	0.5398	0.4515

C.1.4 LightGBM

Table 14: Classification Results across 146 Datasets

Dataset	Accuracy	Precision	Recall	MCC
GAMETES_Epistasis_2_Way_1000atts_0.4H_EDM_1_EDM_1_1	0.4916	0.4924	0.4924	-0.0151
GAMETES_Epistasis_2_Way_20atts_0.1H_EDM_1_1	0.6112	0.6117	0.6115	0.2232
GAMETES_Epistasis_2_Way_20atts_0.4H_EDM_1_1	0.7288	0.7301	0.7283	0.4583
GAMETES_Epistasis_3_Way_20atts_0.2H_EDM_1_1	0.5522	0.5528	0.5528	0.1055
GAMETES_Heterogeneity_20atts_1600_Het_0.4_0.2_50_EDM_2_001	0.6666	0.6673	0.6669	0.3343
GAMETES_Heterogeneity_20atts_1600_Het_0.4_0.2_75_EDM_2_001	0.6919	0.6919	0.6914	0.3834
Hill_Valley_with_noise	0.5988	0.5987	0.5985	0.1973
Hill_Valley_without_noise	0.5712	0.5707	0.5704	0.1410
adult	0.8745	0.8408	0.8002	0.6397
agaricus_lepiota	1.0000	1.0000	1.0000	1.0000
allbp	0.9768	0.7294	0.6928	0.7010
allhyper	0.9886	0.8116	0.6887	0.7890
allhypo	0.9849	0.9128	0.8857	0.8896
allrep	0.9860	0.8063	0.7573	0.7648
anacatdata_aids	0.3900	0.1950	0.5000	0.0000
anacatdata_asbestos	0.7412	0.7584	0.7480	0.5047
anacatdata_authorship	0.9905	0.9921	0.9843	0.9863
anacatdata_bankruptcy	0.6733	0.6524	0.6942	0.3924
anacatdata_boxing1	0.6764	0.6356	0.6053	0.2357
anacatdata_boxing2	0.7975	0.8138	0.7927	0.6055
anacatdata_creditscore	0.9900	0.9844	0.9931	0.9772
anacatdata_cyyoung8092	0.7987	0.7294	0.7150	0.4374
anacatdata_cyyoung9302	0.8421	0.7618	0.7517	0.5091
anacatdata_dmft	0.1950	0.2000	0.1985	0.0354
anacatdata_fraud	0.6741	0.3537	0.5167	0.0000
anacatdata_germangss	0.3697	0.3693	0.3739	0.1631
anacatdata_happiness	0.4389	0.3942	0.4838	0.2180
anacatdata_japansolvent	0.8061	0.8218	0.8096	0.6291
anacatdata_lawsuit	0.9882	0.9577	0.9653	0.9177
ann_thyroid	0.9966	0.9740	0.9877	0.9761

(Continued on next page)

(Continued from previous page)

Dataset	Accuracy	Precision	Recall	MCC
appendicitis	0.8621	0.7839	0.7532	0.5212
auto_insurance_symboling	0.7778	0.7459	0.7414	0.7129
backache	0.8368	0.5588	0.5324	0.0905
balance_scale	0.8660	0.6654	0.6691	0.7634
banana	0.8973	0.8972	0.8950	0.7922
biomed	0.9000	0.8995	0.8854	0.7843
breast_cancer	0.7073	0.6305	0.5962	0.2222
breast_cancer_wisconsin_diagnostic	0.9649	0.9684	0.9564	0.9247
breast_cancer_wisconsin_original	0.9614	0.9553	0.9605	0.9158
bupa	0.5707	0.5737	0.5736	0.1472
calendarDOW	0.6058	0.5830	0.5805	0.5013
car_evaluation	0.9971	0.9956	0.9965	0.9935
cars	0.9655	0.9622	0.9532	0.9364
chess	0.9945	0.9947	0.9943	0.9891
churn	0.9556	0.9504	0.8702	0.8165
clean1	1.0000	1.0000	1.0000	1.0000
clean2	1.0000	1.0000	1.0000	1.0000
cloud	0.4652	0.4904	0.4828	0.2987
coil2000	0.9361	0.5945	0.5180	0.0818
collins	0.9914	0.9887	0.9886	0.9905
confidence	0.7778	0.7767	0.7717	0.7448
congressional_voting_records	0.9555	0.9508	0.9556	0.9064
connect_4	0.8171	0.7325	0.5906	0.6040
contraceptive_method	0.5332	0.5150	0.5096	0.2776
corral	1.0000	1.0000	1.0000	1.0000
credit_approval_australia	0.8529	0.8492	0.8526	0.7017
credit_approval_germany	0.7415	0.6928	0.6630	0.3540
dermatology	0.9626	0.9585	0.9554	0.9532
dis	0.9897	0.8701	0.6935	0.5284
dna	0.9630	0.9551	0.9628	0.9404
ecoli	0.8434	0.7797	0.7244	0.7813
fars	0.6622	0.4116	0.4561	0.5458
flags	0.4907	0.4661	0.4691	0.3448
glass2	0.8758	0.8779	0.8761	0.7538
haberman	0.7151	0.6491	0.6059	0.2508
hayes_roth	0.8125	0.8279	0.8654	0.7085
heart_disease_cleveland	0.8078	0.8067	0.8029	0.6095
heart_disease_hungarian	0.8055	0.7940	0.7901	0.5837
heart_disease_va_long_beach	0.7369	0.6163	0.5793	0.1895
heart_disease_zurich	0.9210	0.5393	0.5640	0.0265
hepatitis	0.8387	0.6646	0.6590	0.3208
horse_colic_lesion_type	0.5179	0.3419	0.3540	0.3101
horse_colic_outcome	0.7095	0.6518	0.5788	0.4396
horse_colic_surgery	0.7375	0.7189	0.7096	0.4279
hypothyroid	0.9806	0.9080	0.8714	0.7773
ionosphere	0.9385	0.9431	0.9195	0.8619
iris	0.9544	0.9562	0.9554	0.9331
irish	1.0000	1.0000	1.0000	1.0000
kddcup	0.9508	0.1954	0.1710	0.9164
kr_vs_kp	0.9920	0.9920	0.9920	0.9840

(Continued on next page)

(Continued from previous page)

Dataset	Accuracy	Precision	Recall	MCC
krkopt	0.6494	0.5646	0.6039	0.6100
labor	0.8375	0.8353	0.8189	0.6498
led24	0.6964	0.6974	0.6967	0.6629
led7	0.7262	0.7296	0.7252	0.6968
letter	0.9662	0.9663	0.9660	0.9649
lupus	0.7389	0.7299	0.7173	0.4454
lymphography	0.8000	0.6780	0.6362	0.6366
magic	0.8830	0.8834	0.8563	0.7392
mfeat_factors	0.9715	0.9715	0.9722	0.9684
mfeat_fourier	0.8430	0.8432	0.8426	0.8259
mfeat_karhunen	0.9615	0.9621	0.9622	0.9573
mfeat_morphological	0.6827	0.6790	0.6825	0.6480
mfeat_pixel	0.9728	0.9726	0.9734	0.9697
mfeat_zernike	0.7847	0.7908	0.7830	0.7610
mnist	0.9771	0.9770	0.9770	0.9746
mofn_3_7_10	1.0000	1.0000	1.0000	1.0000
molecular_biology_promoters	0.8830	0.8855	0.8848	0.7699
monk1	1.0000	1.0000	1.0000	1.0000
monk2	0.9058	0.9051	0.8883	0.7931
monk3	0.9775	0.9776	0.9771	0.9547
movement_libras	0.7588	0.7796	0.7709	0.7434
mushroom	1.0000	1.0000	1.0000	1.0000
mux6	0.8705	0.8739	0.8754	0.7490
new_thyroid	0.9302	0.9498	0.8824	0.8619
nursery	1.0000	1.0000	1.0000	1.0000
optdigits	0.9819	0.9816	0.9819	0.9798
page_blocks	0.9723	0.8486	0.8564	0.8520
parity5	0.3619	0.1810	0.5000	0.0000
parity5+5	0.8751	0.8748	0.8749	0.7496
pendigits	0.9912	0.9913	0.9912	0.9902
penguins	0.9830	0.9839	0.9795	0.9732
phoneme	0.8991	0.8790	0.8771	0.7560
poker	0.6666	0.3216	0.2386	0.3879
postoperative_patient_data	0.7778	0.3889	0.5000	0.0000
prnn_crabs	0.9513	0.9522	0.9532	0.9053
prnn_synth	0.8400	0.8434	0.8395	0.6829
profb	0.6378	0.5802	0.5675	0.1470
ring	0.9718	0.9718	0.9718	0.9437
saheart	0.6745	0.6301	0.6193	0.2489
satimage	0.9240	0.9165	0.9063	0.9065
schizo	0.4974	0.3742	0.3640	0.0277
segmentation	0.9851	0.9853	0.9851	0.9826
shuttle	0.9218	0.3902	0.3820	0.8090
sleep	0.7691	0.7112	0.6464	0.6507
sonar	0.8492	0.8512	0.8518	0.7029
soybean	0.9311	0.9536	0.9473	0.9242
spambase	0.9542	0.9526	0.9518	0.9044
spect	0.8185	0.7373	0.6860	0.4159
spectf	0.8824	0.8573	0.8585	0.7146
splice	0.9603	0.9544	0.9587	0.9362

(Continued on next page)

(Continued from previous page)

Dataset	Accuracy	Precision	Recall	MCC
tae	0.4731	0.4617	0.4477	0.1837
texture	0.9861	0.9864	0.9861	0.9847
threeOf9	1.0000	1.0000	1.0000	1.0000
tic_tac_toe	0.9995	0.9993	0.9996	0.9989
titanic	0.8077	0.7953	0.7452	0.5380
tokyo1	0.9359	0.9310	0.9298	0.8608
twonorm	0.9700	0.9699	0.9700	0.9400
vehicle	0.7665	0.7578	0.7612	0.6888
vowel	0.9505	0.9513	0.9503	0.9457
waveform_21	0.8511	0.8510	0.8510	0.7770
waveform_40	0.8545	0.8545	0.8550	0.7821
wine_quality_red	0.6778	0.3965	0.3687	0.4843
wine_quality_white	0.6689	0.5133	0.3905	0.4930
wine_recognition	0.9352	0.9366	0.9413	0.9066
xd6	1.0000	1.0000	1.0000	1.0000
yeast	0.5818	0.4906	0.4705	0.4495

C.2 Supervised Learning Regression Results

C.2.1 Howso (Targetless)

Table 15: Regression Results across 258 Datasets

Dataset	R^2	Spearman
1027_ESL	0.8033	0.9118
1028_SWD	0.2067	0.5568
1029_LEV	0.4665	0.7092
1030_ERA	0.3372	0.5449
1089_USCrime	0.7240	0.7908
1096_FacultySalaries	0.5929	0.8690
1191_BNG_pbc	0.3086	0.5740
1193_BNG_lowbwt	0.5818	0.7210
1196_BNG_pharynx	0.4863	0.6481
1199_BNG_echoMonths	0.4253	0.6113
1201_BNG_breastTumor	0.1073	0.3425
1203_BNG_pwLinear	0.4808	0.7011
1595_poker	0.6401	0.8685
192_vineyard	0.4278	0.6786
197_cpu_act	0.9748	0.9447
201_pol	0.9521	0.9059
210_cloud	0.7626	0.9177
215_2dplanes	0.9412	0.9704
218_house_8L	0.6157	0.7624
225_puma8NH	0.6726	0.8146
227_cpu_small	0.9674	0.9273
228_elusage	0.5088	0.7795
229_pwLinear	0.5794	0.8036
230_machine_cpu	0.8336	0.8876
294_satellite_image	0.8974	0.9586
344_mv	0.9970	0.9968
4544_GeographicalOriginalofMusic	0.6269	0.7773
485_analcatdata_vehicle	0.4158	0.8109
503_wind	0.7549	0.8688
505_tecator	0.8094	0.8810
519_vinnie	0.6969	0.8440
522_pm10	0.1389	0.4100
523_analcatdata_neavote	0.9250	0.8601
527_analcatdata_election2000	0.9189	0.9765
529_pollen	0.7538	0.8591
537_houses	0.7781	0.8969
542_pollution	0.3670	0.6877
547_no2	0.4616	0.6846
556_analcatdata_apnea2	0.8644	0.5794
557_analcatdata_apnea1	0.8925	0.5775
560_bodyfat	0.9773	0.9937
561_cpu	0.8944	0.9806
562_cpu_small	0.9673	0.9274
564_fried	0.9338	0.9669
573_cpu_act	0.9747	0.9446

(Continued on next page)

(Continued from previous page)

Dataset	R^2	Spearman
574_house_16H	0.5436	0.7848
579_fri_c0_250_5	0.7267	0.8567
581_fri_c3_500_25	0.9030	0.9428
582_fri_c1_500_25	0.8750	0.9369
583_fri_c1_1000_50	0.8907	0.9439
584_fri_c4_500_25	0.8892	0.9325
586_fri_c3_1000_25	0.9293	0.9556
588_fri_c4_1000_100	0.8519	0.9223
589_fri_c2_1000_25	0.8999	0.9389
590_fri_c0_1000_50	0.8150	0.9077
591_fri_c1_100_10	0.8084	0.8907
592_fri_c4_1000_25	0.9316	0.9556
593_fri_c1_1000_10	0.9119	0.9442
594_fri_c2_100_5	0.7489	0.7616
595_fri_c0_1000_10	0.8142	0.9051
596_fri_c2_250_5	0.8534	0.9047
597_fri_c2_500_5	0.8671	0.8975
598_fri_c0_1000_25	0.8169	0.9068
599_fri_c2_1000_5	0.8922	0.9231
601_fri_c1_250_5	0.8779	0.9264
602_fri_c3_250_10	0.8877	0.9465
603_fri_c0_250_50	0.6046	0.8024
604_fri_c4_500_10	0.9217	0.9495
605_fri_c2_250_25	0.7883	0.8797
606_fri_c2_1000_10	0.8813	0.9156
607_fri_c4_1000_50	0.9251	0.9533
608_fri_c3_1000_10	0.9388	0.9628
609_fri_c0_1000_5	0.8407	0.9202
611_fri_c3_100_5	0.8100	0.8708
612_fri_c1_1000_5	0.9123	0.9518
613_fri_c3_250_5	0.8950	0.9204
615_fri_c4_250_10	0.8591	0.9133
616_fri_c4_500_50	0.8860	0.9344
617_fri_c3_500_5	0.9036	0.9433
618_fri_c3_1000_50	0.9197	0.9420
620_fri_c1_1000_25	0.9175	0.9570
621_fri_c0_100_10	0.6125	0.7764
622_fri_c2_1000_50	0.9151	0.9394
623_fri_c4_1000_10	0.9248	0.9567
624_fri_c0_100_5	0.6508	0.8367
626_fri_c2_500_50	0.8534	0.8853
627_fri_c2_500_10	0.8624	0.8964
628_fri_c3_1000_5	0.9261	0.9504
631_fri_c1_500_5	0.8928	0.9400
633_fri_c0_500_25	0.7818	0.8867
634_fri_c2_100_10	0.7213	0.7965
635_fri_c0_250_10	0.7414	0.8652
637_fri_c1_500_50	0.8523	0.9304
641_fri_c1_500_10	0.9027	0.9479
643_fri_c2_500_25	0.8490	0.8792

(Continued on next page)

(Continued from previous page)

Dataset	R^2	Spearman
644_fri_c4_250_25	0.8463	0.9147
645_fri_c3_500_50	0.8603	0.9234
646_fri_c3_500_10	0.9164	0.9507
647_fri_c1_250_10	0.8576	0.9167
648_fri_c1_250_50	0.8233	0.9100
649_fri_c0_500_5	0.7442	0.8655
650_fri_c0_500_50	0.7514	0.8754
651_fri_c0_100_25	0.4835	0.7245
653_fri_c0_250_25	0.7282	0.8367
654_fri_c0_500_10	0.7247	0.8509
656_fri_c1_100_5	0.7581	0.8759
657_fri_c2_250_10	0.8341	0.8292
658_fri_c3_250_25	0.8242	0.9100
659_sleuth_ex1714	0.6487	0.8826
663_rabe_266	0.9833	0.9895
665_sleuth_case2002	0.2900	0.4572
666_rmftsa_ladata	0.5540	0.6142
678_visualizing_environmental	0.1968	0.4940
687_sleuth_ex1605	0.3790	0.6159
690_visualizing_galaxy	0.9730	0.9807
695_chatfield_4	0.8447	0.9310
706_sleuth_case1202	0.4783	0.8049
712_chscase_geyser1	0.7232	0.7125
auto_insurance_losses	0.6267	0.8248
auto_insurance_price	0.8890	0.9407
feynman_III_10_19	0.9991	0.9996
feynman_III_12_43	1.0000	1.0000
feynman_III_13_18	0.9970	0.9992
feynman_III_14_14	0.9910	0.9981
feynman_III_15_12	0.9953	0.9970
feynman_III_15_14	0.9984	0.9998
feynman_III_15_27	0.9991	0.9998
feynman_III_17_37	0.9993	0.9997
feynman_III_19_51	0.8491	0.9831
feynman_III_21_20	0.9973	0.9991
feynman_III_4_32	0.9958	0.9991
feynman_III_4_33	0.9955	0.9969
feynman_III_7_38	0.9994	0.9998
feynman_III_8_54	0.9792	0.9864
feynman_III_9_52	0.9806	0.9921
feynman_II_10_9	0.9994	0.9998
feynman_II_11_20	0.9866	0.9979
feynman_II_11_27	0.9916	0.9978
feynman_II_11_28	1.0000	1.0000
feynman_II_11_3	0.9713	0.9927
feynman_II_13_17	0.9909	0.9993
feynman_II_13_23	0.9995	0.9998
feynman_II_13_34	0.9974	0.9993
feynman_II_15_4	0.9993	0.9996
feynman_II_15_5	0.9993	0.9997

(Continued on next page)

(Continued from previous page)

Dataset	R^2	Spearman
feynman_II_21.32	0.9732	0.9930
feynman_II_24.17	0.9987	0.9993
feynman_II_27.16	0.9997	0.9998
feynman_II_27.18	1.0000	1.0000
feynman_II_2.42	0.9920	0.9986
feynman_II_34.11	0.9970	0.9991
feynman_II_34.2	0.9997	0.9998
feynman_II_34.29a	0.9994	0.9998
feynman_II_34.29b	0.9920	0.9977
feynman_II_34.2a	0.9994	0.9998
feynman_II_35.18	0.9960	0.9980
feynman_II_35.21	0.9968	0.9983
feynman_II_36.38	0.8996	0.9675
feynman_II_37.1	0.9997	0.9998
feynman_II_38.14	1.0000	1.0000
feynman_II_38.3	0.9969	0.9991
feynman_II_3.24	1.0000	1.0000
feynman_II_4.23	0.9992	0.9998
feynman_II_6.11	0.9973	0.9994
feynman_II_6.15a	0.9204	0.9858
feynman_II_6.15b	0.9863	0.9976
feynman_II_8.31	1.0000	1.0000
feynman_II_8.7	0.9991	0.9999
feynman_I_10.7	0.9986	0.9994
feynman_I_11.19	0.9929	0.9969
feynman_I_12.1	1.0000	1.0000
feynman_I_12.11	0.9943	0.9969
feynman_I_12.2	0.9915	0.9993
feynman_I_12.4	0.9985	0.9999
feynman_I_12.5	1.0000	1.0000
feynman_I_13.12	0.9697	0.9959
feynman_I_13.4	0.9986	0.9994
feynman_I_14.3	0.9997	0.9998
feynman_I_14.4	1.0000	1.0000
feynman_I_15.10	0.9962	0.9990
feynman_I_15.3t	0.9955	0.9981
feynman_I_15.3x	0.9934	0.9972
feynman_I_16.6	0.9998	0.9999
feynman_I_18.12	0.9995	0.9997
feynman_I_18.14	0.9987	0.9994
feynman_I_18.4	0.9987	0.9993
feynman_I_24.6	0.9986	0.9995
feynman_I_25.13	1.0000	1.0000
feynman_I_26.2	1.0000	1.0000
feynman_I_27.6	0.9996	0.9998
feynman_I_29.16	0.9968	0.9983
feynman_I_29.4	0.9999	1.0000
feynman_I_30.3	0.9947	0.9964
feynman_I_30.5	0.9993	0.9999
feynman_I_32.17	0.9389	0.9857

(Continued on next page)

(Continued from previous page)

Dataset	R^2	Spearman
feynman_I.32.5	0.9816	0.9993
feynman_I.34.1	0.9996	0.9999
feynman_I.34.14	0.9997	0.9999
feynman_I.34.27	1.0000	1.0000
feynman_I.34.8	0.9970	0.9991
feynman_I.37.4	0.9994	0.9998
feynman_I.38.12	0.9905	0.9992
feynman_I.39.1	1.0000	1.0000
feynman_I.39.11	0.9995	0.9998
feynman_I.39.22	0.9972	0.9991
feynman_I.40.1	0.9851	0.9949
feynman_I.41.16	0.9895	0.9980
feynman_I.43.16	0.9972	0.9991
feynman_I.43.31	0.9997	0.9998
feynman_I.43.43	0.9962	0.9992
feynman_I.44.4	0.9938	0.9984
feynman_I.47.23	0.9996	0.9998
feynman_I.48.2	0.9997	0.9998
feynman_I.50.26	0.9936	0.9953
feynman_I.6.2	1.0000	1.0000
feynman_I.6.2b	0.9995	0.9998
feynman_I.8.14	0.9965	0.9985
feynman_I.9.18	0.9295	0.9740
feynman_test.1	0.8411	0.9559
feynman_test.10	0.9998	0.9999
feynman_test.11	0.9986	0.9993
feynman_test.12	0.9862	0.9952
feynman_test.13	0.9592	0.9910
feynman_test.14	0.8334	0.9519
feynman_test.15	0.9892	0.9962
feynman_test.16	0.9853	0.9910
feynman_test.17	0.9905	0.9986
feynman_test.18	0.9758	0.9958
feynman_test.19	0.9555	0.9532
feynman_test.2	0.9175	0.9769
feynman_test.20	0.5502	0.9048
feynman_test.3	0.9847	0.9951
feynman_test.4	0.9789	0.9900
feynman_test.5	0.9939	0.9979
feynman_test.6	0.9418	0.9868
feynman_test.7	0.9933	0.9969
feynman_test.8	0.9987	0.9993
feynman_test.9	0.9703	0.9980
first_principles_ideal_gas	0.7334	0.8820
first_principles_newton	0.0576	0.6365
first_principles_planck	-2.8546	0.5769
first_principles_rydberg	0.9871	0.9841
nikuradse_1	0.9960	0.9898
solar_flare	-0.1344	0.0856
strogatz_bacres1	0.9978	0.9752

(Continued on next page)

(Continued from previous page)

Dataset	R^2	Spearman
strogatz_bacres2	0.9990	0.9989
strogatz_barmag1	0.9942	0.9967
strogatz_barmag2	0.8938	0.7777
strogatz_glider1	0.9787	0.9887
strogatz_glider2	0.9686	0.9859
strogatz_lv1	0.3866	0.9773
strogatz_lv2	0.5873	0.9736
strogatz_predprey1	0.8934	0.9891
strogatz_predprey2	0.9944	0.9974
strogatz_shearflow1	0.9315	0.9368
strogatz_shearflow2	0.9785	0.9887
strogatz_vdp1	0.9521	0.8630
strogatz_vdp2	0.9959	0.9939

C.2.2 Howso (Single-Target)

Table 16: Regression Results across 258 Datasets

Dataset	R^2	Spearman
1027_ESL	0.8081	0.9116
1028_SWD	0.2573	0.5668
1029_LEV	0.4653	0.7088
1030_ERA	0.3304	0.5447
1089_USCrime	0.7283	0.7728
1096_FacultySalaries	0.6008	0.8553
1191_BNG_pbc	0.3829	0.6331
1193_BNG_lowbwt	0.6047	0.7484
1196_BNG_pharynx	0.5003	0.6618
1199_BNG_echoMonths	0.4605	0.6437
1201_BNG_breastTumor	0.0870	0.3351
1203_BNG_pwLinear	0.6196	0.7956
1595_poker	0.7097	0.9305
192_vineyard	0.4474	0.6861
197_cpu_act	0.9770	0.9534
201_pol	0.9834	0.9684
210_cloud	0.7598	0.9106
215_2dplanes	0.9407	0.9703
218_house_8L	0.6349	0.8079
225_puma8NH	0.6551	0.8032
227_cpu_small	0.9725	0.9418
228_elusage	0.6505	0.8164
229_pwLinear	0.7835	0.8897
230_machine_cpu	0.8001	0.8684
294_satellite_image	0.9029	0.9609
344_mv	0.9997	0.9987
4544_GeographicalOriginalofMusic	0.6509	0.7989
485_analcatdata_vehicle	0.5594	0.8436
503_wind	0.7625	0.8735

(Continued on next page)

(Continued from previous page)

Dataset	R^2	Spearman
505_tecator	0.9920	0.9870
519_vinnie	0.7198	0.8504
522_pm10	0.2516	0.5172
523_analcatdata_neavote	0.9271	0.8612
527_analcatdata_election2000	0.9376	0.9807
529_pollen	0.7573	0.8620
537_houses	0.7443	0.8729
542_pollution	0.2760	0.6442
547_no2	0.4861	0.6787
556_analcatdata_apnea2	0.8700	0.5847
557_analcatdata_apnea1	0.8988	0.5623
560_bodyfat	0.9570	0.9831
561_cpu	0.8895	0.9602
562_cpu_small	0.9728	0.9416
564_fried	0.9307	0.9655
573_cpu_act	0.9770	0.9534
574_house_16H	0.4443	0.7953
579_fri_c0_250_5	0.7496	0.8718
581_fri_c3_500_25	0.8789	0.9279
582_fri_c1_500_25	0.8607	0.9309
583_fri_c1_1000_50	0.8934	0.9441
584_fri_c4_500_25	0.8665	0.9212
586_fri_c3_1000_25	0.9151	0.9477
588_fri_c4_1000_100	0.8483	0.9277
589_fri_c2_1000_25	0.8809	0.9289
590_fri_c0_1000_50	0.8079	0.9046
591_fri_c1_100_10	0.7755	0.8748
592_fri_c4_1000_25	0.9167	0.9425
593_fri_c1_1000_10	0.9297	0.9568
594_fri_c2_100_5	0.7149	0.8244
595_fri_c0_1000_10	0.8346	0.9218
596_fri_c2_250_5	0.8680	0.9174
597_fri_c2_500_5	0.9043	0.9337
598_fri_c0_1000_25	0.8198	0.9101
599_fri_c2_1000_5	0.9289	0.9498
601_fri_c1_250_5	0.8811	0.9316
602_fri_c3_250_10	0.8685	0.9272
603_fri_c0_250_50	0.5748	0.7902
604_fri_c4_500_10	0.9092	0.9433
605_fri_c2_250_25	0.7489	0.8548
606_fri_c2_1000_10	0.8905	0.9244
607_fri_c4_1000_50	0.9096	0.9484
608_fri_c3_1000_10	0.9294	0.9583
609_fri_c0_1000_5	0.8720	0.9411
611_fri_c3_100_5	0.8325	0.8750
612_fri_c1_1000_5	0.9305	0.9629
613_fri_c3_250_5	0.8717	0.9077
615_fri_c4_250_10	0.8298	0.8835
616_fri_c4_500_50	0.8165	0.8978
617_fri_c3_500_5	0.9034	0.9422

(Continued on next page)

(Continued from previous page)

Dataset	R^2	Spearman
618_fri_c3_1000_50	0.9103	0.9379
620_fri_c1_1000_25	0.9061	0.9491
621_fri_c0_100_10	0.5543	0.7534
622_fri_c2_1000_50	0.8831	0.9196
623_fri_c4_1000_10	0.9132	0.9469
624_fri_c0_100_5	0.6985	0.8533
626_fri_c2_500_50	0.8120	0.8515
627_fri_c2_500_10	0.8828	0.9197
628_fri_c3_1000_5	0.9330	0.9566
631_fri_c1_500_5	0.8949	0.9409
633_fri_c0_500_25	0.7671	0.8771
634_fri_c2_100_10	0.6628	0.7812
635_fri_c0_250_10	0.7651	0.8732
637_fri_c1_500_50	0.7556	0.8722
641_fri_c1_500_10	0.9106	0.9513
643_fri_c2_500_25	0.8095	0.8569
644_fri_c4_250_25	0.7605	0.8719
645_fri_c3_500_50	0.8212	0.9034
646_fri_c3_500_10	0.9025	0.9408
647_fri_c1_250_10	0.8598	0.9167
648_fri_c1_250_50	0.7342	0.8612
649_fri_c0_500_5	0.8212	0.9054
650_fri_c0_500_50	0.7282	0.8588
651_fri_c0_100_25	0.4600	0.7262
653_fri_c0_250_25	0.7150	0.8289
654_fri_c0_500_10	0.7529	0.8672
656_fri_c1_100_5	0.7251	0.8585
657_fri_c2_250_10	0.8396	0.8468
658_fri_c3_250_25	0.7829	0.8864
659_sleuth_ex1714	0.6174	0.8582
663_rabe_266	0.9856	0.9906
665_sleuth_case2002	0.3008	0.3890
666_rmftsa_ladata	0.5764	0.6020
678_visualizing_environmental	0.2188	0.5183
687_sleuth_ex1605	0.2866	0.6180
690_visualizing_galaxy	0.9745	0.9818
695_chatfield_4	0.8256	0.9142
706_sleuth_case1202	0.4431	0.7873
712_chscase_geyser1	0.7449	0.7168
auto_insurance_losses	0.8357	0.9267
auto_insurance_price	0.8952	0.9423
feynman_III_10_19	0.9992	0.9997
feynman_III_12_43	1.0000	1.0000
feynman_III_13_18	0.9962	0.9993
feynman_III_14_14	0.9829	0.9983
feynman_III_15_12	0.9952	0.9969
feynman_III_15_14	0.9979	0.9999
feynman_III_15_27	0.9990	0.9998
feynman_III_17_37	0.9995	0.9998
feynman_III_19_51	0.9008	0.9976

(Continued on next page)

(Continued from previous page)

Dataset	R^2	Spearman
feynman_III_21_20	0.9965	0.9991
feynman_III_4_32	0.9947	0.9991
feynman_III_4_33	0.9997	0.9998
feynman_III_7_38	0.9993	0.9998
feynman_III_8_54	0.9837	0.9893
feynman_III_9_52	0.9804	0.9933
feynman_II_10_9	0.9993	0.9999
feynman_II_11_20	0.9819	0.9979
feynman_II_11_27	0.9988	0.9991
feynman_II_11_28	1.0000	1.0000
feynman_II_11_3	0.9940	0.9987
feynman_II_13_17	0.9896	0.9993
feynman_II_13_23	0.9999	1.0000
feynman_II_13_34	0.9997	0.9999
feynman_II_15_4	0.9995	0.9998
feynman_II_15_5	0.9995	0.9998
feynman_II_21_32	0.9871	0.9981
feynman_II_24_17	0.9998	0.9999
feynman_II_27_16	0.9997	0.9999
feynman_II_27_18	1.0000	1.0000
feynman_II_2_42	0.9908	0.9986
feynman_II_34_11	0.9967	0.9991
feynman_II_34_2	0.9997	0.9998
feynman_II_34_29a	0.9993	0.9998
feynman_II_34_29b	0.9905	0.9977
feynman_II_34_2a	0.9993	0.9998
feynman_II_35_18	0.9959	0.9981
feynman_II_35_21	0.9967	0.9983
feynman_II_36_38	0.9616	0.9926
feynman_II_37_1	0.9997	0.9999
feynman_II_38_14	1.0000	1.0000
feynman_II_38_3	0.9965	0.9991
feynman_II_3_24	1.0000	1.0000
feynman_II_4_23	0.9989	0.9998
feynman_II_6_11	0.9964	0.9997
feynman_II_6_15a	0.9863	0.9990
feynman_II_6_15b	0.9954	0.9994
feynman_II_8_31	1.0000	1.0000
feynman_II_8_7	0.9990	0.9999
feynman_I_10_7	0.9999	1.0000
feynman_I_11_19	0.9923	0.9973
feynman_I_12_1	1.0000	1.0000
feynman_I_12_11	0.9974	0.9990
feynman_I_12_2	0.9923	0.9992
feynman_I_12_4	0.9986	0.9999
feynman_I_12_5	1.0000	1.0000
feynman_I_13_12	0.9892	0.9984
feynman_I_13_4	0.9986	0.9995
feynman_I_14_3	0.9997	0.9998
feynman_I_14_4	1.0000	1.0000

(Continued on next page)

(Continued from previous page)

Dataset	R^2	Spearman
feynman_I.15.10	0.9997	0.9999
feynman_I.15.3t	0.9998	0.9999
feynman_I.15.3x	0.9985	0.9994
feynman_I.16.6	0.9998	0.9999
feynman_I.18.12	0.9997	0.9998
feynman_I.18.14	0.9989	0.9996
feynman_I.18.4	0.9991	0.9996
feynman_I.24.6	0.9986	0.9996
feynman_I.25.13	1.0000	1.0000
feynman_I.26.2	1.0000	1.0000
feynman_I.27.6	0.9996	0.9998
feynman_I.29.16	0.9969	0.9986
feynman_I.29.4	0.9999	1.0000
feynman_I.30.3	0.9947	0.9966
feynman_I.30.5	0.9994	0.9999
feynman_I.32.17	0.9832	0.9977
feynman_I.32.5	0.9828	0.9991
feynman_I.34.1	0.9995	0.9999
feynman_I.34.14	0.9997	0.9999
feynman_I.34.27	1.0000	1.0000
feynman_I.34.8	0.9965	0.9991
feynman_I.37.4	0.9996	0.9999
feynman_I.38.12	0.9901	0.9993
feynman_I.39.1	1.0000	1.0000
feynman_I.39.11	0.9993	0.9999
feynman_I.39.22	0.9967	0.9992
feynman_I.40.1	0.9833	0.9946
feynman_I.41.16	0.9909	0.9984
feynman_I.43.16	0.9964	0.9991
feynman_I.43.31	0.9997	0.9998
feynman_I.43.43	0.9951	0.9992
feynman_I.44.4	0.9935	0.9985
feynman_I.47.23	0.9996	0.9998
feynman_I.48.2	0.9999	1.0000
feynman_I.50.26	0.9927	0.9943
feynman_I.6.2	1.0000	1.0000
feynman_I.6.2b	0.9995	0.9998
feynman_I.8.14	0.9964	0.9986
feynman_I.9.18	0.9737	0.9928
feynman_test.1	0.9318	0.9944
feynman_test.10	0.9999	1.0000
feynman_test.11	0.9982	0.9991
feynman_test.12	0.9968	0.9989
feynman_test.13	0.9870	0.9985
feynman_test.14	0.9662	0.9928
feynman_test.15	0.9985	0.9995
feynman_test.16	0.9962	0.9985
feynman_test.17	0.9848	0.9981
feynman_test.18	0.9795	0.9981
feynman_test.19	0.9777	0.9892

(Continued on next page)

(Continued from previous page)

Dataset	R^2	Spearman
feynman_test_2	0.9706	0.9957
feynman_test_20	0.7190	0.9888
feynman_test_3	0.9987	0.9996
feynman_test_4	0.9959	0.9979
feynman_test_5	0.9992	0.9998
feynman_test_6	0.9657	0.9945
feynman_test_7	0.9993	0.9997
feynman_test_8	0.9987	0.9994
feynman_test_9	0.9596	0.9975
first_principles_ideal_gas	0.7099	0.8940
first_principles_newton	0.4408	0.7336
first_principles_planck	-8.3566	0.7243
first_principles_rydberg	0.9818	0.9791
nikuradse_1	0.9974	0.9901
solar_flare	-0.1941	0.1122
strogatz_bacres1	0.9981	0.9693
strogatz_bacres2	0.9981	0.9985
strogatz_barmag1	0.9955	0.9989
strogatz_barmag2	0.9948	0.9976
strogatz_glider1	0.9837	0.9911
strogatz_glider2	0.9566	0.9763
strogatz_lv1	0.4897	0.9947
strogatz_lv2	0.6136	0.9839
strogatz_predprey1	0.9258	0.9935
strogatz_predprey2	0.9934	0.9962
strogatz_shearflow1	0.9669	0.9967
strogatz_shearflow2	0.9920	0.9951
strogatz_vdp1	0.9561	0.9398
strogatz_vdp2	0.9999	1.0000

C.2.3 XGBoost

Table 17: Regression Results across 258 Datasets

Dataset	R^2	Spearman
1027_ESL	0.8024	0.9148
1028_SWD	0.3270	0.5942
1029_LEV	0.5360	0.7324
1030_ERA	0.3501	0.5588
1089_USCrime	0.5860	0.7279
1096_FacultySalaries	0.6673	0.8437
1191_BNG_pbc	0.4416	0.6771
1193_BNG_lowbwt	0.5954	0.7430
1196_BNG_pharynx	0.5134	0.6688
1199_BNG_echoMonths	0.4335	0.6375
1201_BNG_breastTumor	0.1676	0.4111
1203_BNG_pwLinear	0.6222	0.7977
1595_poker	0.6260	0.8402
192_vineyard	0.1822	0.6647

(Continued on next page)

(Continued from previous page)

Dataset	R^2	Spearman
197_cpu_act	0.9839	0.9652
201_pol	0.9855	0.8595
210_cloud	0.7652	0.9074
215_2dplanes	0.9464	0.9724
218_house_8L	0.6593	0.8237
225_puma8NH	0.6332	0.7937
227_cpu_small	0.9776	0.9533
228_elusage	0.6144	0.7893
229_pwLinear	0.8190	0.9004
230_machine_cpu	0.8328	0.8909
294_satellite_image	0.8916	0.9436
344_mv	0.9998	0.9998
4544.GeographicalOriginalofMusic	0.6760	0.8045
485_analcatdata_vehicle	0.4662	0.8552
503_wind	0.7673	0.8744
505_tecator	0.9898	0.9868
519_vinnie	0.6530	0.8242
522_pm10	0.3510	0.6176
523_analcatdata_neavote	0.8782	0.7938
527_analcatdata_election2000	0.7576	0.9674
529_pollen	0.7184	0.8403
537_houses	0.8247	0.9128
542_pollution	0.3147	0.6872
547_no2	0.5712	0.7219
556_analcatdata_apnea2	0.8011	0.5943
557_analcatdata_apnea1	0.8283	0.5459
560_bodyfat	0.9497	0.9867
561_cpu	0.9224	0.9913
562_cpu_small	0.9776	0.9533
564_fried	0.9461	0.9722
573_cpu_act	0.9839	0.9652
574_house_16H	0.6216	0.8097
579_fri_c0_250_5	0.7557	0.8731
581_fri_c3_500_25	0.8831	0.9241
582_fri_c1_500_25	0.8349	0.9101
583_fri_c1_1000_50	0.9047	0.9450
584_fri_c4_500_25	0.8491	0.9003
586_fri_c3_1000_25	0.9071	0.9434
588_fri_c4_1000_100	0.9038	0.9381
589_fri_c2_1000_25	0.9082	0.9451
590_fri_c0_1000_50	0.8411	0.9166
591_fri_c1_100_10	0.7212	0.8274
592_fri_c4_1000_25	0.9118	0.9467
593_fri_c1_1000_10	0.9198	0.9509
594_fri_c2_100_5	0.6873	0.7736
595_fri_c0_1000_10	0.8607	0.9267
596_fri_c2_250_5	0.8448	0.9102
597_fri_c2_500_5	0.9078	0.9394
598_fri_c0_1000_25	0.8478	0.9164
599_fri_c2_1000_5	0.9413	0.9593

(Continued on next page)

(Continued from previous page)

Dataset	R^2	Spearman
601_fri_c1_250_5	0.8529	0.9175
602_fri_c3_250_10	0.8161	0.9053
603_fri_c0_250_50	0.6121	0.8004
604_fri_c4_500_10	0.8882	0.9270
605_fri_c2_250_25	0.7720	0.8538
606_fri_c2_1000_10	0.9142	0.9464
607_fri_c4_1000_50	0.9049	0.9465
608_fri_c3_1000_10	0.9222	0.9563
609_fri_c0_1000_5	0.8911	0.9448
611_fri_c3_100_5	0.6872	0.8152
612_fri_c1_1000_5	0.9323	0.9631
613_fri_c3_250_5	0.8370	0.8840
615_fri_c4_250_10	0.7921	0.8691
616_fri_c4_500_50	0.8509	0.9109
617_fri_c3_500_5	0.9067	0.9478
618_fri_c3_1000_50	0.9065	0.9358
620_fri_c1_1000_25	0.8978	0.9451
621_fri_c0_100_10	0.5422	0.7546
622_fri_c2_1000_50	0.8983	0.9359
623_fri_c4_1000_10	0.9205	0.9492
624_fri_c0_100_5	0.6808	0.8247
626_fri_c2_500_50	0.8406	0.8932
627_fri_c2_500_10	0.8889	0.9319
628_fri_c3_1000_5	0.9315	0.9591
631_fri_c1_500_5	0.8870	0.9382
633_fri_c0_500_25	0.8091	0.8962
634_fri_c2_100_10	0.6484	0.7668
635_fri_c0_250_10	0.7167	0.8537
637_fri_c1_500_50	0.8187	0.8977
641_fri_c1_500_10	0.8932	0.9387
643_fri_c2_500_25	0.8556	0.9052
644_fri_c4_250_25	0.7472	0.8701
645_fri_c3_500_50	0.8576	0.9056
646_fri_c3_500_10	0.8936	0.9329
647_fri_c1_250_10	0.8191	0.8948
648_fri_c1_250_50	0.7508	0.8522
649_fri_c0_500_5	0.8458	0.9135
650_fri_c0_500_50	0.7456	0.8686
651_fri_c0_100_25	0.4494	0.6929
653_fri_c0_250_25	0.6560	0.7823
654_fri_c0_500_10	0.7920	0.8907
656_fri_c1_100_5	0.6789	0.8184
657_fri_c2_250_10	0.8279	0.8681
658_fri_c3_250_25	0.7437	0.8549
659_sleuth_ex1714	0.4084	0.7964
663_rabe_266	0.9931	0.9939
665_sleuth_case2002	-0.0769	0.3392
666_rmftsa_ladata	0.5184	0.5393
678_visualizing_environmental	-0.0436	0.4542
687_sleuth_ex1605	0.3956	0.6277

(Continued on next page)

(Continued from previous page)

Dataset	R^2	Spearman
690_visualizing_galaxy	0.9687	0.9785
695_chatfield_4	0.8141	0.9105
706_sleuth_case1202	0.3978	0.7881
712_chscase_geyser1	0.5854	0.6702
auto_insurance_losses	0.7469	0.8871
auto_insurance_price	0.9096	0.9506
feynman_III_10_19	0.9980	0.9991
feynman_III_12_43	0.9998	0.9999
feynman_III_13_18	0.9955	0.9971
feynman_III_14_14	0.9865	0.9931
feynman_III_15_12	0.9809	0.9863
feynman_III_15_14	0.9973	0.9982
feynman_III_15_27	0.9982	0.9991
feynman_III_17_37	0.9989	0.9995
feynman_III_19_51	0.9471	0.8794
feynman_III_21_20	0.9952	0.9968
feynman_III_4_32	0.9945	0.9968
feynman_III_4_33	0.9995	0.9997
feynman_III_7_38	0.9986	0.9991
feynman_III_8_54	0.7325	0.8578
feynman_III_9_52	0.9601	0.9719
feynman_II_10_9	0.9985	0.9992
feynman_II_11_20	0.9876	0.9920
feynman_II_11_27	0.9978	0.9987
feynman_II_11_28	0.9998	0.9999
feynman_II_11_3	0.9938	0.9969
feynman_II_13_17	0.9929	0.9963
feynman_II_13_23	0.9999	0.9999
feynman_II_13_34	0.9996	0.9998
feynman_II_15_4	0.9988	0.9994
feynman_II_15_5	0.9988	0.9994
feynman_II_21_32	0.9938	0.9973
feynman_II_24_17	0.9996	0.9998
feynman_II_27_16	0.9988	0.9992
feynman_II_27_18	0.9998	0.9999
feynman_II_2_42	0.9905	0.9953
feynman_II_34_11	0.9953	0.9969
feynman_II_34_2	0.9988	0.9992
feynman_II_34_29a	0.9985	0.9991
feynman_II_34_29b	0.9900	0.9925
feynman_II_34_2a	0.9985	0.9990
feynman_II_35_18	0.9922	0.9958
feynman_II_35_21	0.9948	0.9969
feynman_II_36_38	0.9831	0.9916
feynman_II_37_1	0.9988	0.9993
feynman_II_38_14	0.9998	0.9999
feynman_II_38_3	0.9953	0.9969
feynman_II_3_24	0.9997	0.9998
feynman_II_4_23	0.9982	0.9990
feynman_II_6_11	0.9969	0.9990

(Continued on next page)

(Continued from previous page)

Dataset	R^2	Spearman
feynman_II.6.15a	0.9919	0.9940
feynman_II.6.15b	0.9962	0.9984
feynman_II.8.31	0.9998	0.9999
feynman_II.8.7	0.9982	0.9992
feynman_I.10.7	0.9998	0.9999
feynman_I.11.19	0.9893	0.9943
feynman_I.12.1	0.9998	0.9999
feynman_I.12.11	0.9966	0.9984
feynman_I.12.2	0.9941	0.9963
feynman_I.12.4	0.9982	0.9989
feynman_I.12.5	0.9998	0.9999
feynman_I.13.12	0.9925	0.9951
feynman_I.13.4	0.9966	0.9982
feynman_I.14.3	0.9988	0.9992
feynman_I.14.4	0.9998	0.9999
feynman_I.15.10	0.9996	0.9998
feynman_I.15.3t	0.9998	0.9999
feynman_I.15.3x	0.9989	0.9995
feynman_I.16.6	0.9993	0.9996
feynman_I.18.12	0.9992	0.9996
feynman_I.18.14	0.9978	0.9991
feynman_I.18.4	0.9982	0.9991
feynman_I.24.6	0.9965	0.9980
feynman_I.25.13	0.9998	0.9999
feynman_I.26.2	0.9999	0.9999
feynman_I.27.6	0.9989	0.9994
feynman_I.29.16	0.9847	0.9927
feynman_I.29.4	0.9997	0.9998
feynman_I.30.3	0.9893	0.9872
feynman_I.30.5	0.9987	0.9994
feynman_I.32.17	0.9858	0.9883
feynman_I.32.5	0.9903	0.9803
feynman_I.34.1	0.9992	0.9997
feynman_I.34.14	0.9994	0.9998
feynman_I.34.27	0.9998	0.9999
feynman_I.34.8	0.9952	0.9968
feynman_I.37.4	0.9989	0.9995
feynman_I.38.12	0.9931	0.9948
feynman_I.39.1	0.9998	0.9999
feynman_I.39.11	0.9986	0.9992
feynman_I.39.22	0.9952	0.9968
feynman_I.40.1	0.9819	0.9533
feynman_I.41.16	0.9938	0.9931
feynman_I.43.16	0.9953	0.9968
feynman_I.43.31	0.9988	0.9992
feynman_I.43.43	0.9948	0.9970
feynman_I.44.4	0.9922	0.9955
feynman_I.47.23	0.9987	0.9993
feynman_I.48.2	0.9998	0.9999
feynman_I.50.26	0.9846	0.9822

(Continued on next page)

(Continued from previous page)

Dataset	R^2	Spearman
feynman_I.6_2	0.9997	0.9999
feynman_I.6_2b	0.9971	0.9980
feynman_I.8_14	0.9898	0.9961
feynman_I.9_18	0.9776	0.9878
feynman_test_1	0.9530	0.9502
feynman_test_10	0.9997	0.9999
feynman_test_11	0.9968	0.9982
feynman_test_12	0.9973	0.9983
feynman_test_13	0.9917	0.9970
feynman_test_14	0.9767	0.9807
feynman_test_15	0.9986	0.9994
feynman_test_16	0.9961	0.9979
feynman_test_17	0.9894	0.9893
feynman_test_18	0.9904	0.9960
feynman_test_19	0.9904	0.9873
feynman_test_2	0.9717	0.9788
feynman_test_20	0.7631	0.6113
feynman_test_3	0.9979	0.9991
feynman_test_4	0.9978	0.9989
feynman_test_5	0.9984	0.9993
feynman_test_6	0.9754	0.9521
feynman_test_7	0.9994	0.9997
feynman_test_8	0.9973	0.9986
feynman_test_9	0.9677	0.8518
first_principles_ideal_gas	0.4155	0.8381
first_principles_newton	0.6672	0.8585
first_principles_planck	-7.2481	0.9053
first_principles_rydberg	0.9968	0.9889
nikuradse_1	0.9976	0.9896
solar_flare	-0.1444	0.2219
strogatz_bacres1	0.9962	0.9695
strogatz_bacres2	0.9944	0.9958
strogatz_barmag1	0.9814	0.9946
strogatz_barmag2	0.9193	0.9660
strogatz_glider1	0.9642	0.9798
strogatz_glider2	0.9313	0.9702
strogatz_lv1	-4.6152	0.9862
strogatz_lv2	-0.2972	0.9819
strogatz_predprey1	0.8956	0.9931
strogatz_predprey2	0.9918	0.9958
strogatz_shearflow1	0.9311	0.9940
strogatz_shearflow2	0.9703	0.9908
strogatz_vdp1	0.8653	0.9490
strogatz_vdp2	0.9995	0.9996

C.2.4 LightGBM

Table 18: Regression Results across 253 Datasets

Dataset	R^2	Spearman
1027_ESL	0.8477	0.9292
1028_SWD	0.3713	0.6231
1029_LEV	0.5498	0.7410
1030_ERA	0.3559	0.5597
1096_FacultySalaries	0.1822	0.6449
1191_BNG_pbc	0.4284	0.6674
1193_BNG_lowbwt	0.6136	0.7585
1196_BNG_pharynx	0.5136	0.6685
1199_BNG_echoMonths	0.4730	0.6637
1201_BNG_breastTumor	0.1758	0.4201
1203_BNG_pwLinear	0.6225	0.7977
1595_poker	0.2756	0.5468
192_vineyard	0.3144	0.7069
197_cpu_act	0.9864	0.9658
201_pol	0.9870	0.8632
210_cloud	0.6118	0.8819
215_2dplanes	0.9486	0.9724
218_house_8L	0.6939	0.8412
225_puma8NH	0.6697	0.8124
227_cpu_small	0.9803	0.9531
228_elusage	0.3925	0.6795
229_pwLinear	0.8483	0.9241
230_machine_cpu	0.6315	0.8215
294_satellite_image	0.9016	0.9476
344_mv	0.9998	0.9998
4544_GeographicalOriginalofMusic	0.7177	0.8405
503_wind	0.7945	0.8903
505_tecator	0.9776	0.9882
519_vinnie	0.7114	0.8404
522_pm10	0.4448	0.6783
523_analcatdata_neavote	0.8813	0.8367
527_analcatdata_election2000	0.2175	0.7768
529_pollen	0.7667	0.8655
537_houses	0.8299	0.9149
542_pollution	0.2520	0.6312
547_no2	0.6084	0.7582
556_analcatdata_apnea2	0.7042	0.4480
557_analcatdata_apnea1	0.7311	0.3930
560_bodyfat	0.9596	0.9896
561_cpu	0.6541	0.9141
562_cpu_small	0.9803	0.9531
564_fried	0.9530	0.9760
573_cpu_act	0.9864	0.9658
574_house_16H	0.6632	0.8326
579_fri.c0.250.5	0.8290	0.9103
581_fri.c3.500.25	0.9022	0.9423
582_fri.c1.500.25	0.8842	0.9348
583_fri.c1.1000.50	0.9253	0.9565
584_fri.c4.500.25	0.8687	0.9195

(Continued on next page)

(Continued from previous page)

Dataset	R^2	Spearman
586_fri_c3_1000_25	0.9296	0.9581
588_fri_c4_1000_100	0.9145	0.9449
589_fri_c2_1000_25	0.9219	0.9577
590_fri_c0_1000_50	0.8836	0.9407
591_fri_c1_100_10	0.4334	0.6518
592_fri_c4_1000_25	0.9173	0.9538
593_fri_c1_1000_10	0.9391	0.9653
594_fri_c2_100_5	0.5540	0.7418
595_fri_c0_1000_10	0.8984	0.9458
596_fri_c2_250_5	0.8389	0.9084
597_fri_c2_500_5	0.9272	0.9534
598_fri_c0_1000_25	0.8868	0.9436
599_fri_c2_1000_5	0.9399	0.9612
601_fri_c1_250_5	0.8853	0.9353
602_fri_c3_250_10	0.8337	0.9162
603_fri_c0_250_50	0.7864	0.8924
604_fri_c4_500_10	0.9069	0.9401
605_fri_c2_250_25	0.8124	0.8961
606_fri_c2_1000_10	0.9324	0.9617
607_fri_c4_1000_50	0.9156	0.9518
608_fri_c3_1000_10	0.9297	0.9610
609_fri_c0_1000_5	0.9159	0.9551
611_fri_c3_100_5	0.6066	0.7015
612_fri_c1_1000_5	0.9425	0.9697
613_fri_c3_250_5	0.8520	0.9007
615_fri_c4_250_10	0.8145	0.8881
616_fri_c4_500_50	0.8697	0.9210
617_fri_c3_500_5	0.9012	0.9505
618_fri_c3_1000_50	0.9175	0.9450
620_fri_c1_1000_25	0.9280	0.9594
621_fri_c0_100_10	0.7654	0.8648
622_fri_c2_1000_50	0.9185	0.9487
623_fri_c4_1000_10	0.9250	0.9486
624_fri_c0_100_5	0.6900	0.8258
626_fri_c2_500_50	0.8604	0.9122
627_fri_c2_500_10	0.8988	0.9415
628_fri_c3_1000_5	0.9375	0.9641
631_fri_c1_500_5	0.9049	0.9485
633_fri_c0_500_25	0.8707	0.9303
634_fri_c2_100_10	0.5585	0.7385
635_fri_c0_250_10	0.8209	0.9032
637_fri_c1_500_50	0.8813	0.9367
641_fri_c1_500_10	0.9112	0.9523
643_fri_c2_500_25	0.8776	0.9261
644_fri_c4_250_25	0.7670	0.8880
645_fri_c3_500_50	0.8434	0.9032
646_fri_c3_500_10	0.8989	0.9397
647_fri_c1_250_10	0.8775	0.9269
648_fri_c1_250_50	0.8335	0.9020
649_fri_c0_500_5	0.8954	0.9445

(Continued on next page)

(Continued from previous page)

Dataset	R^2	Spearman
650_fri_c0.500.50	0.8378	0.9143
651_fri_c0.100.25	0.5150	0.7462
653_fri_c0.250.25	0.7745	0.8564
654_fri_c0.500.10	0.8729	0.9344
656_fri_c1.100.5	0.6286	0.8248
657_fri_c2.250.10	0.8459	0.8747
658_fri_c3.250.25	0.7373	0.8573
663_rabe_266	0.9435	0.9709
665_sleuth_case2002	0.1711	0.4230
666_rmftsa_ladata	0.4321	0.6046
678_visualizing_environmental	0.1584	0.4936
687_sleuth_ex1605	0.2421	0.5276
690_visualizing_galaxy	0.9675	0.9775
695_chatfield_4	0.8253	0.9069
706_sleuth_case1202	0.5381	0.7661
712_chscase_geyser1	0.7251	0.7061
auto_insurance_losses	0.6849	0.8396
auto_insurance_price	0.8747	0.9395
feynman_III.10.19	0.9988	0.9994
feynman_III.12.43	0.9998	0.9999
feynman_III.13.18	0.9970	0.9978
feynman_III.14.14	0.9909	0.9952
feynman_III.15.12	0.9426	0.9660
feynman_III.15.14	0.9984	0.9986
feynman_III.15.27	0.9987	0.9992
feynman_III.17.37	0.9990	0.9995
feynman_III.19.51	0.9482	0.9548
feynman_III.21.20	0.9969	0.9978
feynman_III.4.32	0.9964	0.9976
feynman_III.4.33	0.9996	0.9998
feynman_III.7.38	0.9989	0.9992
feynman_III.8.54	0.5515	0.7869
feynman_III.9.52	0.9575	0.9720
feynman_II.10.9	0.9988	0.9993
feynman_II.11.20	0.9911	0.9943
feynman_II.11.27	0.9985	0.9988
feynman_II.11.28	0.9998	0.9998
feynman_II.11.3	0.9959	0.9978
feynman_II.13.17	0.9949	0.9970
feynman_II.13.23	0.9999	1.0000
feynman_II.13.34	0.9997	0.9999
feynman_II.15.4	0.9990	0.9995
feynman_II.15.5	0.9990	0.9995
feynman_II.21.32	0.9959	0.9980
feynman_II.24.17	0.9997	0.9998
feynman_II.27.16	0.9991	0.9994
feynman_II.27.18	0.9998	0.9999
feynman_II.2.42	0.9912	0.9960
feynman_II.34.11	0.9968	0.9978
feynman_II.34.2	0.9990	0.9993

(Continued on next page)

(Continued from previous page)

Dataset	R^2	Spearman
feynman_II_34_29a	0.9988	0.9992
feynman_II_34_29b	0.9936	0.9954
feynman_II_34_2a	0.9989	0.9992
feynman_II_35_18	0.9948	0.9974
feynman_II_35_21	0.9966	0.9980
feynman_II_36_38	0.9877	0.9950
feynman_II_37_1	0.9991	0.9994
feynman_II_38_14	0.9998	0.9999
feynman_II_38_3	0.9968	0.9978
feynman_II_3_24	0.9998	0.9998
feynman_II_4_23	0.9987	0.9992
feynman_II_6_11	0.9977	0.9991
feynman_II_6_15a	0.9945	0.9938
feynman_II_6_15b	0.9969	0.9983
feynman_II_8_31	0.9998	0.9999
feynman_II_8_7	0.9987	0.9992
feynman_I_10_7	0.9999	1.0000
feynman_I_11_19	0.9944	0.9971
feynman_I_12_1	0.9998	0.9999
feynman_I_12_11	0.9969	0.9985
feynman_I_12_2	0.9962	0.9971
feynman_I_12_4	0.9987	0.9990
feynman_I_12_5	0.9998	0.9999
feynman_I_13_12	0.9925	0.9959
feynman_I_13_4	0.9981	0.9990
feynman_I_14_3	0.9990	0.9993
feynman_I_14_4	0.9998	0.9999
feynman_I_15_10	0.9997	0.9999
feynman_I_15_3t	0.9999	0.9999
feynman_I_15_3x	0.9993	0.9997
feynman_I_16_6	0.9993	0.9996
feynman_I_18_12	0.9993	0.9996
feynman_I_18_14	0.9983	0.9993
feynman_I_18_4	0.9986	0.9993
feynman_I_24_6	0.9980	0.9988
feynman_I_25_13	0.9998	0.9999
feynman_I_26_2	0.9999	0.9999
feynman_I_27_6	0.9992	0.9995
feynman_I_29_16	0.9776	0.9897
feynman_I_29_4	0.9997	0.9998
feynman_I_30_3	0.9689	0.9633
feynman_I_30_5	0.9990	0.9995
feynman_I_32_17	0.9895	0.9909
feynman_I_32_5	0.9919	0.9899
feynman_I_34_1	0.9994	0.9998
feynman_I_34_14	0.9996	0.9998
feynman_I_34_27	0.9998	0.9999
feynman_I_34_8	0.9969	0.9978
feynman_I_37_4	0.9991	0.9995
feynman_I_38_12	0.9953	0.9956

(Continued on next page)

(Continued from previous page)

Dataset	R^2	Spearman
feynman_I_39_1	0.9998	0.9999
feynman_I_39_11	0.9989	0.9992
feynman_I_39_22	0.9969	0.9978
feynman_I_40_1	0.9843	0.9818
feynman_I_41_16	0.9957	0.9945
feynman_I_43_16	0.9968	0.9978
feynman_I_43_31	0.9990	0.9993
feynman_I_43_43	0.9964	0.9977
feynman_I_44_4	0.9925	0.9961
feynman_I_47_23	0.9990	0.9994
feynman_I_48_2	0.9998	0.9998
feynman_I_50_26	0.9754	0.9697
feynman_I_6_2	0.9998	0.9999
feynman_I_6_2b	0.9976	0.9987
feynman_I_8_14	0.9867	0.9962
feynman_I_9_18	0.9873	0.9948
feynman_test_1	0.9656	0.9834
feynman_test_10	0.9998	0.9999
feynman_test_11	0.9976	0.9986
feynman_test_12	0.9982	0.9987
feynman_test_13	0.9933	0.9974
feynman_test_14	0.9737	0.9818
feynman_test_15	0.9988	0.9995
feynman_test_16	0.9977	0.9987
feynman_test_17	0.9927	0.9914
feynman_test_18	0.9937	0.9973
feynman_test_19	0.9926	0.9910
feynman_test_2	0.9560	0.9657
feynman_test_20	0.7215	0.9191
feynman_test_3	0.9985	0.9995
feynman_test_4	0.9987	0.9993
feynman_test_5	0.9991	0.9996
feynman_test_6	0.9800	0.9810
feynman_test_7	0.9996	0.9998
feynman_test_8	0.9984	0.9991
feynman_test_9	0.9716	0.9678
first_principles_planck	-11.9371	0.5233
first_principles_rydberg	0.6534	0.8704
nikuradse_1	0.9922	0.9852
solar_flare	-0.1965	0.2186
strogatz_bacres1	0.9747	0.9251
strogatz_bacres2	0.9857	0.9878
strogatz_barmag1	0.9591	0.9818
strogatz_barmag2	0.8519	0.9537
strogatz_glider1	0.9322	0.9623
strogatz_glider2	0.8832	0.9375
strogatz_lv1	-4.9581	0.4009
strogatz_lv2	-0.8227	0.8175
strogatz_predprey1	0.5780	0.9332
strogatz_predprey2	0.9854	0.9925

(Continued on next page)

(Continued from previous page)

Dataset	R^2	Spearman
strogatz_shearflow1	0.7893	0.9023
strogatz_shearflow2	0.9536	0.9847
strogatz_vdp1	0.7794	0.8616
strogatz_vdp2	0.9981	0.9991

C.3 Feature Importance Validation Results

This section provides detailed results from the ROAR (RemOve And Retrain) validation [Hooker et al., 2019] comparing Howso’s feature importance methods (Prediction Contributions and Accuracy Contributions) with SHAP [Lundberg and Lee, 2017].

Table 19: ROAR Comparison Results: Howso Prediction Contributions, Howso Accuracy Contributions, and SHAP Performance by Dataset and Removal Level

Dataset	Task	Method	Removed	Baseline	After	Change	Relative	Seeds		
diabetes	Regression (MAE)	Prediction Contrib.	0% (0)	49.3	49.3	0.0	0.0%	3		
		Prediction Contrib.	10% (1)	49.3	52.3	+3.6	+7.2%	3		
		Prediction Contrib.	20% (2)	49.3	55.7	+6.4	+13.0%	3		
		Prediction Contrib.	50% (5)	49.3	61.3	+12.0	+24.4%	3		
		Accuracy Contrib.	0% (0)	49.3	49.3	0.0	0.0%	3		
		Accuracy Contrib.	10% (1)	49.3	52.3	+3.0	+6.1%	3		
		Accuracy Contrib.	20% (2)	49.3	55.7	+6.4	+13.0%	3		
		Accuracy Contrib.	50% (5)	49.3	58.2	+8.9	+18.0%	3		
		SHAP	0% (0)	49.3	49.3	0.0	0.0%	3		
		SHAP	10% (1)	49.3	50.7	+1.4	+2.8%	3		
		SHAP	20% (2)	49.3	55.7	+6.4	+13.0%	3		
		SHAP	50% (5)	49.3	56.0	+6.7	+13.6%	3		
		breast_cancer	Classification (Acc)	Prediction Contrib.	0% (0)	97.4%	97.4%	0.0 pp	0.0%	3
				Prediction Contrib.	10% (3)	97.4%	95.6%	-1.8 pp	-1.8%	3
Prediction Contrib.	20% (6)			97.4%	96.5%	-0.9 pp	-0.9%	3		
Prediction Contrib.	50% (15)			97.4%	96.5%	-0.9 pp	-0.9%	3		
Accuracy Contrib.	0% (0)			97.4%	97.4%	0.0 pp	0.0%	3		
Accuracy Contrib.	10% (3)			97.4%	97.4%	0.0 pp	0.0%	3		
Accuracy Contrib.	20% (6)			97.4%	95.6%	-1.8 pp	-1.8%	3		
Accuracy Contrib.	50% (15)			97.4%	95.6%	-1.8 pp	-1.8%	3		
SHAP	0% (0)			97.4%	97.4%	0.0 pp	0.0%	3		
SHAP	10% (3)			97.4%	97.4%	0.0 pp	0.0%	3		
SHAP	20% (6)			97.4%	97.4%	0.0 pp	0.0%	3		
SHAP	50% (15)			97.4%	94.7%	-0.9 pp	-0.9%	3		

Note: Values are medians across 3 random seeds. Numbers in parentheses indicate the count of features removed. MAE = Mean Absolute Error (lower is better). Acc = Accuracy (higher is better). pp = percentage points. All tests performed on XGBoost models.

C.4 Anomaly Detection Results

Table 20: Anomaly Detection Results across Datasets

Metric	Dataset	PR-AUC	ROC-AUC
CBLOF	10_cover	0.0932	0.5130
CBLOF	12_fault	0.2136	0.5605
CBLOF	14_glass	0.0621	0.6300
CBLOF	15_Hepatitis	0.1970	0.6559
CBLOF	16_http	0.0200	0.4207

(Continued on next page)

(Continued from previous page)

Metric	Dataset	PR-AUC	ROC-AUC
CBLOF	18_Ionosphere	0.2368	0.7047
CBLOF	19_landsat	0.2585	0.7408
CBLOF	1_ALOI	0.0328	0.4428
CBLOF	20_letter	0.0970	0.7089
CBLOF	21_Lymphography	0.0411	0.3769
CBLOF	22_magic.gamma	0.2351	0.6151
CBLOF	23_mammography	0.0907	0.7392
CBLOF	24_mnist	0.1243	0.4617
CBLOF	25_musk	0.0930	0.6308
CBLOF	26_optdigits	0.1025	0.6732
CBLOF	27_PageBlocks	0.0472	0.4964
CBLOF	28_pendigits	0.1161	0.6788
CBLOF	29_Pima	0.2093	0.5770
CBLOF	2_annthyroid	0.0760	0.4719
CBLOF	30_satellite	0.3509	0.8474
CBLOF	31_satimage-2	0.0943	0.7443
CBLOF	32_shuttle	0.0692	0.5460
CBLOF	33_skin	0.1706	0.5995
CBLOF	34_smtpt	0.0001	0.0152
CBLOF	35_SpamBase	0.1749	0.4047
CBLOF	36_speech	0.2593	0.8649
CBLOF	37_Stamps	0.0349	0.3651
CBLOF	38_thyroid	0.0635	0.5200
CBLOF	39_vertebral	0.1476	0.5205
CBLOF	40_vowels	0.2774	0.8707
CBLOF	41_Waveform	0.1579	0.6446
CBLOF	42_WBC	0.0660	0.5672
CBLOF	43_WDBC	0.0794	0.6059
CBLOF	44_Wilt	0.0742	0.6802
CBLOF	45_wine	0.1361	0.6230
CBLOF	46_WPBC	0.1594	0.5555
CBLOF	47_yeast	0.2041	0.5984
CBLOF	4_breastw	0.1761	0.4623
CBLOF	5_campaign	0.1908	0.5933
CBLOF	6_cardio	0.1899	0.7974
CBLOF	7_Cardiotocography	0.1404	0.4658
COF	10_cover	0.1293	0.7050
COF	12_fault	0.3152	0.7435
COF	14_glass	0.2912	0.9435
COF	15_Hepatitis	0.3015	0.8260
COF	16_http	0.1270	0.9212
COF	18_Ionosphere	0.3357	0.7790
COF	19_landsat	0.2745	0.7851
COF	1_ALOI	0.1546	0.7091
COF	20_letter	0.2925	0.8606
COF	21_Lymphography	0.2068	0.8774
COF	22_magic.gamma	0.3036	0.7468
COF	23_mammography	0.1524	0.8397
COF	24_mnist	0.1751	0.6670
COF	25_musk	0.2979	0.9667

(Continued on next page)

(Continued from previous page)

Metric	Dataset	PR-AUC	ROC-AUC
COF	26_optdigits	0.2082	0.8599
COF	27_PageBlocks	0.1969	0.8261
COF	28_pendigits	0.1393	0.7858
COF	29_Pima	0.2930	0.7199
COF	2_annthyroid	0.1582	0.7984
COF	30_satellite	0.3080	0.7411
COF	31_satimage-2	0.1025	0.8088
COF	32_shuttle	0.1628	0.7396
COF	33_skin	0.1342	0.6205
COF	34_smtpt	1.0000	1.0000
COF	35_SpamBase	0.2490	0.5751
COF	36_speech	0.0638	0.4539
COF	37_Stamps	0.1219	0.6646
COF	38_thyroid	0.0682	0.7084
COF	39_verttebral	0.2429	0.7147
COF	40_vowels	0.3219	0.9706
COF	41_Waveform	0.2265	0.9388
COF	42_WBC	0.1973	0.8300
COF	43_WDBC	0.3301	0.9487
COF	44_Wilt	0.1453	0.7606
COF	45_wine	0.2020	0.7022
COF	46_WPBC	0.2831	0.7689
COF	47_yeast	0.2209	0.6376
COF	4_breastw	0.2601	0.6733
COF	5_campaign	0.1928	0.6709
COF	6_cardio	0.2457	0.8888
COF	7_Cardiotocography	0.2469	0.7309
COPOD	10_cover	0.2806	0.8820
COPOD	12_fault	0.3253	0.8047
COPOD	14_glass	0.3594	0.9468
COPOD	15_Hepatitis	0.2628	0.8583
COPOD	16_http	0.1413	0.9313
COPOD	18_Ionosphere	0.3044	0.7275
COPOD	19_landsat	0.1922	0.7557
COPOD	1_ALOI	0.1993	0.7840
COPOD	20_letter	0.1164	0.7025
COPOD	21_Lymphography	0.4791	0.9184
COPOD	22_magic.gamma	0.2720	0.7223
COPOD	23_mammography	0.2394	0.8148
COPOD	24_mnist	0.2831	0.8396
COPOD	25_musk	0.2722	0.8528
COPOD	26_optdigits	0.2404	0.8868
COPOD	27_PageBlocks	0.1852	0.7955
COPOD	28_pendigits	0.2049	0.8610
COPOD	29_Pima	0.3415	0.7884
COPOD	2_annthyroid	0.2541	0.8390
COPOD	30_satellite	0.2801	0.7605
COPOD	31_satimage-2	0.2403	0.9161
COPOD	32_shuttle	0.2288	0.8351
COPOD	33_skin	0.1697	0.6963

(Continued on next page)

(Continued from previous page)

Metric	Dataset	PR-AUC	ROC-AUC
COPOD	34_smtpt	1.0000	1.0000
COPOD	35_SpamBase	0.3239	0.7338
COPOD	36_speech	0.2702	0.8568
COPOD	37_Stamps	0.2880	0.8675
COPOD	38_thyroid	0.2986	0.8233
COPOD	39_vertrebral	0.2415	0.7457
COPOD	40_vowels	0.2751	0.7936
COPOD	41_Waveform	0.3236	0.9090
COPOD	42_WBC	0.1979	0.8979
COPOD	43_WDBC	0.2095	0.7451
COPOD	44_Wilt	0.1776	0.7994
COPOD	45_wine	0.3133	0.8913
COPOD	46_WPBC	0.3238	0.7937
COPOD	47_yeast	0.3177	0.8061
COPOD	4_breastw	0.3280	0.7638
COPOD	5_campaign	0.2997	0.8147
COPOD	6_cardio	0.2808	0.8575
COPOD	7_Cardiotocography	0.3304	0.8573
ECOD	10_cover	0.2944	0.8659
ECOD	12_fault	0.3360	0.8152
ECOD	14_glass	0.3400	0.9408
ECOD	15_Hepatitis	0.2583	0.8658
ECOD	16_http	0.1928	0.9601
ECOD	18_Ionosphere	0.2950	0.7302
ECOD	19_landsat	0.2437	0.7744
ECOD	1_ALOI	0.1955	0.7504
ECOD	20_letter	0.1188	0.7303
ECOD	21_Lymphography	0.4837	0.9329
ECOD	22_magic.gamma	0.2908	0.7494
ECOD	23_mammography	0.2627	0.8765
ECOD	24_mnist	0.2787	0.8258
ECOD	25_musk	0.2783	0.8661
ECOD	26_optdigits	0.2445	0.9165
ECOD	27_PageBlocks	0.1861	0.7891
ECOD	28_pendigits	0.2013	0.8760
ECOD	29_Pima	0.3432	0.7807
ECOD	2_annthyroid	0.2612	0.8413
ECOD	30_satellite	0.2623	0.7570
ECOD	31_satimage-2	0.2447	0.9105
ECOD	32_shuttle	0.2151	0.8429
ECOD	33_skin	0.2188	0.7153
ECOD	34_smtpt	1.0000	1.0000
ECOD	35_SpamBase	0.3237	0.7212
ECOD	36_speech	0.2593	0.8649
ECOD	37_Stamps	0.2784	0.8876
ECOD	38_thyroid	0.3018	0.8176
ECOD	39_vertrebral	0.2387	0.7521
ECOD	40_vowels	0.2728	0.7809
ECOD	41_Waveform	0.3034	0.9004
ECOD	42_WBC	0.2116	0.8854

(Continued on next page)

(Continued from previous page)

Metric	Dataset	PR-AUC	ROC-AUC
ECOD	43_WDBC	0.2293	0.7804
ECOD	44_Wilt	0.1720	0.8127
ECOD	45_wine	0.3232	0.9004
ECOD	46_WPBC	0.3385	0.8006
ECOD	47_yeast	0.3288	0.8228
ECOD	4_breastw	0.3244	0.7648
ECOD	5_campaign	0.2969	0.8147
ECOD	6_cardio	0.2992	0.8801
ECOD	7_Cardiotocography	0.3210	0.8592
FeatureBagging	10_cover	0.1224	0.7047
FeatureBagging	12_fault	0.3137	0.7584
FeatureBagging	14_glass	0.4062	0.9646
FeatureBagging	15_Hepatitis	0.2980	0.8058
FeatureBagging	16_http	0.2009	0.9686
FeatureBagging	18_Ionosphere	0.3472	0.8062
FeatureBagging	19_landsat	0.3001	0.8138
FeatureBagging	1_ALOI	0.1722	0.7780
FeatureBagging	20_letter	0.3113	0.8791
FeatureBagging	21_Lymphography	0.4761	0.9361
FeatureBagging	22_magic.gamma	0.3108	0.7616
FeatureBagging	23_mammography	0.1724	0.8633
FeatureBagging	24_mnist	0.1869	0.6698
FeatureBagging	25_musk	0.3882	0.9903
FeatureBagging	26_optdigits	0.2764	0.8548
FeatureBagging	27_PageBlocks	0.1894	0.8163
FeatureBagging	28_pendigits	0.1994	0.7976
FeatureBagging	29_Pima	0.3132	0.7435
FeatureBagging	2_annthyroid	0.2262	0.8483
FeatureBagging	30_satellite	0.3249	0.7550
FeatureBagging	31_satimage-2	0.3346	0.9895
FeatureBagging	32_shuttle	0.2034	0.8222
FeatureBagging	33_skin	0.1507	0.6684
FeatureBagging	34_smtpt	1.0000	1.0000
FeatureBagging	35_SpamBase	0.2563	0.6131
FeatureBagging	36_speech	0.2001	0.9158
FeatureBagging	37_Stamps	0.1439	0.7377
FeatureBagging	38_thyroid	0.0777	0.7151
FeatureBagging	39_vertrebral	0.2932	0.8345
FeatureBagging	40_vowels	0.4064	0.9832
FeatureBagging	41_Waveform	0.3747	0.9872
FeatureBagging	42_WBC	0.2018	0.9070
FeatureBagging	43_WDBC	0.3972	0.9622
FeatureBagging	44_Wilt	0.1683	0.8066
FeatureBagging	45_wine	0.2386	0.9094
FeatureBagging	46_WPBC	0.2878	0.7644
FeatureBagging	47_yeast	0.2192	0.6769
FeatureBagging	4_breastw	0.2808	0.6907
FeatureBagging	5_campaign	0.2209	0.6773
FeatureBagging	6_cardio	0.3238	0.9398
FeatureBagging	7_Cardiotocography	0.2403	0.7210

(Continued on next page)

(Continued from previous page)

Metric	Dataset	PR-AUC	ROC-AUC
HBOS	10_cover	0.2851	0.8755
HBOS	12_fault	0.3159	0.7669
HBOS	14_glass	0.3343	0.9244
HBOS	15_Hepatitis	0.2540	0.8424
HBOS	16_http	0.0991	0.6272
HBOS	18_Ionosphere	0.2874	0.7332
HBOS	19_landsat	0.2330	0.7773
HBOS	1_ALOI	0.1887	0.7648
HBOS	20_letter	0.1390	0.7143
HBOS	21_Lymphography	0.4133	0.8970
HBOS	22_magic.gamma	0.2878	0.7403
HBOS	23_mammography	0.2329	0.7449
HBOS	24_mnist	0.2897	0.7424
HBOS	25_musk	0.2938	0.8575
HBOS	26_optdigits	0.2447	0.7785
HBOS	27_PageBlocks	0.1603	0.7433
HBOS	28 PENDIGITS	0.1989	0.8517
HBOS	29_Pima	0.3423	0.7829
HBOS	2_annthyroid	0.2598	0.8310
HBOS	30_satellite	0.3072	0.7780
HBOS	31_satimage-2	0.2797	0.8996
HBOS	32_shuttle	0.2041	0.7976
HBOS	33_skin	0.2117	0.7103
HBOS	34_smtpt	1.0000	1.0000
HBOS	35_SpamBase	0.2952	0.6558
HBOS	36_speech	0.2480	0.8495
HBOS	37_Stamps	0.2870	0.8776
HBOS	38_thyroid	0.2051	0.8264
HBOS	39_verttebral	0.2178	0.7428
HBOS	40_vowels	0.2956	0.7840
HBOS	41_Waveform	0.3685	0.8864
HBOS	42_WBC	0.2026	0.8863
HBOS	43_WDBC	0.2752	0.7697
HBOS	44_Wilt	0.1763	0.7795
HBOS	45_wine	0.3280	0.8857
HBOS	46_WPBC	0.3307	0.7948
HBOS	47_yeast	0.2991	0.7853
HBOS	4_breastw	0.3125	0.7421
HBOS	5_campaign	0.2899	0.7580
HBOS	6_cardio	0.2613	0.8201
HBOS	7_Cardiotocography	0.3323	0.8215
IForest	10_cover	0.2847	0.8850
IForest	12_fault	0.3397	0.8270
IForest	14_glass	0.3195	0.9370
IForest	15_Hepatitis	0.2821	0.8733
IForest	16_http	0.1869	0.9588
IForest	18_Ionosphere	0.3233	0.7856
IForest	19_landsat	0.2902	0.8520
IForest	1_ALOI	0.2269	0.8285
IForest	20_letter	0.1327	0.7961

(Continued on next page)

(Continued from previous page)

Metric	Dataset	PR-AUC	ROC-AUC
IForest	21_Lymphography	0.3897	0.9271
IForest	22_magic.gamma	0.3058	0.7762
IForest	23_mammography	0.2206	0.8085
IForest	24_mnist	0.2969	0.7736
IForest	25_musk	0.2641	0.9392
IForest	26_optdigits	0.2395	0.8298
IForest	27_PageBlocks	0.1890	0.8098
IForest	28_pendigits	0.2115	0.9054
IForest	29_Pima	0.3457	0.7923
IForest	2_annthyroid	0.2617	0.8639
IForest	30_satellite	0.3431	0.8512
IForest	31_satimage-2	0.2983	0.9566
IForest	32_shuttle	0.2447	0.8593
IForest	33_skin	0.2717	0.7966
IForest	34_smtpt	0.5000	0.9999
IForest	35_SpamBase	0.2951	0.6947
IForest	36_speech	0.3179	0.8409
IForest	37_Stamps	0.3080	0.8862
IForest	38_thyroid	0.2661	0.8134
IForest	39_vertrebral	0.2715	0.8142
IForest	40_vowels	0.2223	0.8731
IForest	41_Waveform	0.3532	0.9318
IForest	42_WBC	0.2278	0.9108
IForest	43_WDBC	0.2649	0.8490
IForest	44_Wilt	0.1872	0.8310
IForest	45_wine	0.3549	0.9055
IForest	46_WPBC	0.3406	0.8354
IForest	47_yeast	0.3123	0.8014
IForest	4_breastw	0.3270	0.7525
IForest	5_campaign	0.3042	0.8107
IForest	6_cardio	0.2916	0.8595
IForest	7_Cardiotocography	0.3322	0.8479
KNN	10_cover	0.3173	0.9490
KNN	12_fault	0.3813	0.8393
KNN	14_glass	0.3654	0.9499
KNN	15_Hepatitis	0.3272	0.9015
KNN	16_http	0.1243	0.9273
KNN	18_Ionosphere	0.3675	0.8409
KNN	19_landsat	0.2988	0.8623
KNN	1_ALOI	0.2023	0.8284
KNN	20_letter	0.2252	0.9214
KNN	21_Lymphography	0.4463	0.9274
KNN	22_magic.gamma	0.3229	0.8140
KNN	23_mammography	0.1759	0.7640
KNN	24_mnist	0.2219	0.8223
KNN	25_musk	0.3958	0.9886
KNN	26_optdigits	0.2289	0.9452
KNN	27_PageBlocks	0.1866	0.8405
KNN	28_pendigits	0.2301	0.9524
KNN	29_Pima	0.3385	0.7847

(Continued on next page)

(Continued from previous page)

Metric	Dataset	PR-AUC	ROC-AUC
KNN	2_annthyroid	0.2243	0.8888
KNN	30_satellite	0.3403	0.8271
KNN	31_satimage-2	0.3372	0.9817
KNN	32_shuttle	0.2639	0.9374
KNN	33_skin	0.2565	0.8043
KNN	34_smtpt	1.0000	1.0000
KNN	35_SpamBase	0.2971	0.6820
KNN	36_speech	0.2754	0.9201
KNN	37_Stamps	0.2301	0.8971
KNN	38_thyroid	0.1870	0.8738
KNN	39_vertrebral	0.2942	0.8943
KNN	40_vowels	0.4080	0.9641
KNN	41_Waveform	0.3267	0.9783
KNN	42_WBC	0.2971	0.9385
KNN	43_WDBC	0.2904	0.9418
KNN	44_Wilt	0.1882	0.8782
KNN	45_wine	0.3090	0.9266
KNN	46_WPBC	0.3531	0.8942
KNN	47_yeast	0.2729	0.7319
KNN	4_breastw	0.2817	0.7192
KNN	5_campaign	0.2560	0.8132
KNN	6_cardio	0.2749	0.9087
KNN	7_Cardiotocography	0.3001	0.8158
LODA	10_cover	0.2448	0.8012
LODA	12_fault	0.3137	0.7803
LODA	14_glass	0.2541	0.8490
LODA	15_Hepatitis	0.2773	0.8336
LODA	16_http	0.0119	0.3390
LODA	18_Ionosphere	0.2843	0.6550
LODA	19_landsat	0.2511	0.7661
LODA	1_ALOI	0.1949	0.8015
LODA	20_letter	0.1091	0.6688
LODA	21_Lymphography	0.5325	0.8943
LODA	22_magic.gamma	0.2868	0.7325
LODA	23_mammography	0.1305	0.7540
LODA	24_mnist	0.2646	0.7997
LODA	25_musk	0.2159	0.8411
LODA	26_optdigits	0.2143	0.8373
LODA	27_PageBlocks	0.1774	0.6547
LODA	28_pendigits	0.1978	0.8232
LODA	29_Pima	0.3298	0.7537
LODA	2_annthyroid	0.2424	0.7428
LODA	30_satellite	0.2571	0.6980
LODA	31_satimage-2	0.3083	0.8501
LODA	32_shuttle	0.1924	0.6798
LODA	33_skin	0.1892	0.6601
LODA	34_smtpt	0.0002	0.4931
LODA	35_SpamBase	0.2867	0.6735
LODA	36_speech	0.2998	0.8631
LODA	37_Stamps	0.3540	0.8260

(Continued on next page)

(Continued from previous page)

Metric	Dataset	PR-AUC	ROC-AUC
LODA	38_thyroid	0.2469	0.7860
LODA	39_vertеbral	0.2058	0.6910
LODA	40_vowels	0.2691	0.7354
LODA	41_Waveform	0.3249	0.8935
LODA	42_WBC	0.2925	0.9346
LODA	43_WDBC	0.3129	0.7081
LODA	44_Wilt	0.1842	0.7109
LODA	45_wine	0.4263	0.8828
LODA	46_WPBC	0.2963	0.7696
LODA	47_yeast	0.2564	0.6835
LODA	4_breastw	0.2739	0.6689
LODA	5_campaign	0.3071	0.8408
LODA	6_cardio	0.2795	0.7975
LODA	7_Cardiotocography	0.3130	0.7973
LOF	10_cover	0.1391	0.6844
LOF	12_fault	0.3191	0.7298
LOF	14_glass	0.3330	0.9214
LOF	15_Hepatitis	0.2936	0.8099
LOF	16_http	0.1634	0.8970
LOF	18_Ionosphere	0.3506	0.8108
LOF	19_landsat	0.2984	0.8166
LOF	1_ALOI	0.1687	0.7366
LOF	20_letter	0.3082	0.8783
LOF	21_Lymphography	0.5399	0.9307
LOF	22_magic.gamma	0.3045	0.7488
LOF	23_mammography	0.1842	0.8607
LOF	24_mnist	0.1860	0.6757
LOF	25_musk	0.3757	0.9901
LOF	26_optdigits	0.2665	0.8433
LOF	27_PageBlocks	0.1822	0.8110
LOF	28_pendigits	0.2099	0.7940
LOF	29_Pima	0.3056	0.7289
LOF	2_annthyroid	0.2054	0.8329
LOF	30_satellite	0.3231	0.7574
LOF	31_satimage-2	0.3290	0.9891
LOF	32_shuttle	0.1814	0.7579
LOF	33_skin	0.1447	0.6554
LOF	34_smtп	1.0000	1.0000
LOF	35_SpamBase	0.2640	0.6186
LOF	36_speech	0.2015	0.9118
LOF	37_Stamps	0.1168	0.7053
LOF	38_thyroid	0.0623	0.6747
LOF	39_vertеbral	0.2735	0.7739
LOF	40_vowels	0.4549	0.9847
LOF	41_Waveform	0.4081	0.9882
LOF	42_WBC	0.1763	0.9079
LOF	43_WDBC	0.4270	0.9700
LOF	44_Wilt	0.1439	0.7863
LOF	45_wine	0.3213	0.9193
LOF	46_WPBC	0.2841	0.7555

(Continued on next page)

(Continued from previous page)

Metric	Dataset	PR-AUC	ROC-AUC
LOF	47_yeast	0.2106	0.6604
LOF	4_breastw	0.2812	0.6909
LOF	5_campaign	0.2290	0.6834
LOF	6_cardio	0.3288	0.9387
LOF	7_Cardiotocography	0.2405	0.7239
MCD	10_cover	0.3398	0.9453
MCD	12_fault	0.3666	0.8513
MCD	14_glass	0.3099	0.9155
MCD	15_Hepatitis	0.2365	0.8061
MCD	16_http	0.1280	0.9646
MCD	18_Ionosphere	0.3854	0.8553
MCD	19_landsat	0.2842	0.8633
MCD	1_ALOI	0.2811	0.8983
MCD	20_letter	0.1128	0.7918
MCD	21_Lymphography	0.3050	0.8701
MCD	22_magic.gamma	0.3353	0.8310
MCD	23_mammography	0.1492	0.7608
MCD	24_mnist	0.1850	0.8180
MCD	25_musk	0.3718	0.9148
MCD	26_optdigits	0.1070	0.7361
MCD	27_PageBlocks	0.1740	0.8360
MCD	28_pendigits	0.2644	0.9331
MCD	29_Pima	0.3340	0.8040
MCD	2_annthyroid	0.2919	0.9253
MCD	30_satellite	0.3708	0.8858
MCD	31_satimage-2	0.2923	0.9517
MCD	32_shuttle	0.2211	0.8989
MCD	33_skin	0.2545	0.8049
MCD	34_smtip	1.0000	1.0000
MCD	35_SpamBase	0.2688	0.7036
MCD	36_speech	0.3329	0.9940
MCD	37_Stamps	0.3098	0.9021
MCD	38_thyroid	0.2313	0.9174
MCD	39_verttebral	0.2774	0.8974
MCD	40_vowels	0.2124	0.9189
MCD	41_Waveform	0.3967	0.9841
MCD	42_WBC	0.2267	0.8549
MCD	43_WDBC	0.4884	0.9853
MCD	44_Wilt	0.2056	0.8569
MCD	45_wine	0.3629	0.9266
MCD	46_WPBC	0.3618	0.8894
MCD	47_yeast	0.3564	0.8643
MCD	4_breastw	0.3092	0.7330
MCD	5_campaign	0.3253	0.9326
MCD	6_cardio	0.2261	0.8995
MCD	7_Cardiotocography	0.3276	0.8764
MOGAAL	10_cover	0.0205	0.7520
MOGAAL	12_fault	0.2561	0.6496
MOGAAL	14_glass	0.0146	0.2783
MOGAAL	15_Hepatitis	0.0994	0.4083

(Continued on next page)

(Continued from previous page)

Metric	Dataset	PR-AUC	ROC-AUC
MOGAAL	16_http	0.0885	0.8565
MOGAAL	18_Ionosphere	0.1255	0.3832
MOGAAL	19_landsat	0.0959	0.5788
MOGAAL	1_ALOI	0.0564	0.7043
MOGAAL	20_letter	0.0228	0.4121
MOGAAL	21_Lymphography	0.0159	0.2628
MOGAAL	22_magic.gamma	0.2464	0.6509
MOGAAL	23_mammography	0.0467	0.7232
MOGAAL	24_mnist	0.1602	0.7433
MOGAAL	25_musk	0.0858	0.3429
MOGAAL	26_optdigits	0.0745	0.6557
MOGAAL	27_PageBlocks	0.0985	0.5655
MOGAAL	28_pendigits	0.0112	0.4192
MOGAAL	29_Pima	0.1308	0.4031
MOGAAL	2_annthyroid	0.0522	0.5362
MOGAAL	30_satellite	0.0894	0.3914
MOGAAL	31_satimage-2	0.0067	0.5130
MOGAAL	32_shuttle	0.0569	0.5587
MOGAAL	33_skin	0.0858	0.5230
MOGAAL	34_smtpt	0.0039	0.9871
MOGAAL	35_SpamBase	0.2447	0.5735
MOGAAL	36_speech	0.1987	0.8082
MOGAAL	37_Stamps	0.0538	0.4156
MOGAAL	38_thyroid	0.0176	0.5175
MOGAAL	39_vertebral	0.0572	0.3801
MOGAAL	40_vowels	0.2069	0.7205
MOGAAL	41_Waveform	0.0232	0.4908
MOGAAL	42_WBC	0.0960	0.4957
MOGAAL	43_WDBC	0.0956	0.4303
MOGAAL	44_Wilt	0.0192	0.4303
MOGAAL	45_wine	0.0417	0.4059
MOGAAL	46_WPBC	0.1188	0.3864
MOGAAL	47_yeast	0.2493	0.6280
MOGAAL	4_breastw	0.1169	0.3806
MOGAAL	5_campaign	0.1592	0.6534
MOGAAL	6_cardio	0.1874	0.7182
MOGAAL	7_Cardiotocography	0.1691	0.5382
OCSVM	10_cover	0.3253	0.8913
OCSVM	12_fault	0.3563	0.8158
OCSVM	14_glass	0.3664	0.9339
OCSVM	15_Hepatitis	0.2653	0.8557
OCSVM	16_http	0.0965	0.8050
OCSVM	18_Ionosphere	0.3152	0.7403
OCSVM	19_landsat	0.2885	0.8558
OCSVM	1_ALOI	0.2256	0.8317
OCSVM	20_letter	0.1317	0.7755
OCSVM	21_Lymphography	0.3473	0.8803
OCSVM	22_magic.gamma	0.3070	0.7784
OCSVM	23_mammography	0.1814	0.7867
OCSVM	24_mnist	0.2645	0.7691

(Continued on next page)

(Continued from previous page)

Metric	Dataset	PR-AUC	ROC-AUC
OCSVM	25_musk	0.2950	0.9563
OCSVM	26_optdigits	0.2345	0.8203
OCSVM	27_PageBlocks	0.1955	0.7991
OCSVM	28_pendigits	0.2411	0.9102
OCSVM	29_Pima	0.3312	0.7767
OCSVM	2_annthyroid	0.2583	0.8596
OCSVM	30_satellite	0.3141	0.7805
OCSVM	31_satimage-2	0.3832	0.9584
OCSVM	32_shuttle	0.1991	0.8171
OCSVM	33_skin	0.2742	0.7878
OCSVM	34_smtpt	1.0000	1.0000
OCSVM	35_SpamBase	0.3106	0.7097
OCSVM	36_speech	0.2809	0.8802
OCSVM	37_Stamps	0.2576	0.8798
OCSVM	38_thyroid	0.1916	0.8153
OCSVM	39_verttebral	0.2688	0.7587
OCSVM	40_vowels	0.2755	0.8669
OCSVM	41_Waveform	0.3450	0.9420
OCSVM	42_WBC	0.2823	0.9112
OCSVM	43_WDBC	0.2578	0.8385
OCSVM	44_Wilt	0.2170	0.8166
OCSVM	45_wine	0.3335	0.9079
OCSVM	46_WPBC	0.3332	0.8232
OCSVM	47_yeast	0.2855	0.7392
OCSVM	4_breastw	0.3216	0.7361
OCSVM	5_campaign	0.2998	0.8230
OCSVM	6_cardio	0.2238	0.8532
OCSVM	7_Cardiotocography	0.3379	0.8184
PCA	10_cover	0.2896	0.8867
PCA	12_fault	0.3236	0.7946
PCA	14_glass	0.3188	0.9129
PCA	15_Hepatitis	0.2469	0.8488
PCA	16_http	0.0946	0.7808
PCA	18_Ionosphere	0.2691	0.7025
PCA	19_landsat	0.2496	0.7893
PCA	1_ALOI	0.2707	0.8342
PCA	20_letter	0.1165	0.7438
PCA	21_Lymphography	0.3608	0.8825
PCA	22_magic.gamma	0.2946	0.7501
PCA	23_mammography	0.1637	0.7618
PCA	24_mnist	0.2989	0.7692
PCA	25_musk	0.2877	0.8746
PCA	26_optdigits	0.2035	0.8088
PCA	27_PageBlocks	0.1904	0.7584
PCA	28_pendigits	0.2043	0.8689
PCA	29_Pima	0.3154	0.7595
PCA	2_annthyroid	0.2634	0.8478
PCA	30_satellite	0.2271	0.6739
PCA	31_satimage-2	0.2891	0.9144
PCA	32_shuttle	0.2267	0.7937

(Continued on next page)

(Continued from previous page)

Metric	Dataset	PR-AUC	ROC-AUC
PCA	33_skin	0.2376	0.7126
PCA	34_smtpt	1.0000	1.0000
PCA	35_SpamBase	0.3153	0.7163
PCA	36_speech	0.2826	0.8780
PCA	37_Stamps	0.2767	0.8736
PCA	38_thyroid	0.2798	0.8137
PCA	39_vertrebral	0.2534	0.7797
PCA	40_vowels	0.3243	0.7847
PCA	41_Waveform	0.3169	0.9008
PCA	42_WBC	0.2199	0.8909
PCA	43_WDBC	0.2648	0.8095
PCA	44_Wilt	0.1766	0.7987
PCA	45_wine	0.3133	0.9045
PCA	46_WPBC	0.3302	0.8058
PCA	47_yeast	0.2872	0.7423
PCA	4_breastw	0.3140	0.7256
PCA	5_campaign	0.2887	0.8218
PCA	6_cardio	0.2563	0.8261
PCA	7_Cardiotocography	0.3219	0.8093
SOD	10_cover	0.3167	0.9520
SOD	12_fault	0.3605	0.8116
SOD	14_glass	0.4198	0.9644
SOD	15_Hepatitis	0.2910	0.8524
SOD	16_http	0.1873	0.8874
SOD	18_Ionosphere	0.3517	0.8283
SOD	19_landsat	0.2895	0.8483
SOD	1_ALOI	0.1756	0.7669
SOD	20_letter	0.2749	0.9306
SOD	21_Lymphography	0.2757	0.9114
SOD	22_magic.gamma	0.3047	0.7679
SOD	23_mammography	0.1519	0.7779
SOD	24_mnist	0.1689	0.7610
SOD	25_musk	0.3992	0.9864
SOD	26_optdigits	0.2973	0.9562
SOD	27_PageBlocks	0.2073	0.8523
SOD	28_pendigits	0.2055	0.9248
SOD	29_Pima	0.3158	0.7431
SOD	2_annthyroid	0.2253	0.8379
SOD	30_satellite	0.3373	0.8190
SOD	31_satimage-2	0.2959	0.9883
SOD	32_shuttle	0.2467	0.9169
SOD	33_skin	0.2047	0.6932
SOD	34_smtpt	1.0000	1.0000
SOD	35_SpamBase	0.2782	0.6570
SOD	36_speech	0.1930	0.8460
SOD	37_Stamps	0.2879	0.9286
SOD	38_thyroid	0.1085	0.8933
SOD	39_vertrebral	0.3000	0.8705
SOD	40_vowels	0.3552	0.9642
SOD	41_Waveform	0.2634	0.9211

(Continued on next page)

(Continued from previous page)

Metric	Dataset	PR-AUC	ROC-AUC
SOD	42_WBC	0.3048	0.8601
SOD	43_WDBC	0.2172	0.9519
SOD	44_Wilt	0.1772	0.8318
SOD	45_wine	0.2972	0.8869
SOD	46_WPBC	0.3393	0.8976
SOD	47_yeast	0.2531	0.6765
SOD	4_breastw	0.2746	0.6931
SOD	5_campaign	0.2122	0.7603
SOD	6_cardio	0.2538	0.8666
SOD	7_Cardiotocography	0.2635	0.8004
SOGAAL	10_cover	0.0082	0.7046
SOGAAL	12_fault	0.2592	0.6327
SOGAAL	14_glass	0.1416	0.6219
SOGAAL	15_Hepatitis	0.0957	0.4005
SOGAAL	16_http	0.0056	0.8039
SOGAAL	18_Ionosphere	0.1288	0.4475
SOGAAL	19_landsat	0.0999	0.5895
SOGAAL	1_ALOI	0.0373	0.7324
SOGAAL	20_letter	0.0596	0.3845
SOGAAL	21_Lymphography	0.1652	0.5958
SOGAAL	22_magic.gamma	0.2043	0.6585
SOGAAL	23_mammography	0.0257	0.7510
SOGAAL	24_mnist	0.1206	0.7179
SOGAAL	25_musk	0.0399	0.3929
SOGAAL	26_optdigits	0.0526	0.7032
SOGAAL	27_PageBlocks	0.0582	0.5529
SOGAAL	28_pendigits	0.0158	0.6160
SOGAAL	29_Pima	0.1453	0.4253
SOGAAL	2_annthyroid	0.0798	0.7629
SOGAAL	30_satellite	0.0893	0.3900
SOGAAL	31_satimage-2	0.0090	0.6566
SOGAAL	32_shuttle	0.0774	0.7012
SOGAAL	33_skin	0.0878	0.5581
SOGAAL	34_smtpt	0.0005	0.8900
SOGAAL	35_SpamBase	0.2542	0.6076
SOGAAL	36_speech	0.1739	0.8065
SOGAAL	37_Stamps	0.0527	0.4886
SOGAAL	38_thyroid	0.0326	0.7205
SOGAAL	39_verttebral	0.0685	0.4905
SOGAAL	40_vowels	0.1629	0.7123
SOGAAL	41_Waveform	0.0154	0.5361
SOGAAL	42_WBC	0.0199	0.4828
SOGAAL	43_WDBC	0.1029	0.5989
SOGAAL	44_Wilt	0.0430	0.6637
SOGAAL	45_wine	0.0584	0.4696
SOGAAL	46_WPBC	0.1062	0.4364
SOGAAL	47_yeast	0.2253	0.6613
SOGAAL	4_breastw	0.1481	0.4921
SOGAAL	5_campaign	0.1507	0.7314
SOGAAL	6_cardio	0.1506	0.7137

(Continued on next page)

(Continued from previous page)

Metric	Dataset	PR-AUC	ROC-AUC
SOGAAL	7_Cardiotocography	0.1601	0.5097
conviction_dynamic	10_cover	0.2441	0.9774
conviction_dynamic	12_fault	0.3936	0.8828
conviction_dynamic	14_glass	0.3856	0.9603
conviction_dynamic	15_Hepatitis	0.2586	0.8318
conviction_dynamic	16_http	0.0701	0.9246
conviction_dynamic	18_Ionosphere	0.3891	0.8655
conviction_dynamic	19_landsat	0.3336	0.8998
conviction_dynamic	1_ALOI	0.2455	0.9211
conviction_dynamic	20_letter	0.3343	0.9694
conviction_dynamic	21_Lymphography	0.4462	0.9358
conviction_dynamic	22_magic.gamma	0.3450	0.8483
conviction_dynamic	23_mammography	0.2743	0.9183
conviction_dynamic	24_mnist	0.2694	0.8770
conviction_dynamic	25_musk	0.4295	0.9859
conviction_dynamic	26_optdigits	0.2261	0.9671
conviction_dynamic	27_PageBlocks	0.2219	0.8806
conviction_dynamic	28_pendigits	0.1968	0.9321
conviction_dynamic	29_Pima	0.3480	0.8119
conviction_dynamic	2_annthyroid	0.2518	0.8825
conviction_dynamic	30_satellite	0.3898	0.8878
conviction_dynamic	31_satimage-2	0.2499	0.9752
conviction_dynamic	32_shuttle	0.3175	0.9446
conviction_dynamic	33_skin	0.2460	0.7996
conviction_dynamic	34_smtpt	1.0000	1.0000
conviction_dynamic	35_SpamBase	0.2891	0.7224
conviction_dynamic	36_speech	0.1836	0.7222
conviction_dynamic	37_Stamps	0.2568	0.9082
conviction_dynamic	38_thyroid	0.1124	0.8056
conviction_dynamic	39_verttebral	0.2844	0.8824
conviction_dynamic	40_vowels	0.3767	0.9847
conviction_dynamic	41_Waveform	0.3473	0.9863
conviction_dynamic	42_WBC	0.1918	0.8815
conviction_dynamic	43_WDBC	0.3656	0.9879
conviction_dynamic	44_Wilt	0.2021	0.8769
conviction_dynamic	45_wine	0.4003	0.9526
conviction_dynamic	46_WPBC	0.4375	0.9182
conviction_dynamic	47_yeast	0.2467	0.6849
conviction_dynamic	4_breastw	0.3053	0.7905
conviction_dynamic	5_campaign	0.3018	0.8906
conviction_dynamic	6_cardio	0.3111	0.9429
conviction_dynamic	7_Cardiotocography	0.3356	0.9003
distance_contribution_conviction	10_cover	0.2665	0.9593
distance_contribution_conviction	12_fault	0.3986	0.8400
distance_contribution_conviction	14_glass	0.4409	0.9563
distance_contribution_conviction	15_Hepatitis	0.3338	0.8948
distance_contribution_conviction	16_http	0.1068	0.9277
distance_contribution_conviction	18_Ionosphere	0.3525	0.8393
distance_contribution_conviction	19_landsat	0.3012	0.8576
distance_contribution_conviction	1_ALOI	0.1832	0.8240

(Continued on next page)

(Continued from previous page)

Metric	Dataset	PR-AUC	ROC-AUC
distance_contribution_conviction	20_letter	0.2523	0.9176
distance_contribution_conviction	21_Lymphography	0.2260	0.9300
distance_contribution_conviction	22_magic.gamma	0.3172	0.8108
distance_contribution_conviction	23_mammography	0.1729	0.7693
distance_contribution_conviction	24_mnist	0.1750	0.7937
distance_contribution_conviction	25_musk	0.4599	0.9891
distance_contribution_conviction	26_optdigits	0.1891	0.9307
distance_contribution_conviction	27_PageBlocks	0.1870	0.8386
distance_contribution_conviction	28_pendigits	0.2148	0.9402
distance_contribution_conviction	29_Pima	0.3362	0.7773
distance_contribution_conviction	2_annthyroid	0.2334	0.8721
distance_contribution_conviction	30_satellite	0.3397	0.8234
distance_contribution_conviction	31_satimage-2	0.2717	0.9793
distance_contribution_conviction	32_shuttle	0.2692	0.9351
distance_contribution_conviction	33_skin	0.2468	0.8010
distance_contribution_conviction	34_smtpt	1.0000	1.0000
distance_contribution_conviction	35_SpamBase	0.2928	0.6556
distance_contribution_conviction	36_speech	0.1823	0.7468
distance_contribution_conviction	37_Stamps	0.2427	0.9077
distance_contribution_conviction	38_thyroid	0.1481	0.8593
distance_contribution_conviction	39_vertrebral	0.3213	0.8907
distance_contribution_conviction	40_vowels	0.3617	0.9674
distance_contribution_conviction	41_Waveform	0.2945	0.9787
distance_contribution_conviction	42_WBC	0.2544	0.9197
distance_contribution_conviction	43_WDBC	0.3201	0.9729
distance_contribution_conviction	44_Wilt	0.2111	0.8715
distance_contribution_conviction	45_wine	0.3168	0.9380
distance_contribution_conviction	46_WPBC	0.3243	0.8881
distance_contribution_conviction	47_yeast	0.2965	0.7964
distance_contribution_conviction	4_breastw	0.2891	0.7222
distance_contribution_conviction	5_campaign	0.2321	0.8271
distance_contribution_conviction	6_cardio	0.2596	0.9119
distance_contribution_conviction	7_Cardiotocography	0.2932	0.8336
similarity_conviction	10_cover	0.1877	0.7506
similarity_conviction	12_fault	0.2460	0.6364
similarity_conviction	14_glass	0.3405	0.8895
similarity_conviction	15_Hepatitis	0.3095	0.8088
similarity_conviction	16_http	0.0414	0.7807
similarity_conviction	18_Ionosphere	0.3210	0.7460
similarity_conviction	19_landsat	0.2862	0.7859
similarity_conviction	1_ALOI	0.1920	0.8167
similarity_conviction	20_letter	0.3608	0.9010
similarity_conviction	21_Lymphography	0.1681	0.7769
similarity_conviction	22_magic.gamma	0.2930	0.7330
similarity_conviction	23_mammography	0.2249	0.8061
similarity_conviction	24_mnist	0.1012	0.5795
similarity_conviction	25_musk	0.4242	0.8731
similarity_conviction	26_optdigits	0.3429	0.8872
similarity_conviction	27_PageBlocks	0.1619	0.7750
similarity_conviction	28_pendigits	0.1873	0.7939

(Continued on next page)

(Continued from previous page)

Metric	Dataset	PR-AUC	ROC-AUC
similarity_conviction	29_Pima	0.2846	0.7137
similarity_conviction	2_annthyroid	0.0859	0.6836
similarity_conviction	30_satellite	0.3057	0.7492
similarity_conviction	31_satimage-2	0.2051	0.8206
similarity_conviction	32_shuttle	0.1798	0.7627
similarity_conviction	33_skin	0.1284	0.6237
similarity_conviction	34_smtpt	1.0000	1.0000
similarity_conviction	35_SpamBase	0.2502	0.6450
similarity_conviction	36_speech	0.1887	0.7225
similarity_conviction	37_Stamps	0.1531	0.7158
similarity_conviction	38_thyroid	0.0660	0.6253
similarity_conviction	39_verttebral	0.2918	0.7552
similarity_conviction	40_vowels	0.3349	0.9856
similarity_conviction	41_Waveform	0.2321	0.8816
similarity_conviction	42_WBC	0.2157	0.7807
similarity_conviction	43_WDBC	0.3190	0.9872
similarity_conviction	44_Wilt	0.1256	0.7512
similarity_conviction	45_wine	0.1689	0.6806
similarity_conviction	46_WPBC	0.3571	0.7666
similarity_conviction	47_yeast	0.2025	0.6205
similarity_conviction	4_breastw	0.2783	0.6889
similarity_conviction	5_campaign	0.2375	0.7420
similarity_conviction	6_cardio	0.3212	0.8876
similarity_conviction	7_Cardiotocography	0.2109	0.7014

C.5 Reinforcement Learning: Detailed Results

C.5.1 CartPole Results

Metric	Value
Total Runs	5
Winning Runs	5
Win Rate (%)	100.00
Median Rounds to Win	273
IQR Rounds to Win	38.00
Median High Score	500.00
Median Total Cases	26564

Table 21: CartPole Summary Statistics

Iteration	Win	Rounds	Avg Score (Final)	Avg Score (Total)	High Score	Total Cases
0	Yes	100	252.42	252.42	500	22191
1	Yes	273	195.09	116.14	500	25564
2	Yes	791	196.79	123.35	500	71117
3	Yes	287	195.11	143.84	500	30427
4	Yes	249	196.16	136.71	500	26564

Table 22: CartPole Detailed Run Results

C.5.2 Wafer-Thin-Mints Results

Metric	Value
Total Runs	20
Winning Runs	14
Win Rate (%)	70.00
Median Rounds to Win	150.00
IQR Rounds to Win	0.00
Median High Score	9.00
Median Total Cases	1189.50

Table 23: Wafer-Thin-Mints Summary Statistics

Iteration	Win	Rounds	Avg Score (Final)	Avg Score (Total)	High Score	Total Cases
0	No	150	3.92	3.92	5	738
1	Yes	150	6.15	6.15	9	1130
2	No	150	4.43	4.43	8	815
3	No	150	5.74	5.74	9	1182
4	Yes	150	7.31	7.31	9	1342
5	Yes	150	7.44	7.44	9	1361
6	Yes	150	6.99	6.99	9	1237
7	Yes	150	7.10	7.10	9	1329
8	Yes	150	6.97	6.97	9	1253
9	Yes	150	7.10	7.10	9	1291
10	Yes	150	6.35	6.35	9	1197
11	Yes	150	7.00	7.00	9	1352
12	Yes	150	6.20	6.20	9	1156
13	Yes	150	6.53	6.53	9	1168
14	No	150	5.01	5.01	6	901
15	No	150	4.51	4.51	6	845
16	Yes	150	6.92	6.92	9	1264
17	Yes	150	7.50	7.50	9	1351
18	No	150	1.52	1.52	2	378
19	Yes	150	6.65	6.65	9	1166

Table 24: Wafer-Thin-Mints Detailed Run Results

C.6 Synthetic Data Generation: Detailed Results

Table 25: Synthetic Data Generation: Regression Datasets (Spearman Correlation)

Dataset	Original	Generated
1199_BNG_echoMonths	0.8296	0.8083
197_cpu_act	0.9832	0.9754
537_houses	0.9553	0.9464
574_house_16H	0.9144	0.9018

Table 26: Synthetic Data Generation: Classification Datasets

Dataset	Accuracy		F1-Score		MCC	
	Orig	Gen	Orig	Gen	Orig	Gen
letter	0.953	0.901	0.954	0.902	0.952	0.897
magic	0.879	0.851	0.879	0.852	0.732	0.667
mushroom	1.000	1.000	1.000	1.000	1.000	0.999
pendigits	0.992	0.986	0.992	0.986	0.992	0.984
ring	0.971	0.886	0.971	0.896	0.942	0.791

C.7 Adversarial Robustness Results

C.7.1 Aggregate Results

Table 27: Mean accuracy degradation under adversarial attack across 27 datasets

Attack	Model	Clean Acc	Adv Acc	Δ (Adv - Clean)
K=3 (approx)	Decision Tree	0.783	0.564	-0.220
	Howso	0.819	0.596	-0.223
	k-NN	0.796	0.436	-0.360
	LightGBM	0.835	0.619	-0.216
	Logistic Regression	0.795	0.684	-0.111
	XGBoost	0.834	0.633	-0.201
K=1 (exact)	Decision Tree	0.783	0.641	-0.142
	Howso	0.819	0.737	-0.082
	k-NN	0.796	0.757	-0.039
	LightGBM	0.835	0.717	-0.119
	Logistic Regression	0.795	0.742	-0.053
	XGBoost	0.834	0.691	-0.143

C.7.2 Per-Dataset Results

Complete per-dataset results for Howso are provided below.

Table 28: Summary statistics of accuracy degradation by model and attack

Attack	Model	Median Δ	Mean Δ	Min Δ	Q1	Q3	Worst-5 Mean
K=3	Dec. Tree	-0.167	-0.220	-0.530	-0.341	-0.104	-0.441
	Howso	-0.179	-0.223	-0.550	-0.349	-0.070	-0.482
	k-NN	-0.333	-0.360	-0.803	-0.460	-0.163	-0.728
	LightGBM	-0.166	-0.216	-0.535	-0.308	-0.116	-0.476
	Log. Reg.	-0.067	-0.111	-0.463	-0.167	-0.021	-0.308
	XGBoost	-0.195	-0.201	-0.550	-0.271	-0.090	-0.479
K=1	Dec. Tree	-0.097	-0.142	-0.420	-0.193	-0.052	-0.345
	Howso	-0.056	-0.082	-0.420	-0.107	-0.016	-0.248
	k-NN	-0.023	-0.039	-0.233	-0.052	0.000	-0.123
	LightGBM	-0.083	-0.119	-0.420	-0.183	-0.033	-0.303
	Log. Reg.	-0.038	-0.053	-0.333	-0.078	0.000	-0.161
	XGBoost	-0.119	-0.143	-0.450	-0.212	-0.048	-0.334

Table 29: Howso per-dataset robustness results

Dataset	Attack	Clean Acc	Adv Acc	Δ	N Test
biomed	K=3	1.000	0.833	-0.167	42
breast_w	K=3	0.950	0.771	-0.179	140
cars	K=3	1.000	0.696	-0.304	79
cleveland	K=3	0.443	0.262	-0.180	61
cloud	K=3	0.364	0.318	-0.045	22
confidence	K=3	0.933	0.533	-0.400	15
d_breast_cancer	K=3	0.974	0.667	-0.307	114
d_digits	K=3	0.967	0.475	-0.492	360
d_iris	K=3	0.833	0.533	-0.300	30
d_wine	K=3	1.000	0.583	-0.417	36
ecoli	K=3	0.879	0.803	-0.076	66
haberman	K=3	0.661	0.629	-0.032	62
heart_statlog	K=3	0.759	0.667	-0.093	54
hepatitis	K=3	0.839	0.774	-0.065	31
irish	K=3	1.000	0.450	-0.550	100
labor	K=3	0.917	0.667	-0.250	12
lupus	K=3	0.611	0.556	-0.056	18
lymphography	K=3	0.833	0.700	-0.133	30
new_thyroid	K=3	0.953	0.512	-0.442	43
penguins	K=3	0.985	0.478	-0.507	67
postoperative_patient_data	K=3	0.833	0.833	0.000	18
prnn_fglass	K=3	0.707	0.317	-0.390	41
saheart	K=3	0.710	0.645	-0.065	93
sonar	K=3	0.810	0.690	-0.119	42
uci_glass	K=3	1.000	0.721	-0.279	43
uci_heart_disease	K=3	0.467	0.433	-0.033	60
wine_quality_red	K=3	0.678	0.537	-0.141	320
biomed	K=1	1.000	0.881	-0.119	42
breast_w	K=1	0.950	0.886	-0.064	140
cars	K=1	1.000	0.797	-0.203	79
cleveland	K=1	0.443	0.426	-0.016	61
cloud	K=1	0.364	0.364	0.000	22
confidence	K=1	0.933	0.933	0.000	15
d_breast_cancer	K=1	0.974	0.965	-0.009	114
d_digits	K=1	0.967	0.928	-0.039	360
d_iris	K=1	0.833	0.633	-0.200	30
d_wine	K=1	1.000	0.944	-0.056	36
ecoli	K=1	0.879	0.864	-0.015	66
haberman	K=1	0.661	0.677	0.016	62
heart_statlog	K=1	0.759	0.722	-0.037	54
hepatitis	K=1	0.839	0.742	-0.097	31
irish	K=1	1.000	0.580	-0.420	100
labor	K=1	0.917	0.833	-0.083	12
lupus	K=1	0.611	0.556	-0.056	18
lymphography	K=1	0.833	0.800	-0.033	30
new_thyroid	K=1	0.953	0.698	-0.256	43
penguins	K=1	0.985	0.896	-0.090	67
postoperative_patient_data	K=1	0.833	0.833	0.000	18
prnn_fglass	K=1	0.707	0.610	-0.098	41
saheart	K=1	0.710	0.677	-0.032	93
sonar	K=1	0.810	0.786	-0.024	42
uci_glass	K=1	1.000	0.837	-0.163	43
uci_heart_disease	K=1	0.467	0.467	0.000	60
wine_quality_red	K=1	0.678	0.562	-0.116	320